

**MAREES TERRESTRES**  
**BULLETIN D'INFORMATIONS**

**INTERNATIONAL CENTER FOR EARTH TIDES**  
**CENTRE INTERNATIONAL DES MAREES TERRESTRES**



**International Association of Geodesy - International Gravity Field Service**  
**(IAG – IGFS)**

**Publié par l'Université de la Polynésie française**

**BIM n° 148**

**ISSN n°0542-6766**

**1 SEPTEMBRE 2014**

*Editeur: Prof. Jean-Pierre BARRIOT*  
*Observatoire Géodésique de Tahiti*  
*Université de Polynésie française*  
*BP6570 – 98702 Faaa*  
*Tahiti-Polynésie française*

BLANK PAGE

The precious help of Prof. Bernard Ducarme is gracefully acknowledged for his guidance and help in completing this issue of the BIM.

All the issues of the BIM can be downloaded from [bim-icet.org](http://bim-icet.org)

BLANK PAGE

BIM 148

1<sup>er</sup> septembre 2014

**SPECIAL ISSUE**  
**17th International Symposium on Earth Tides**  
**“Understand the Earth”**  
**15-19 April, 2013**  
**Warsaw, Poland**

MIERCZYK Z.....	
Rector Military University of Technology Welcome Address.....	11907
DUCARME B. ....	
Citation for the Paul Melchior Medal 2013 – Prof. Houtze Hsu.....	11909
BARRIOT J.-P. ....	
Minutes of the Directing Board of ICET meeting.....	11913
PAGIATAKIS S., BOGUSZ J. ....	
Resolutions ETS2013.....	11915
ETS2013 SUMMARY and LIST OF PARTICIPANTS.....	11917
LIST OF PREVIOUS EARTH TIDES MEETINGS.....	11921

**SCIENTIFIC PAPERS**

VIRTANEN H., BILKER-KOIVULA M., MÄKINEN J., NÄRÄNEN J., RAJA-HALLI A., RUOTSALAINEN H. Comparison between measurements with the superconducting gravimeter T020 and the absolute gravimeter FG5-221 at Metsähovi, Finland in 2003-2012.....	11923
CADICHEANU N., VAN RUYMBEKE M., PING ZHU..... On the variability of the coupling between some Earth tides periodicities and earthquake triggering from three important seismic nest regions on Earth.....	11929
PING ZHU, VAN RUYMBEKE M., QUINIF Y., CAMELBEECK TH., MEUS PH. .... Hydrological and tectonic strain forces measured from a karstic cave using extensometers .....	11945
VAN RUYMBEKE M., WIELANT F., NOËL J.-P., DUMONT PH. .... Calibration of pendulum by sinusoidal torque induced with the needles of a watch turning in the gravity field of the Earth.....	11961
VOLKOV V.A., DUBROV M.N. .... Geodynamical observations using spatially distributed gravimeters, tiltmeters, and laser strainmeters...11971	

## ADDITIONAL SCIENTIFIC PAPER

ZHANG MIAOMIAO, XU JIANQIAO, SUN HEPING, SHEN WENBIN, CHEN XIAODONG.....	
Comparison of noise levels of the new <i>i</i> Grav-007 superconducting gravimeter and the SG-065	
superconducting gravimeter in Wuhan (China).....	11987

## **Rector Military University of Technology Welcome Address**

Dear participants of the 17th International Symposium on Earth Tides,

I would like to warmly welcome you to Poland, to the Military University of Technology.

The framework for your discussion will be “Understand the Earth”. Although there are many influential factors, the understanding of the Earth system with its major processes and its trends is one of the requirements for a sustainable development. Earth observations are not only necessary for the scientific understandings, they are fundamental for most societal activities ranging from disaster prevention and mitigation, over the provision of resources such as energy, water and food, the understanding of climate change, the protection of the biosphere, the environment, and human health, to the building and management of a prosperous and sustainable global society. Geodesy is fundamental in meeting this global challenge: geodesy provides the foundation on which all Earth observation systems are built. In this function, geodesy provides comprehensive observations of changes in the Earth’s shape, gravity field and rotation.

From the other side that knowledge can be used as a tool to help oneself lead a better life. Education is crucial to each society’s success and universities have a vital role to play in this regard. Higher education generates, transfers and applies the knowledge required for development to take place. This is very important task in the Information Age with its knowledge-based economy.

The 17th Symposium is held at the Military University of Technology, so please let me briefly introduce the University to you.

I would like to emphasize that since the opening for the civil students, several study programmes have been developed, including geodesy with the issues related to the geodynamics and physical geodesy.

We realise that to take advantage of the full potential of higher education we need critical knowledge partnership for development. This Symposium is a good opportunity to exchange experiences and form long term relationships and collaboration between our various institutions and countries represented here. I want to encourage all participants to make the most of this opportunity.

I wish you a pleasant stay in Warsaw and very fruitful deliberations at the Symposium.

Gen. Prof. Zygmunt Mierczyk  
Rector of the Military University of Technology



Warsaw, April 17, 2013

### **Earth Tides Commission Medal**

Ladies and Gentlemen,  
Dear Colleagues and Friends,

It is for me an honour and a pleasure to introduce Professor Hsu Hou-Tse. He is not only an eminent scientist, member of the prestigious Chinese Academy of Sciences, but also as he likes to say himself an “old friend”. It is always a pleasure indeed to meet him and enjoy his sense of humor. He has the remarkable quality of inducing his audience to be happy in the pursuit of science and glad to be talking about it. In a few words he is able to express clearly the conclusions of a long and sometimes tedious scientific discussion.

Prof. Hsu started his scientific life in physical geodesy under the guidance of Professor Fang Jun in the middle of the 1950's and, for more than 50 years now, he was exploring all the aspects of this rich subject that led him to travel all around the world and tomorrow, at least mentally, to the planet Mars. With more than 200 scientific publications and several books Prof. Hsu is certainly one leading scientist of our tidal community.

Prof Hsu Hou-Tse started international cooperation for Earth Tides studies in continental China as early as 1978, when he took part to the scientific mission that the Chinese Academy of Sciences and the State Seismological Bureau sent to the Royal Observatory of Belgium under the direction of Prof. Fang Jun. Between 1979 and 1982 he was personally involved in the installation of the 8 stations of the Earth tidal profile developed across China by Prof Paul Melchior and his staff. I had personally the privilege to install with him stations not only in Wuhan but also in Canton and in Wulumuchi. This project was only a starting point for his activity in Earth tides research. He purchased modern instrumentation to supersede the old ASKANIA gravimeters available in China at that time, starting with LaCoste & Romberg model G and ET meters. He continued tidal gravity observations in China and he has successfully operated a first Superconducting gravimeter in Wuhan since 1985. This early instrument was renewed and a new permanent station, installed in 1997 for the Global Geodynamics Project, is still in operation.

Under his leadership the Institute of Geodesy and Geophysics of the Chinese Academy of Sciences became a Centre for Earth Tidal Research in China. Prof Hsu sent many young scientists abroad to create a scientific task force able to develop theoretical and experimental research in Earth gravity tides, with applications in oceanic loading, atmospheric pressure, Earth's free oscillations and Free Core Nutation.

As president of the IAG Commission on Earth Tides, he worked for the international organization of the Earth's Tidal research during a period of 8 years. The Global Geodynamics Project was launched in 1997 during his mandate.

Besides his commitment to Earth Tides community as scientist, Director of the Institute of Geodesy and Geophysics of the Chinese Academy of Sciences and former President of the Earth Tides Commission, Prof Hsu was a personal friend of Paul Melchior, who would certainly appreciate that the first medal awarded under his name is granted to Prof. Hsu.

Bernard Ducarme,  
Georges Lemaître Centre for Earth and Climate Research,  
Earth and Life Institute, Catholic University of Louvain.

International Association of Geodesy  
Commission 3 “Earth Rotation and Geodynamics”  
Sub-Commission 3.1 „Earth Tides and Geodynamics”  
awards

**EARTH TIDES  
COMMISSION MEDAL**

to

**Professor Houtze Hsu**

in recognition of his outstanding service and leadership  
in Geodesy and Earth Tides.

This presentation is made the 17th day of April, 2013  
at the

17th International Symposium on Earth Tides in Warsaw, Poland.

Spiros Pagiatakis  
Chair

Janusz Bogusz  
Co-Chair

Earth Tides Commission Medal Diploma



Earth Tides Commission Medal



Warsaw, April 16, 2013

## **Minutes of the Directing Board of International Centre for Earth Tides**

Present at the meeting: Heping Sun (representing Harald Schuh), Spiros Pagiatakis, Jean-Pierre Barriot, David Crossley, Bernard Ducarme and Walter Zuern (invited).

After some discussion, the Directing Board of ICET unanimously agreed on the following points:

1. GGP matters:
  - a. concerning the end-user products of GGP, the exact data flows and data formats must be precisely defined by a group of experts designed by the Directing Board of ICET. A proposal should be submitted to Subcommission 3.1 at the next IAG meeting in Postdam in September 2013.
  - b. a centralized data center seems to be the best way to guarantee a uniform data editing for GGP.
  - c. ICET will continue its support to GGP, until at least the next IUGG meeting, including the timely delivery of one-minute validated data.
  - d. in addition, ICET will provide the end-user a track of all the corrections applied to the raw GGP data, from the beginning of all GGP time series.
2. ICET matters:
  - a. ICET will continue to publish on a yearly basis the BIM, that will be available online on both the GGP and ICET websites. In particular, some of the papers from the 18th Int. Symposium on Earth Tides will be published on the BIM (on a special issue if we have a sufficient number of papers).
  - b. As the spectrum of instruments dedicated to the study of Earth Tides is much larger than the supraconducting gravimeter, it seems better to have two separate services under the umbrella of IGFS. About half of the communications at the 18th Int. Symposium on Earth Tides reporting instrumental results were dedicated to studies outside the scope of GGP.

It is to be noted that many of these points have yet to be discussed and finalized by ICET and GGP. In any case, more detailed proposals from ICET and GGP will be presented at the IAG meeting in Postdam in September 2013. A Directing Board of ICET will take place during this event.

J.-P. Barriot, Director of ICET



## Resolutions – ETS2013

- 1) The participants of the 17<sup>th</sup> International Symposium on Earth Tides taking into consideration
  - a. the Terms of Reference and Objectives of the IAG SC-3.1
  - b. the increased activities in multidisciplinary research in geodynamics, and
  - c. the widening frequency band and extension of spatial scales of the geodynamic phenomena that can be captured by a large variety of sensors and observing systems,

Recommend that

- a. the name of the SC-3.1 be changed to “Geodynamics and Earth Tides” to better reflect the nature of the research activities,
  - b. the name of the “International Symposium on Earth Tides” be changed accordingly to “International Symposium on Geodynamics and Earth Tides”,
  - c. the international symposia under the new name be numbered consecutively from the previous conferences to ensure continuation,
  - d. the above changes be effective after the next IUGG General Assembly in 2015, in compliance with the IAG status and bylaws.
- 2) The participants of the 17<sup>th</sup> International Symposium on Earth Tides recognizing
  - a. the significant and continued contribution of GGP to geodynamics research,
  - b. the increased demand for GGP data and relevant products for multidisciplinary research, engineering and operational applications and experimentation,
  - c. the increased demand for data and relevant products observed by a wide range of sensors including, but not limited to, tilt meters, strain-meters, and spring gravimeters, for multidisciplinary research, engineering and operational applications and experimentation, and
  - d. the need to provide the users with the above data and data products in complete, uniform, authoritative and timely fashion

Recommend that

- a. a new IAG Service be created under the umbrella of IGFS,
  - b. the new service be named “GGP- ICET Service”,
  - c. the new service include two components namely “Global Geodynamics Project - GGP” and “International Centre of Earth Tides - ICET”.

Furthermore, they recommend that

- d. a working group be formed immediately to carry out a thorough analysis of the needs of, and prepare a proposal for the creation of the new service, its terms of reference, goals and objectives and structure,
  - e. ICET continue to operate as usual, provide support to GGP, make available to the end-user a track of all corrections applied to the GGP data, and publish BIM.
- 3) The participants of the 17<sup>th</sup> International Symposium on Earth Tides recognizing the importance of dissemination of the scientific contributions of the symposium recommend that:
  - a. a number of manuscripts be submitted to the Journal of Geodynamics for publication for a future Special Edition (SI). The submissions must be within the scope of Journal of Geodynamics and go through the standard peer-review process. The limit will be set at 25 published papers. The Editor-in-chief will have the final say regarding the acceptance/rejection of manuscripts submitted to Journal of Geodynamics.
  - b. papers with technical and/or instrumentation development and calibration content will be published in BIM.

- 4) The delegates of the 17<sup>th</sup> International Symposium on Earth Tides accept the proposal by Prof. Carla Braitenberg to hold the 18<sup>th</sup> International Symposium on Earth Tides in Trieste, Italy, in 2016.
- 5) The participants of the 17<sup>th</sup> International Symposium on Earth Tides, the IAG Commission 3, the IAG Sub-commission 3.1 and the Global Geodynamics Project thank the Military University of Technology (MUT), and the sponsors of the symposium, namely the International Association of Geodesy, the Rector of MUT and the Committee for Geodesy, Polish Academy of Sciences for hosting and supporting this event. Moreover, the delegates thank the Local Organising Committee (LOC), Janusz Bogusz (Head of LOC), Marcin Gałuszkiewicz, Andrzej Araszkiewicz, Katarzyna Kamińska, Anna Kłos, Lidia Rachoń and Karolina Szafranek for their warm welcome and flawless organisation that made the 17<sup>th</sup> International Symposium on Earth Tides a great scientific success.

Spiros Pagiatakis, Chair of the Sub-Commission 3.1

Janusz Bogusz, Co-Chair of the Sub-Commission 3.1

## ETS2013 Summary

73 participant from 3 different continents, 7 thematic sessions with 55 oral and 32 poster presentations.

### List of participants

<b>No.</b>	<b>First name</b>	<b>Name</b>	<b>e-mail</b>
1	Maiko	Abe	abe@gfz-potsdam.de
2	Andrzej	Araszkiewicz	aaraszkiewicz@wat.edu.pl
3	Jose	Arnosó	arnoso@ucm.es
4	Jean-Pierre	Barriot	jean-pierre.barriot@upf.pf
5	Janusz	Bogusz	jbogusz@wat.edu.pl
6	Jean-Paul	Boy	jeanpaul.boy@unistra.fr
7	Ladislav	Brimich	geofbrim@savba.sk
8	Aleksander	Brzeziński	alek@cbk.waw.pl
9	Marta	Calvo García-Maroto	mcalvo@fomento.es
10	Cedric	Champollion	cedric.champollion@gmail.com
11	Joanne	Chauveau	joanne.chauveau@etu.unistra.fr
12	Xiaodong	Chen	chenxd@whigg.ac.cn
13	Beatriz	Cordoba	b.cordoba@oan.es
14	David	Crossley	crossley@eas.slu.edu
15	Ove Christian	Dahl Omang	ove.christian.dahl.omang@kartverket.no
16	Mstislav	Dubrov	start1mn@mail.ru
17	Bernard	Ducarme	bf.ducarme@gmail.com
18	Christoph	Foerste	foer@gfz-potsdam.de
19	Jeff	Freymueller	liuzw.99@gmail.com
20	Marcin	Galuszkiewicz	mgaluszkiewicz@wat.edu.pl
21	Andreas	Güntner	guentner@gfz-potsdam.de
22	Rüdiger	Haas	rudiger.haas@chalmers.se
23	Basile	Hector	basile.hector@unistra.fr
24	Christine	Heimlich	christine.heimlich@unistra.fr
25	Jacques	Hinderer	jhinderer@unistra.fr
26	H.-T.	Hsu	hsuh@asch.whigg.ac.cn
27	Xiao Gang	Hu	hxg432@whigg.ac.cn
28	Thomas	Jahr	thomas.jahr@uni-jena.de
29	Marek	Kaczorowski	marekk@cbk.waw.pl
30	Jeff	Kennedy	jkennedy@usgs.gov
31	Marta	Kis	kis.marta@mfgi.hu
32	Anna	Klos	aklos@wat.edu.pl
33	Andras	Koppan	koppan.andras@mfgi.hu
34	Wiesław	Kosek	kosek@cbk.waw.pl
35	Hana	Krasna	hana.krasna@tuwien.ac.at
36	Nicolas	Le Moigne	nicolas.lemoigne@gm.univ-montp2.fr
37	Hui	LI	lihuidz@public.wh.hb.cn
38	Shaocong	Luo	luosc@asch.whigg.ac.cn
39	Anthony	Memín	Anthony.Memin@utas.edu.au
40	Gyula	Mentes	mentes@ggki.hu
41	Bruno	Meurers	bruno.meurers@univie.ac.at
42	Vadim	Milyukov	milyukov@sai.msu.ru

43	Jolanta	Nastula	nastula@cbk.waw.pl
44	Tomasz	Olszak	t.olszak@gik.pw.edu.pl
45	Spiros	Pagiatakis	spiros@yorku.ca
46	Vojtech	Palinkas	vojtech.palinkas@pecny.cz
47	Lidia	Rachon	lrachon@wat.edu.pl
48	Arttu	Raja-Halli	arttu.raja-halli@fgi.fi
49	Marcin	Rajner	mrajner@gik.pw.edu.pl
50	Umberto	Riccardi	umbricca@unina.it
51	Bernd	Ritschel	rit@gfz-potsdam.de
52	Yves	Rogister	yves.rogister@unistra.fr
53	Severine	Rosat	Severine.Rosat@unistra.fr
54	Pierre	Rouleau	prouleau@grenfell.mun.ca
55	Hannu	Ruotsalainen	hannu.ruotsalainen@fgi.fi
56	Peter	Schindler	peter.schindler@uni-jena.de
57	Harald	Schuh	schuh@gfz-potsdam.de
58	Holger	Steffen	holger-soren.steffen@lm.se
59	Rebekka	Steffen	rsteffen@ucalgary.ca
60	He-Ping	Sun	heping@asch.whigg.ac.cn
61	Karolina	Szafranek	kszafranek@wat.edu.pl
62	Małgorzata	Świerczyńska	goswierk@gmail.com
63	Milos	Valko	mvalko@kma.zcu.cz
64	Michele	van Ruymbeke	labvrui@oma.be
65	Heikki	Virtanen	heikki.virtanen@fgi.fi
66	Viktor A.	Volkov	vav_volkov@mail.ru
67	Herbert	Wilmes	herbert.wilmes@bkg.bund.de
68	Hartmut	Wziontek	Hartmut.Wziontek@bkg.bund.de
69	Cui	Xiaoming	cxm02010331@163.com
70	Baili	Zhou	Zhoubl@asch.whigg.ac.cn
71	Jiangcun	Zhou	zjc@asch.whigg.ac.cn
72	Ping	Zhu	zhuping@oma.be
73	Walter	Zürn	walter.zuern@partner.kit.edu



ETS2013 Group Photo



### List of Previous Earth Tides Meetings

1	24-26.04.1957	Brussels, Belgium
2	21-26.07.1958	Munich, Germany
3	06-11.07.1959	Trieste, Italy
4	05-10.06.1961	Brussels, Belgium
5	01-06.06.1964	Brussels, Belgium
6	15-20.09.1969	Strasbourg, France
7	10-14.09.1973	Sopron, Hungary
8	19-24.09.1977	Bonn, Germany
9	17-22.08.1981	New York, USA
10	23-27.09.1985	Madrid, Spain
11	31.07-5.08.1989	Helsinki, Finland
12	04-07.08.1993	Beijing, China
13	22-25.07.1997	Brussels, Belgium
14	28.08-1.09.2000	Mizusawa, Japan
15	02-06.08.2004	Ottawa, Canada
16	01-05.09.2008	Jena, Germany
17	15-18.04.2013	Warsaw, Poland



## **Comparison between measurements with the superconducting gravimeter T020 and the absolute gravimeter FG5-221 at Metsähovi, Finland in 2003-2012**

H. Virtanen, M. Bilker-Koivula, J. Mäkinen J. Näränen, A. Raja-Halli, H. Ruotsalainen

Finnish Geodetic Institute

heikki.virtanen@fgi.fi

The superconducting gravimeter (SG) T020 is recording at Metsähovi gravity laboratory since 1994. Regular absolute gravimeter (AG) measurements have taken place between 1988 and 2002 with the JILAg-5 gravimeter and from 2003 onwards with the FG5-221. We have compared results of the SG and the AG between 2003 and 2012.

The SG is a relative instrument, which should regularly be compared with an AG for determination of drift, to connect SG data after longer gaps, and to remove big offsets. Additionally, the scale factor of the SG needs to be determined using simultaneous observations with an AG. Conversely, comparison of SG and AG time series can support AG observations by detecting possible instrument problems in the AG.

For calibration we have used the time series of both instruments without any corrections. For drift comparison we have corrected the time series of both instruments in a similar way for three effects: tides, polar motion and influence of the atmosphere.

When a discrepancy appears between the SG and the AG time series, it may indicate a problem with one of the instruments. For determining which instrument is producing the more plausible result we can compare their data with models of environmental effects in gravity, not included in the above-mentioned three standard corrections. In Metsähovi, the hydrological variation (local-regional-global) is the largest effect. Seasonal variation can be up to 8  $\mu\text{gal}$  peak-to-peak. In addition, loading by the Baltic Sea causes effects up to 3  $\mu\text{gal}$ . The hydrological signal is seen in both the SG and AG data. More generally, most of the variation in AG time series is also seen in the SG data and can therefore be attributed to the same environmental effects.

Finally, correcting the AG record on the basis of models confirmed by the SG can improve the precision of determination of the gravity trend due to postglacial rebound.

### **Introduction**

The superconducting gravimeter (SG) is a relative instrument, and as such should regularly be compared with an absolute gravimeter (AG) for determination of drift, to connect SG data after longer gaps, and to remove big offsets. Additionally, the scale factor of the SG needs to be determined using simultaneous observations with an AG. Conversely, comparison of SG and AG time series can support AG observations by detecting possible instrument problems in the AG. The SG T020 has been recording at Metsähovi (Finland) gravity laboratory since August 1994. Regular AG measurements have taken place between 1988 and 2002 with the JILAg-5 gravimeter and from 2003 onwards with the FG5-221. Determination of the gravity trend due to postglacial rebound has also been carried out.

Here we present results from comparisons of SG data and specific AG measurements campaigns aimed at calibrating the SG.

## SG calibration

The scale factor for SG (T020) was first calibrated using simultaneous observations with the absolute gravimeter JILAg-5 in 1995. From that calibration we adopted the value  $110.7 \pm 0.30$  ( $\mu\text{Gal}/\text{V}$ ). Thereafter calibration has been checked occasionally. Some comparisons with ocean loading models seem to indicate that the value above is too high by 0.3 % (Baker and Bos, 2001; 2003). To obtain a large tidal amplitude, the AG-based calibrations were carried out near new or full moon. Typically, 2400 drops in the absolute gravimeter per day were carried out, the whole calibration lasting 2-7 days (mean 3.5 days).

We have about 130 common datasets at Metsähovi, most of them are short (1 day) and used for checking FG5-221 and for geodynamics studies. We have selected to this study 24 datasets, with durations of 2-7 days. For calibration we have used the time series of both instruments without any corrections. Data of SG was 1-second records in Volts. The data of AG consist of 50 drops in sets of 30 minute intervals. Duration of a set was 500 seconds (50 drops, every 10 second). We have regressed the gravity value (mean time of 50 drops) and SG data of  $\pm 250$  seconds. We have tested several methods for determining the best mean of 500 SG gravity value e.g. mean, median and filtering to 1-minute. Results were practically the same. For AG observations g7 software was used. As weights in regression we have used the drop scatter error ( $g7$ ). There was no significant difference in the results, regardless of either precision or uncertainty errors were applied or not. Used datasets are presented in the **Table 1**. An example of one dataset is shown in the **Fig 1**. Results from the comparisons are presented in **Fig 2**, showing both calibration factor and the linear drift of the SG. The drift of the SG includes also the trend of the Fennoscandian postglacial rebound (2 mm/year). The new calibration factor for SG T020 is  $110.43 \pm 0.12$   $\mu\text{Gal}/\text{V}$ .

**Table 1.** Calibration data sets and results. Numbers 1-20 were measured at pillar AB and numbers 21 – 24 at pillar AC. Total of 4033 sets including 201650 drops. Dur= Duration in days, Amp= max amplitude in  $\mu\text{gals}$ . In calculation a constant value (98191000) were subtracted. Cal=calculated calibration factor and standard error of result. Nset=number of dropping sets used.

Number	Date	Dur	Ampl	Constant	Cal	Err	Nset	
1	2003 11 15 22	4	2	140	6698.518	-109.891	0.601	96
2	2003 11 25 13	19	2	208	6697.768	-110.963	0.471	70
3	2004 10 7 21	1	2	116	6697.788	-109.045	0.980	77
4	2004 11 2 22	39	2	141	6697.543	-111.703	0.712	94
5	2004 12 16 18	39	2	159	6701.405	-111.888	0.950	89
6	2005 1 8 4	2	5	<b>231</b>	6697.780	-109.918	0.387	232
7	2005 1 12 16	2	4	213	6697.874	-110.801	0.512	185
8	2005 1 23 16	24	4	170	6696.671	-109.852	0.428	201
9	2005 8 5 4	39	2	137	6699.339	-109.093	0.792	63
10	2006 6 6 7	29	2	92	6699.465	-109.487	1.121	89
11	2006 6 14 7	9	4	202	6699.657	-110.388	0.334	183
12	2006 7 12 8	36	3	201	6688.106	-110.060	0.357	164
13	2007 12 25 2	56	3	220	6695.660	-110.570	0.595	124
14	2008 1 23 17	57	6	202	6697.636	-109.736	0.446	248
15	2008 6 18 2	49	3	167	6687.720	-110.544	0.298	142
16	2008 11 15 0	34	5	212	6672.160	-110.818	0.286	235
17	2008 12 14 3	6	5	225	6675.679	-110.898	0.266	237
18	2010 12 6 3	2	7	187	6673.467	-110.191	0.265	331
19	2012 6 3 19	39	7	198	6672.307	-110.376	0.221	316
20	2012 8 18 20	9	<b>7</b>	143	6671.595	-110.500	0.170	265
21	2004 4 10 13	54	2	162	6709.243	-110.561	0.642	96
22	2004 5 4 21	24	2	177	6707.056	-110.037	0.485	96
23	2004 8 21 14	44	2	106	6699.916	-111.439	1.004	96
24	2005 6 7 17	41	3	176	6700.378	-111.025	0.378	126

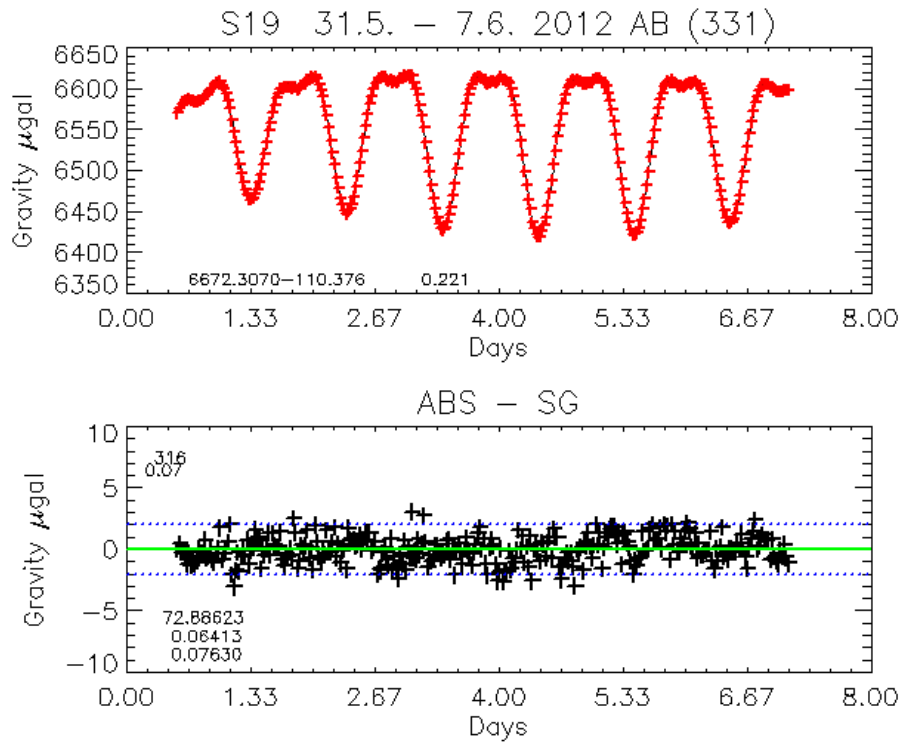


Fig 1: Data set number 19, Top: SG solid black line, AG marked with red cross. Bottom scattering of AG measurements after regression, dotted lines shows limits of  $2\mu\text{gals}$ .

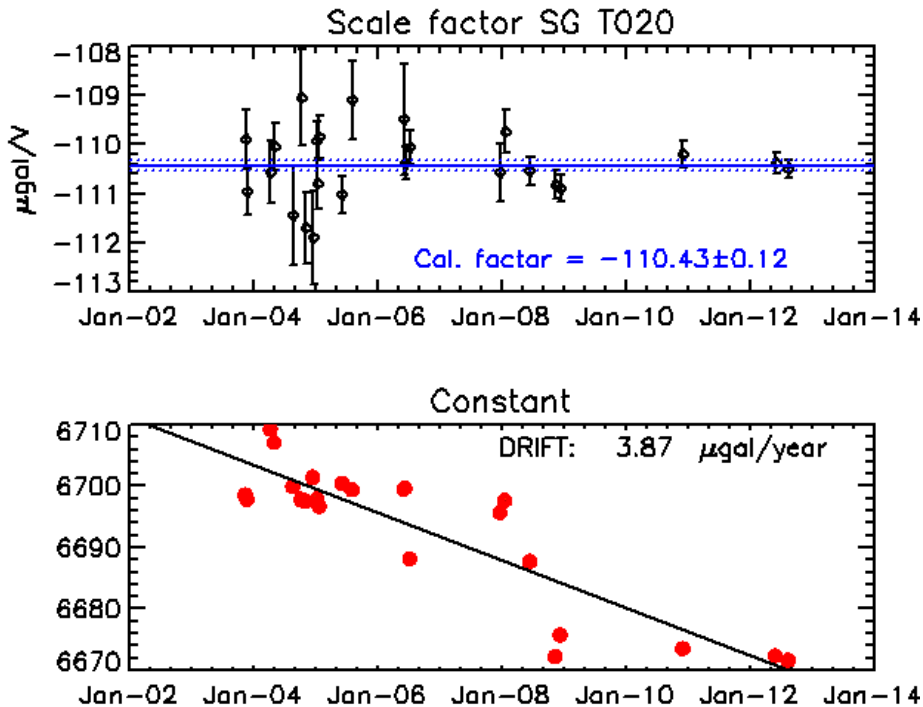


Fig 2. Top: Calculated scale factors and errors for 24 datasets. The new calibration factor is weighted mean of all datasets and shown with blue line. Bottom: Linear drift calculated from constant value of regressions.

## Comparisons of long period time series

We have used hourly SG data from November 2003 to September 2012 and 165 datasets of AG (pillar AB 110 and pillar AC 55). A constant value of 981916515 was subtracted from AG observations. Some offsets in SG due to long-term disturbances have been corrected with the help of the AG data. In addition a preliminary drift rate has been estimated from AG. For comparison we have corrected the time series of both instruments in a similar way for three effects: tides, polar motion and influence of the atmosphere. When a discrepancy appears between the SG and the AG time series, it may indicate a problem with one of the instruments. For determining which instrument is producing the more plausible result we can compare their data with models of environmental effects in gravity, not included in the above-mentioned three standard corrections. At Metsähovi, the hydrological variation (local-regional-global) is the largest gravimetric effect. Seasonal variation can be up to 8  $\mu\text{gal}$  peak-to-peak. In addition, loading by the Baltic Sea causes the effects up to 3  $\mu\text{gal}$ . The hydrological signal is seen in both the SG and AG data. More generally, most of the variation in the AG time series is also seen in the SG data and can therefore be attributed to the same environmental effects. Correcting the AG record on the basis of models confirmed by the SG can improve the precision of determination of the gravity trend due to postglacial rebound.

In **Fig. 3** we have presented AG and SG measurements with a trend and without it. Trends were removed with linear regressions. We have used pillar AB for trend determination.

In **Fig. 4** we show the observed gravity with SG, together with gravity effects due to hydrology and the Baltic Sea. We present the gravity effect of the global hydrological model GLDAS including 4 soilmoisture layers and snow. Green's function formalism was applied for the calculations. Gravity effects for local groundwater (GW) (Virtanen 2006), WSFS (Watershed Simulation and Forecast System by Finnish Environmental Institute, Vehviläinen 2002) and the Baltic Sea (HSL) were calculated by regressions (Virtanen 2004). We have used tide gauge record in Helsinki 30 km away. The Metsähovi station is 10 km from the nearest bay of the Baltic Sea and 15 km from the open sea. Then we have applied different corrections for AG data, subtracting these gravity effects. We have used the mean value from these correcting time-series, using the same time intervals as used in datasets of AG. Results are given in **Table 2**.

**Table 2.** Trend determination with different correction methods for AG

<b>Treatment</b>	<b>Trend (<math>\mu\text{gal}/\text{year}</math>)</b>	<b>Error</b>
None	-0.49	0.08
SG	-0.47	0.08
GLDAS	-0.39	0.07
WSFS	-0.47	0.08
HSL	-0.43	0.09
GW	-0.41	0.08

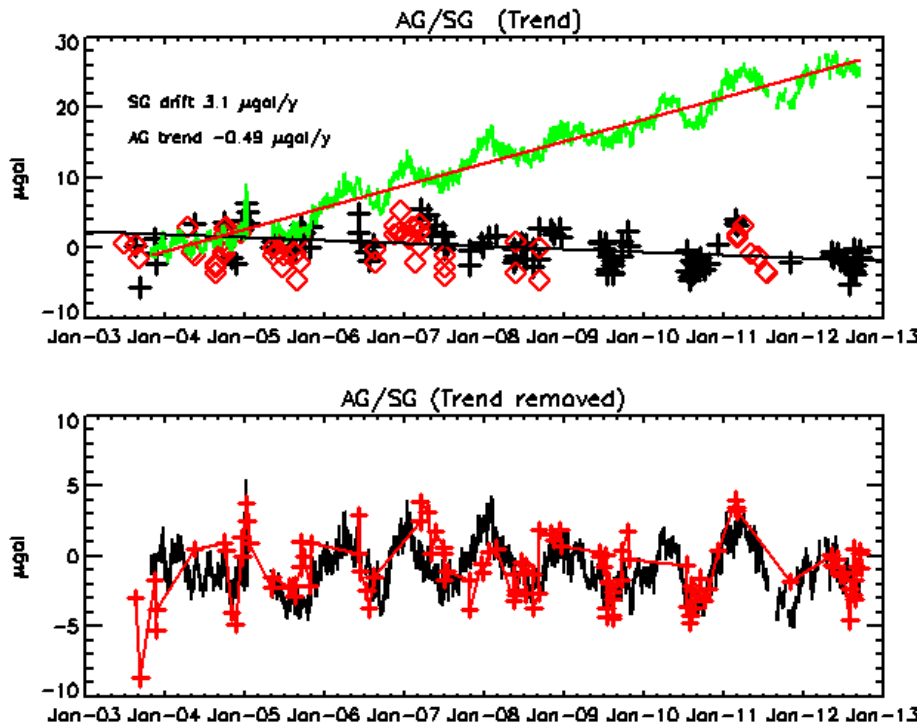


**Fig 3.** Top: Green curve shows SG gravity. The fitted drift is shown with red line, AG measurements are with black cross (AB) and with red diamond (AC). Bottom linear drift/trend removed: Black curve shows SG data and AG is marked with red cross and solid line.

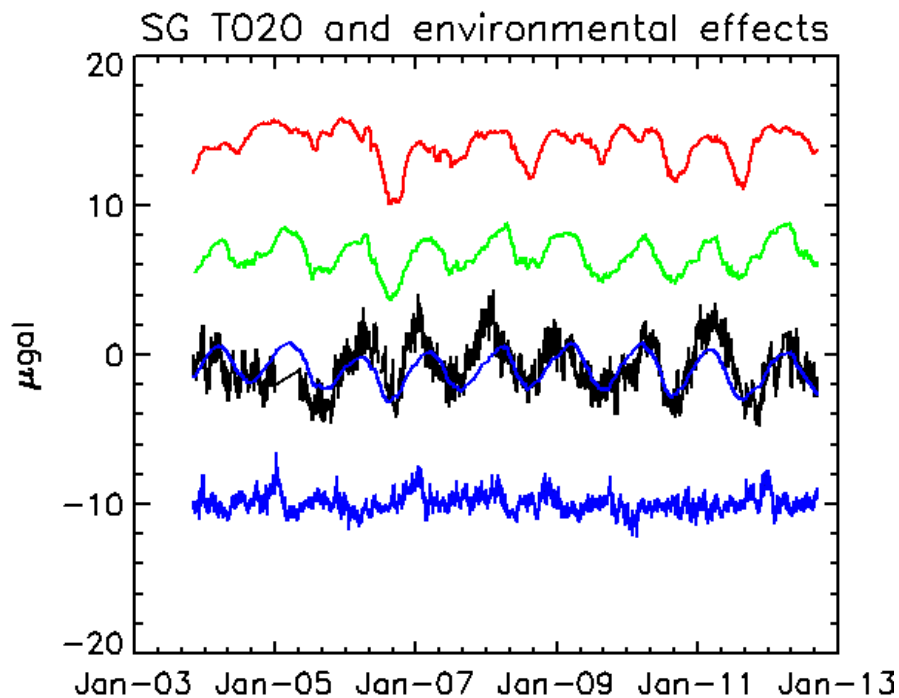


**Fig 4.** From top: Gravity effects of local groundwater (red), WSFS (green), GLDAS blue, for comparisons SG (black) and HSL (blue).

## Conclusions

A new calibration factor has been determined for SG T020 with AG FG5-221 (**110.43±0.12  $\mu\text{Gal/V}$** ). This result is 0.3% smaller than the factor used at present. The results agree with earlier studies (Baker and Bos 2001, 2003). The observed instrumental drift of SG seems to be 3.6  $\mu\text{gal/y}$  (3.1±0.5). Postglacial rebound is at Metsähovi about 2 mm/yr and the expected gravity change due to it about 0.7  $\mu\text{Gals/y}$ . Earlier studies have given as the trend about 0.5  $\mu\text{gals/y}$  at Metsähovi (Bilker-Koivula 2008). In this study, AG corrected using SG gives compatible results. It seems that hydrological corrections have small effect on the trend determinations, due to long timeseries (9 years with FG5). Two instruments are necessary to ensure that the AG measurements are referencing the mean station gravity and not short-term gravity perturbations due to, for example hydrology and meteorology. Hydrological variations from local to global are the largest unmodeled effect on AG measurements. SG can provide correction parameters due to environmental effects for AG and AG can give drift control for SG. SGs and AGs are thus very complementary instruments (Crossley et al 2009). They serve to check each other by independent measurements. We have in this study used rather simple methods, more advanced methods have also been presented (Wziontek et al 2006).

## References:

- Baker, T. and Bos M (2001) Tidal Gravity Observations and Ocean Tide Models, *J. Geod. Soc. Japan* 47(1), 76-81
- Baker, T. and Bos M (2003) Validating Earth and ocean tide models using tidal gravity measurements. *Geophys. J. Int.*, 152, 468-485
- Bilker-Koivula, M., J. Mäkinen, L. Timmen, O. Gitlein, F. Klopping, R. Falk (2008): 'Repeated Absolute Gravity Measurements in Finland.' In Peshekhonov (Ed.): *International Symposium Terrestrial Gravimetry: Static and Mobile Measurements – Proceedings, 20.-23.8.2007*, St. Petersburg, Russia, State Research Center of Russia Elektropribor, 2008. pp. 147-15
- Crossley, D., Hinderer, J., 2009. The Contribution of GGP Superconducting Gravimeters to GGCOS. M.G. Sideris (ed.), *Observing our Changing Earth*, International Association of Geodesy Symposia 133, Springer-Verlag Berlin, pp 841-852.
- Vehviläinen B (2007) Hydrological Forecasting and Real-Time Monitoring: The Watershed Simulation and Forecasting System (WSFS) DOI: 10.1002/9780470511121.ch2
- Virtanen H (2004): Loading effects in Metsähovi from the atmosphere and the Baltic Sea. *J Geodynamics* 38: 407–422
- Virtanen H et al (2006) Comparison of superconducting gravimeter observations with hydrological models of various spatial extents, *Bull Inf Marées Terrestres* 142: 11361–11368
- Wziontek, H., R. Falk, H. Wilmes, P. Wolf, 2006, Rigorous combination of superconducting and absolute gravity measurements with respect to instrumental properties, *Bull. d'Inf. Marees Terr.* 142, 11417–11422.

# On the variability of the coupling between some earth tides periodicities and earthquake triggering from three important seismic nest regions on Earth

Nicoleta Cadicheanu<sup>a,\*</sup>, Michel van Ruymbeke<sup>b</sup> & Ping Zhu<sup>b</sup>

<sup>a</sup> Institute of Geodynamics of the Romanian Academy, 19-21, Jean-Louis Calderon St., Bucharest-37, 020032, Romania

<sup>b</sup> Royal Observatory of Belgium, ORB-avenue circulaire 3, 1180, Bruxelles, Belgium

## ABSTRACT

Currently, many studies confirm the involvement of Earth tides in the earthquake triggering at the regional level. On a global scale, however, this has not been found. Statistical approach plays an important role in the methodology of the correlation analyses. With the help of such method based on histogram cumulating, a specific technique for assessing the statistical parameter  $p$  of correlation between some earth tides periodicities and earthquakes was established.

The data base includes temporal series of intermediate-depth seismic events that took place from 1980 to 2012, corresponding to three seismic nest regions characterized by strong heterogeneities: Vrancea (Romania), Bucaramanga (Colombia) and Hindu Kush (Afghanistan).

Special attention is given to result validation of the correlation statistical parameter  $p$ , calculated in the temporal sliding windows and spatial sliding windows (statistical tidal tomography) by means of random synthetically time series.

**Keywords:** Earth tides,  $p$  correlation parameter, HiCum, tomography, seismic nest, random time series.

## 1. Introduction

In a seismic zone, geology and tectonics have a leading role in the energy accumulation process. Moon and Sun tidal attractions induce elastic deformations of the solid Earth corresponding to a stress variation usually with two orders larger than tectonic stress variation (Stavinschi and Souchay, 2003; Tanaka et al., 2006). But Earth tides stress modulation is energetically a non-cumulative process while the variation in tectonic stress leads to accumulation of such energy after a long time. Earth tides could influence also physical parameters related to important geophysical phenomena like atmospheric circulation, fluid flow (water, lava, etc.), thermo-mechanical or tectonic processes involved in crustal and sub-crustal stress accumulation.

This means that Earth tides could be a good candidate to influence the earthquakes triggering. But this fact has not yet been clearly demonstrated on a global scale even though the concept of tidal triggering is more than 110 years old (Ping Zhu, 2010; Emter, 1997; Schuster, 1897). But currently, many studies confirm the involvement of Earth tides in the earthquake triggering at the regional level (Cochran et al., 2004; Tanaka et al., 2002; Kasahara, 2002;

Tolstoy et al., 2002; Wilcock, 2001; Tsuruoka et al., 1995; Zugravescu et al., 1989; Souriau et al., 1982; van Ruymbeke et al., 1981; Heaton, 1975). The gravitational attraction of the Moon and Sun is the principal external force that modulates at the depth the intermediate (60 km to 300 km) and deep earthquakes (focal depth > 300 km) (Cadicheanu, 2008; Ismail-Zadeh, 2005). It could affect the dynamic of the Earth with periodicities in mainly diurnal and semi-diurnal band (Melchior, 1978).

The influences of the tidal semidiurnal waves on the intermediate depth seismic activity in Vrancea (Romania) were found previously (Cadicheanu et al., 2007). The analysis was extended to two other long time series of intermediate-depth earthquakes (Fig.1) in Vrancea (Romania), Bucaramanga (Columbia) and Hindu Kush (Afghanistan) nest seismic zones (Cadicheanu et al., 2008a).

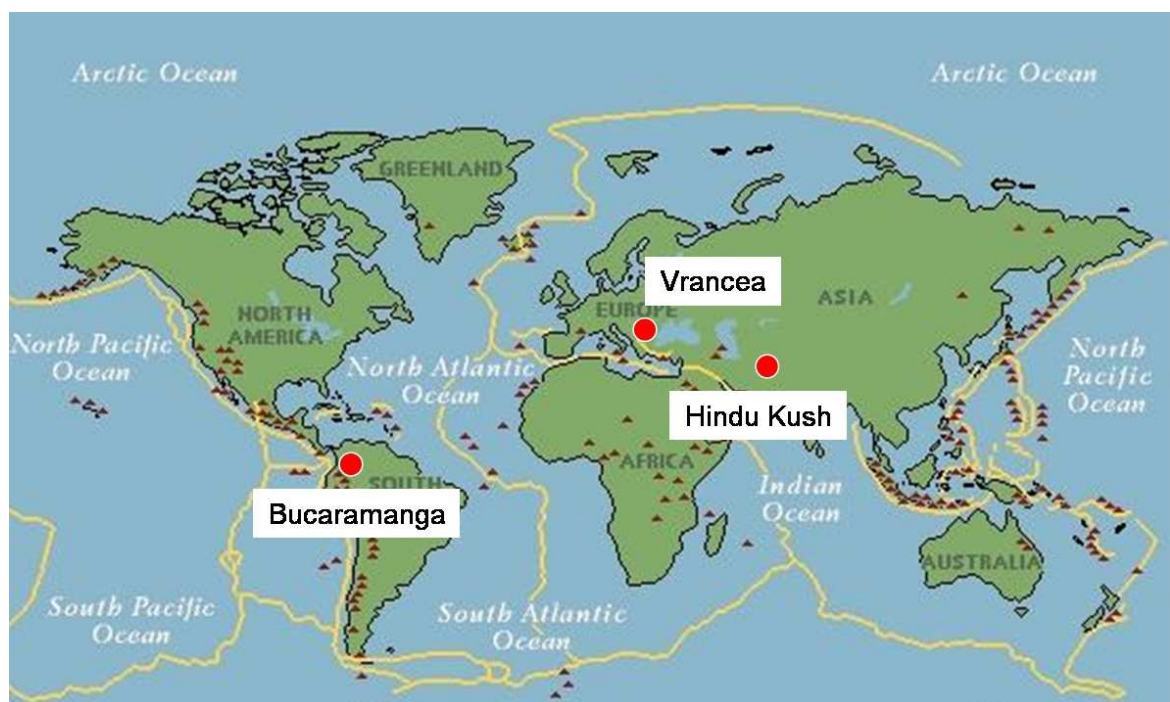


**Fig.1.** Geographical positioning of three seismic zones: Vrancea, Bucaramanga and Hindu Kush

## 2. Data

The input data for our study were obtained from RomPlus catalogue of seismic events occurred between 1980 and 2012 for Vrancea seismic zone (3604 intermediate events with  $M_w \geq 2.9$ ), from IRIS catalogue for Bucaramanga seismic zone (3219 intermediate events with  $M_w \geq 3.0$ ) and for Hindu Kush seismic zone (4662 intermediate events with  $M_w \geq 3.6$ ). All the depth intermediate earthquakes were taken in account, main shocks and aftershocks also.

The nest intermediate-depth seismic activity represents the common feature of the three analyzed seismic zones (Zarifi and Havskov, 2003), tectonically very different.

These seismic zones are localized in the North hemisphere of the Earth and the catalogues cover the following geographical rectangles:

- 1) Vrancea (Romania):  $45.0^\circ - 46.0^\circ\text{N}$ ,  $26.0^\circ - 27.0^\circ\text{E}$ ,
- 2) Bucaramanga (Colombia):  $5.0^\circ - 9.5^\circ\text{N}$ ,  $72.5^\circ - 74.5^\circ\text{W}$  and
- 3) Hindu Kush (Afghanistan):  $35.0^\circ\text{N} - 38.0^\circ\text{N}$ ,  $68.0^\circ\text{E} - 72.0^\circ\text{E}$ .

### 3. Method

#### 3.1. HiCum method and statistical tests of validation

In order to investigate the correlation between Earth tide  $M2$  component and seismic activity in the three seismic regions we have chosen the histogram cumulating method (HiCum) applied on the events distributions (van Ruymbeke et al., 2003). This method is very efficient for the stable phenomena like Earth tides that represent an astronomical clock. The HiCum algorithm is capable to evaluate very precisely the amplitude of a periodical component included in a repetitive process. In the case of a random distribution of events such as a time series of earthquakes, we search for a specified periodicity  $M2$  in the seismic activity. Each event  $E_i$  occurred at time  $t_i$  is characterized by a phase  $\alpha_i$  defined in the interval  $360^\circ$ , corresponding to the phase of a selected harmonic signal (Fig.2).

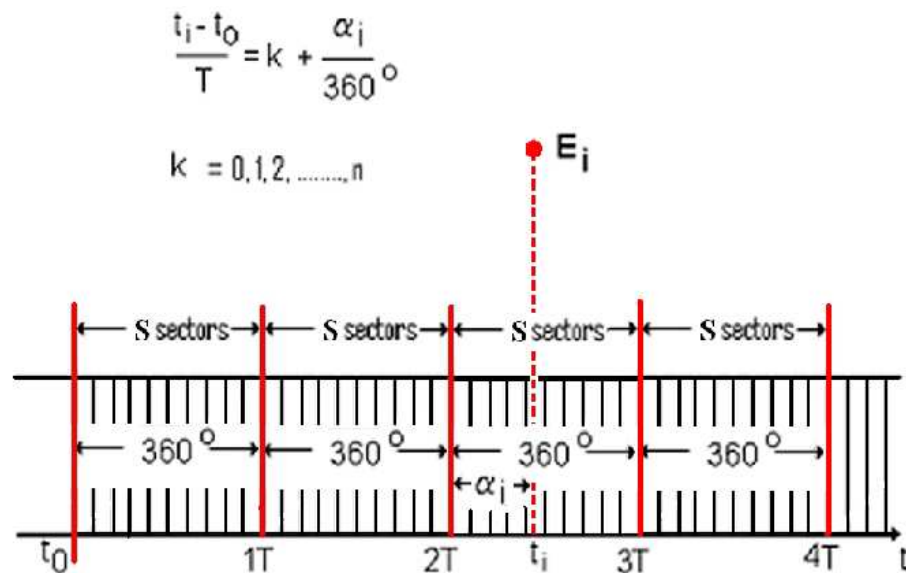


**Fig. 2.** Time series partition into selected time period  $T$ . An event  $E_i$  occurring at time  $t_i$  is defined by an angle  $\alpha_i$

The stacking analysis method HiCum consists in adjusting a cosine function to the histogram of the  $\alpha_i$  (Fig.3.).

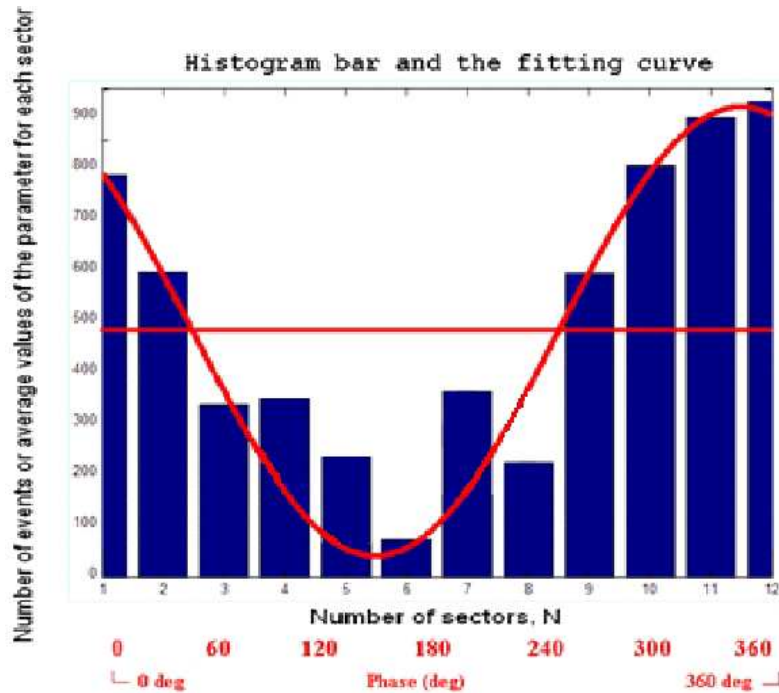


Fig. 3. The fitting curve of the HICUM stacking by a cosinusoidal function.

The amplitude and phase of this cosine show the relation, in terms of modulation, between the stacked events and the semidiurnal tidal component. The stacking function could be applied in sliding windows in the time domain, respectively in the space domain.

Shuster test is usually applied to analyze the correlation between earthquakes occurrences and a selected earth tide component by the coefficient  $p$ . It is evaluated for a specified significance level that characterizes the null hypothesis rejection (Schuster, 1897).

$$Ps = \exp(-D^2/N) \quad (1)$$

where  $N$  is the number of earthquakes and  $D$  represents the length of the vectorial sum of all unit length vectors defined by their angle phase.

But we concluded that Schuster test must be supplemented by another test capable to detect the staining of a random distribution aspect using, if is possible, a different mathematical approach. Permutation test (Pitman, 1938) was our second choice because it does not use any a priori assumption.

$$\text{for } A_j > A_0 \text{ (j=0,1,2,\dots,m); } p_p = m/n \quad (2)$$

where  $A_j$  represents the amplitude of the sinusoids obtained for every permutation in the HiCum initial distribution ( $A_0$  is the amplitude of the initial seismic event distribution),  $n$  is the number of permutation,  $m \leq n$ .

Thus, the parameter  $p$  used to validate the correlation was statistically defined by means of two independent statistical tests.

Our next approach investigated and validated the sensibility of a statistical parameter  $p$  to transient features around strong seismic events for  $M2$  component (Cadicheanu, 2008).

### 3.2 Temporal and 3D sliding windows

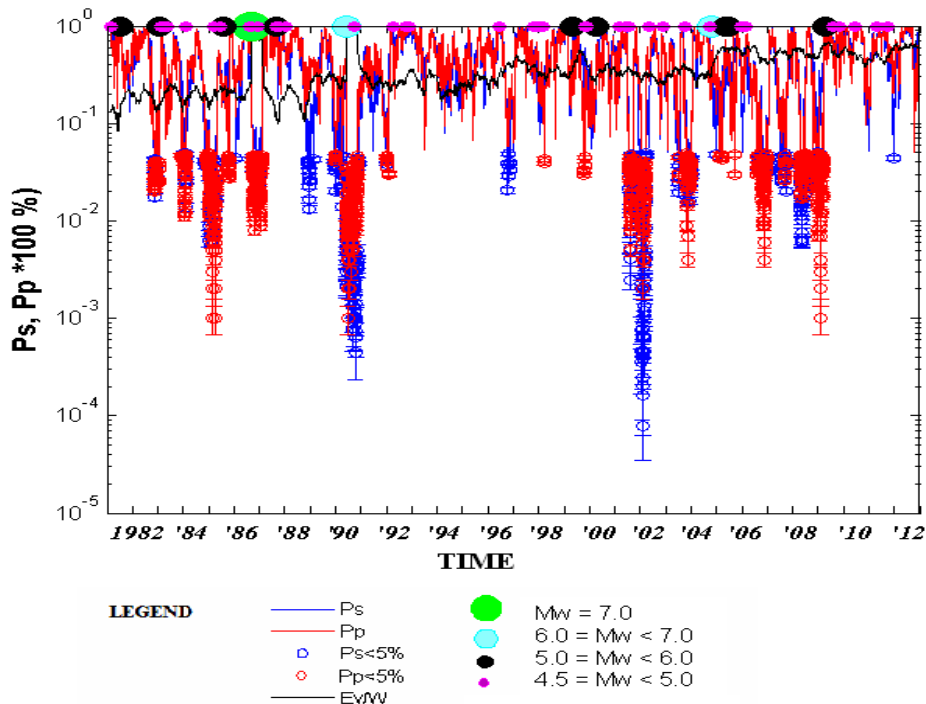
We introduce the temporal variability of the two statistical coefficients  $p$  applied on two kinds of temporal sliding windows defined respectively with constant time intervals shifted by a fixed number of  $M2$  Earth tide period, and windows containing constant number of events,  $N_{fix}$  and shifted also by constant number of events. This number  $N_{fix}$  is obtained by an algorithm based on empirical Sturges (1926) formula (3).

$$K=(N_{max} - N_{min})/(1+3.22 *lg N_{tot}) \quad (3)$$

where  $K$  is the constant number of bin which characterizes the cumulative histogram resulted by stacking analysis ,  $N_{max}$  and  $N_{min}$  are the maximum, respectively minimum number of events obtained by counting events in each window shifted by a fixed number of  $M2$  Earth tide period , and  $N_{tot}$  represents the total number of events. The average amplitude of all adjusting cosine functions applied to the cumulative histograms represents  $N_{fix}$ .

The  $p$ -values are plotted at the end of each window. For example, we choose the time series of intermediate-depth earthquakes that occurred in Vrancea seismic zone from 1980 to 2012 (3604 intermediate events with  $M_w \geq 2.9$ ). (Fig. 4). We fund, for a fixed time interval of 170 days shifted by two  $M2$  intervals (about one day),  $N_{max}= 150$  events,  $N_{min}=1$  event and  $K=12$ . The average amplitude for all adjusting cosine functions applied to the cumulative histograms of each sliding window gives the constant number of events  $N_{fix}=50$  events.

In both cases the variation of  $p$ -values has the same behavior. This can be considered a good result concerning the choice of the method.



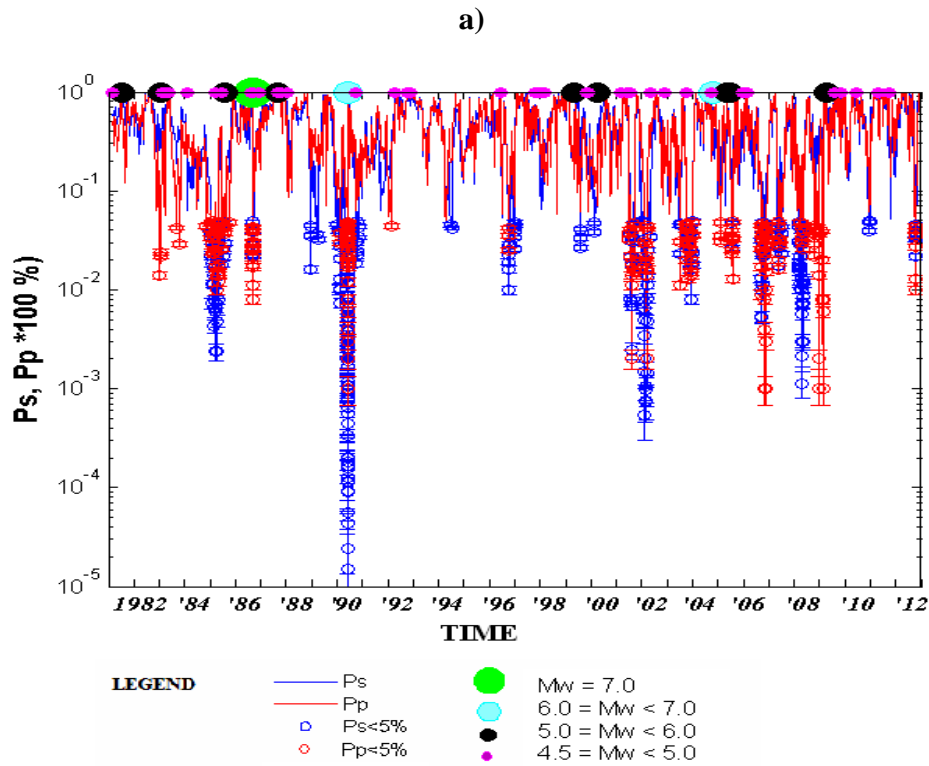


**Fig. 4.** Vrancea seismic zone exemple. Statistical coefficient  $p$  values for Schuster's test,  $p_S$ , (in blue) and permutation test,  $p_p$ , (in red), marked with circles for  $p < 5\%$ . The magenta circles are for earthquakes with  $4.5 \leq M_w < 5.0$ . Earthquakes with magnitude  $5.0 \leq M_w < 6.0$  are represented by black circles, with magnitude  $6.0 \leq M_w < 7.0$  are represented by cyan circles and the green circle is for earthquakes with  $M_w \geq 7.0$ . The upper graph (a) shows results for the sliding windows defined by the fixed time interval 170 days shifted by two  $M2$  intervals (about one day). The black curve represents the variation of the number of events in each window,  $E_v/W$ . The lower graph (b) corresponds to sliding windows with fixed number of events ( $N_{fix} = 50$  seismic events) shifted with one event. In this case, black curve is not represented because  $E_v/W = const = N_{fix}$ , for every sliding windows we have the same number of events  $N_{fix}$

In addition to the temporal sliding windows, we investigate the mentioned coupling between  $M2$  and intermediate-depth seismic activity using the new concept of “3-D statistical tidal tomography” (Cadicheanu et al., 2008). In this case, the  $p$ -coefficients are calculated for events located within box volumes (Fig.5) shifted in horizontal, respectively vertically plans. From statistical reasons only the series equal or larger than 25 events are considered. The dimension of the box is function of the average density of the seismic events in the considered area, the reported localization errors of the earthquake hypocenters and the minimum number of events required for statistical reason.

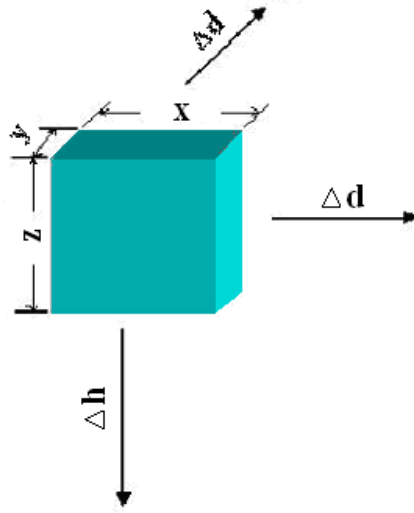
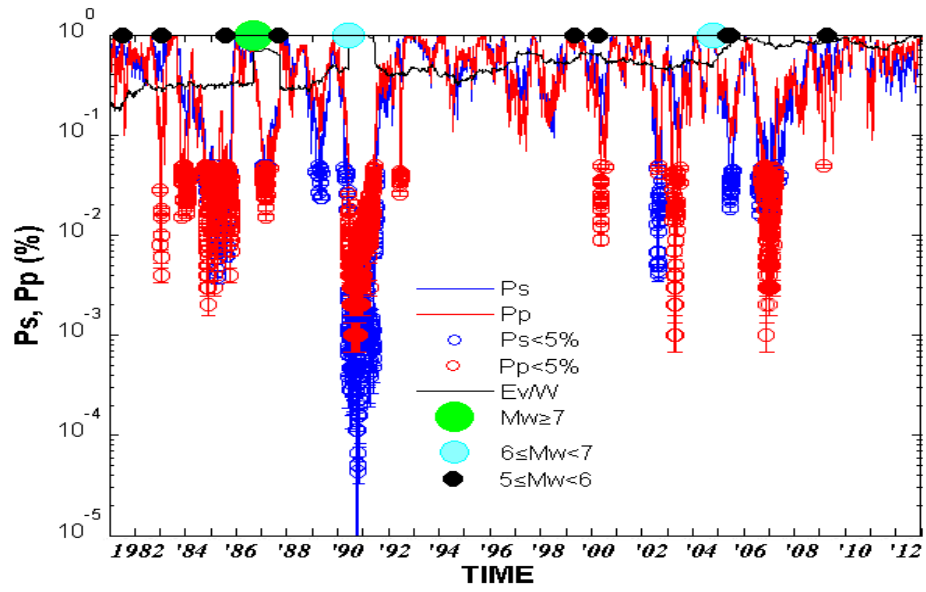


**Fig. 5.** The “statistical tidal tomography” map of  $p$  statistical coefficients is obtained when stacking function is applied to 3-D geometry following the earthquake distribution. The calculations are carried out for spatial box volume windows covering the entire hypocenter zone area. The horizontally and respectively vertically sliding steps are in according to the reported localization errors of the earthquake hypocenters.

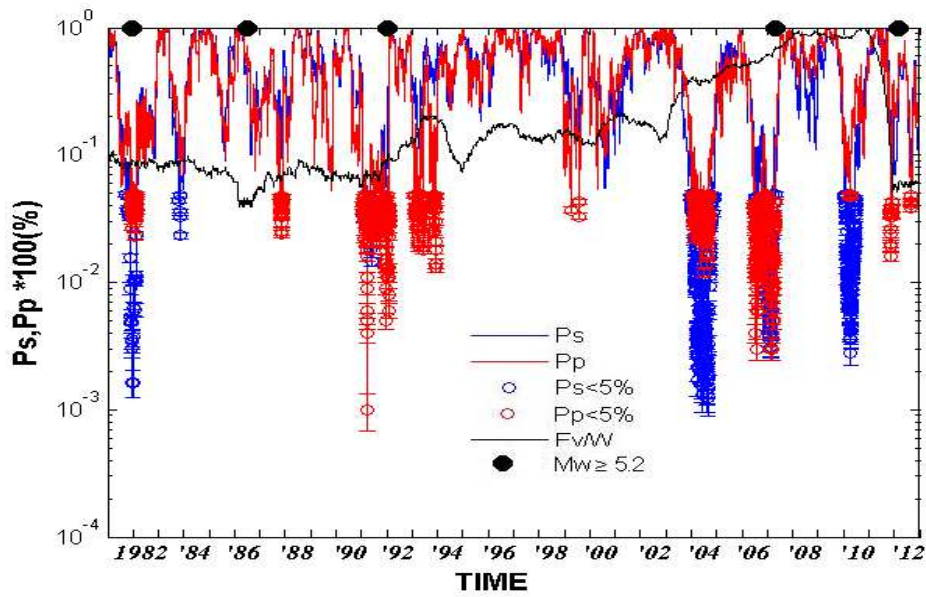
#### 4. RESULTS AND DISCUSSION

Statistical  $p$  –values are calculated for each sliding window of a year shifted by two  $M2$  periods. A systematic temporal pattern of the  $p$ -values preceding or following the meaningful earthquakes was observed for the analyzed seismic zones (Fig.6). It is represented by a number of temporal windows, in which  $p$  –values are less than the 5% or express a frequent descending tendency toward smaller values of  $p$ . This behavior is observed from a few weeks in some cases, to a few years in other, before an important event or immediately after its occurrence.

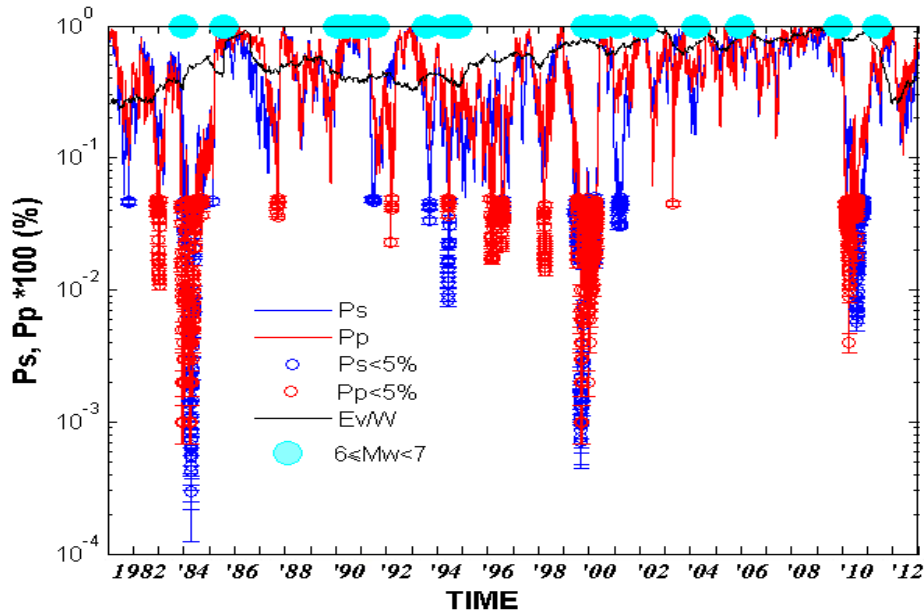
Therefore, we identify this feature for Vrancea (Romania) before the 1986, 1990 and 2004 large earthquakes ( $M_w \geq 6.0$ ) and for the most part of earthquakes with  $M_w \geq 5.0$  (Fig.6a). In Bucaramanga (Columbia) seismic region we observe this aspect before the 1981, 1992, 1992, 2007 and 2012 earthquakes (Fig.6b), but here the intervals between two successive large earthquakes are very short comparing with Vrancea seismic zone. It means that the periods of energy recharge and release are not adequate for an earth tide triggering. The gravitational stress variation is not efficient in such a case where the main source of stress variations is each large event. We encounter a similar situation in Hindu Kush (Afghanistan) seismic region where the earthquakes with  $M_w \geq 6.0$  are also frequent (Fig.6c).”



(a)



(b)



(c)

**Fig.6.** Statistical  $p$  value variations for the intermediate-depth seismic zones Vrancea (a), Bucaramanga (b) and Hindu Kush (c). Statistical coefficient  $p$  values for Schuster's test (in blue) and permutation test (in red) are marked with circles for  $p < 5\%$ .

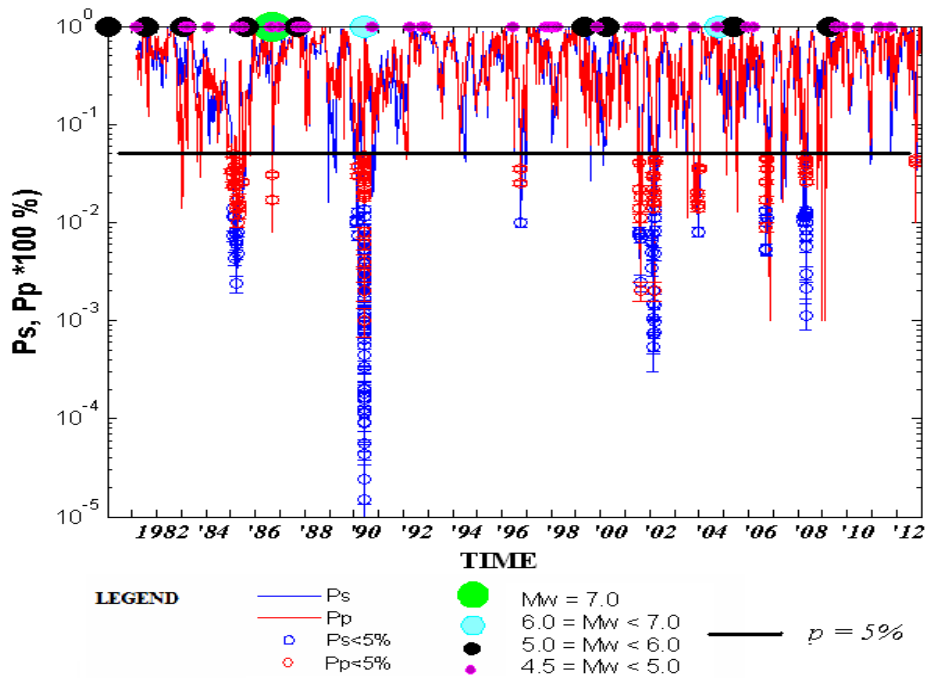
An important step of our approach was the result validation of the correlation statistical parameter  $p$  by means of random synthetically time series.

We have constructed hundred random synthetically time series of seismic events for each seismic zone taking in account the real intervals between two successive events from the observation series of earthquakes. We applied a randomization algorithm by permutation of these intervals and each time we calculated the correlation parameter  $p$  in the same way as for real data.

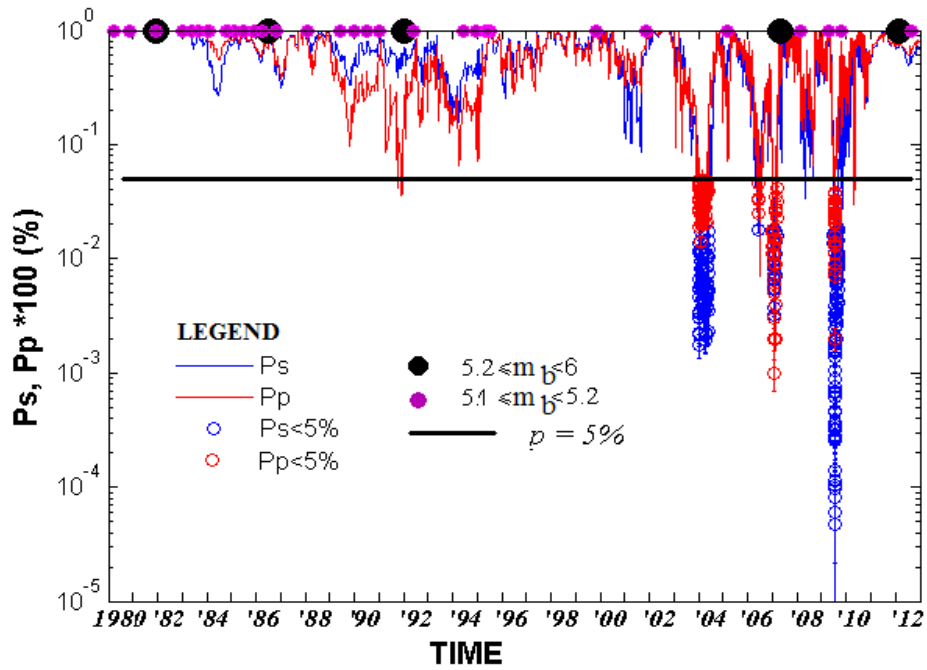
We calculated the average and the dispersion  $\sigma$  for the amplitude  $A$  of the fitting sinusoidal function in the all windows in which  $p < 5\%$  for random synthetically data. We considered the presence of correlation between seismic activity and earth tide component  $M2$  only in all the windows in which the following relation is true:

$$A_{W_{eq}}(p < 5\%) > \max(A_{\text{mean\_syn\_eq}}(p < 5\%) + \sigma) \quad (3)$$

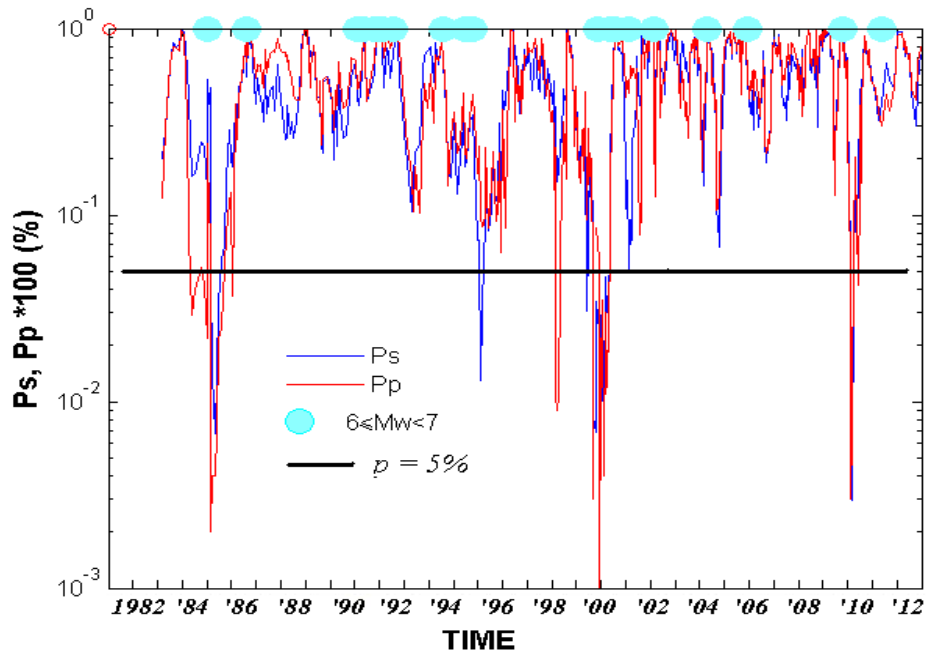
where, for a specified seismic area,  $A_{W_{eq}}$  is the amplitude of the fitting sinusoidal curve calculated for each real data window with  $p < 5\%$ ,  $A_{\text{mean\_syn\_eq}}$  represents the average amplitude of all fitting sinusoidal curve amplitudes of the windows with  $p < 5\%$  for each random synthetically series and  $\sigma$  the corresponding dispersion. We established the largest  $A_{\text{mean\_syn\_eq}}$  value of the one hundred as the lower limit for validate the presence of correlation between  $M2$  earth tide component and seismic activity in the case of the time windows where  $p < 5\%$  (Fig.7).



(a)



(b)



(c)

**Fig. 7.** Validation of the correlation time windows between M2 earth tide component and seismic activity for Vrancea (a), Bucaramanga (b) and Hindu Kush (c) intermediate-depth seismic zones. Validated statistical coefficient  $p < 5\%$  values for Schuster's test  $p_S$  and permutation test  $p_P$  are marked with blue, respectively red circles. The black line delineates  $p \leq 5\%$  zone of the  $p > 5\%$  zone. The  $p$  values of the figure 7a (Vrancea) correspond to sliding windows with fixed number of 50 seismic events shifted with one event, the  $p$  values of the figure 7b (Bucaramanga) correspond to sliding windows with fixed number of 125 seismic events shifted with one event while the  $p$  values of the figure 7c (Hindu Kush) correspond to sliding windows with fixed number of 150 seismic events shifted with 10 events.

We observe a good percentage of validation for Vrancea seismic region, fewer in Bucaramanga and not any window of correlation validated for Hindu Kush seismic region. We assume that gravitational processes are not the only dominating phenomenon neither in time nor in space. Other complex processes such as thermal or electromagnetic could play an important role in the triggering of earthquakes.

There are significant tectonical differences between the three seismic zones. Bucaramanga is characterized by a double process of oceanic subduction (Pulido, 2003). As regards Hindu Kush seismicity, it is affected by a dynamical process of continental subduction (Replumaz et al., 2013; Pegler and Das, 1998).

From this point of view, the Vrancea seismic region seems to be a good choice for the study of correlation between Earth tides and earthquakes. For this reason we have considered important to extend our temporal and spatial analysis in particular for this seismic area.

An attempt to analyze the  $p$ -value variations for Vrancea, 1934 -2007 in sliding windows of 365 days shifted by 50 days was also performed (Fig.8).

By applying the FFT to the 5th-order polynomial least squares fit of  $p$ -values, we obtain a quasi-long period of 17 years of correlation between earthquake occurrences and M2 tidal waves.

This period is in good agreement with the behavior of other characteristics of the seismic activity retrieved by Enescu et al.(1999): the same periodicity was observed concerning the magnitude limit values and fault plane solutions alternation. Intervals where the NE–SW orientation of the fault planes is dominant, maximum magnitudes are  $M_{w_{max}} > 6.7$ , while in intervals dominated by the NW–SE orientation of the fault planes, maximum magnitudes are  $M_{w_{max}} \leq 6.7$  (Fig.8).

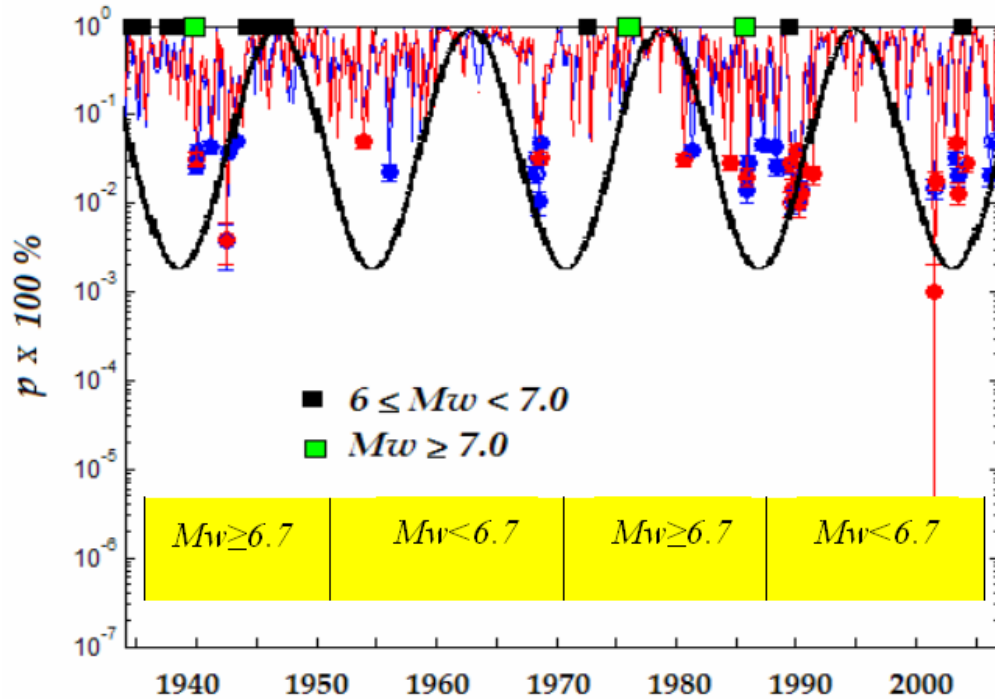


**Fig. 8.**  $p_s$  (blue line and circles) and  $p_p$  (red line and circles) -values variations for Vrancea seismic zone, 1934 - 2007 interval, in sliding windows of 365 days shifted by 50 days . A quasi-long period of 17 years in the variation of the  $p$ - value is pointed out. The same periodicity was observed by Enescu et al. (1999) concerning the magnitude limit values and fault plane solutions alternation. Intervals where the NE–SW orientation of the fault planes is dominant, maximum magnitudes are  $M_{w_{max}} > 6.7$ , while in intervals dominated by the NW–SE orientation of the fault planes, maximum magnitudes are  $M_{w_{max}} \leq 6.7$  (yellow rectangles separated by black lines).

#### 4.1. 3-D statistical tidal tomography

To improve our observations on Vrancea seismic region we have extend in space the possibility of statistical parameter  $p$  applying the new concept of statistical tomography (Cadicheanu, 2008; Cadicheanu et al., 2008).

A "statistical tidal tomography" map for each intermediate-depth seismic zone is obtained when stacking function is shifted in 3D geometry following the hypocenter distribution. We assume that the tidal tomography patterns represent the response of the regional tectonic structure to the earth-tides.

The space distribution of the volumes in which the statistical parameter  $p$  of correlation is smaller than 5% agrees with the model of the distribution of seismicity for the Vrancea

seismic zone (Radulian et al., 2008). Taking into account the assumption according to which gravitational forces dominate the volumes with  $p < 5\%$ , we obtain a special map of their action on the Vrancea intermediate-depth seismic activity (Fig.9) maybe related to the torsion movement funded here by Stanica et al. (2004). Small white squares represent the positions of the elementary volumes in which  $p < 5\%$  and colorbar gives the number of earthquakes for each small elementary volume at different levels.

From tectonic point of view, among the three seismic regions, only Vrancea shows a peculiar feature related to the presence of a detached slab immersed into the asthenosphere (Ismail-Zadeh et al., 2005). Due to this greater freedom of movement in asthenosphere, the seismic volume will be more sensitive to the action of gravitational forces than other areas and thus to the action of the earth tides. But we observe that the coupling between earth tides and seismic activity is not constant. This means that any seismic region is subject to complex physical factors, not only gravitational, that impose various physical parameters measurements.

## 5. CONCLUSIONS

Different signatures of the  $p$  variation are observed in the neighborhood of the stronger earthquakes. Coupling tendencies between some earth tide components (semi-diurnal  $M2$  wave especially) and seismic activity for three important seismic regions of the world (Vrancea, Bucaramanga and Hindu Kush) are studied by means of the statistical  $p$ -value and validated by means of random synthetically time series. We suppose that statistical  $p$ -value, could have a potential capacity to identify the existence of transient features around strong seismic events.

In the triggering mechanisms, important factors could be: the variations of the heat flow distribution in the earth mantel, the fluid flow in the porous medium, in terms of physical characteristics of contact with magma in the areas of the crustal and sub-crustal discontinuity, the large seismic events and the earth tides that induce periodical variations of the gravitational forces at large scale. All these factors are capable to modify the energetic potential of a region inducing variations of the stress at the fault level. Our results confirm the existence of a structure and tectonic dynamics specific to each of the three analyzed areas. ). In particular, in Vrancea region, the immersed seismic volume into the asthenosphere makes the seismic activity more sensitive to the action of gravitational forces than other similar areas and thus to the action of the earth tides.

In this context, Vrancea seismic region is the suitable zone for studies of the correlation between Earth tides and earthquake occurrences.

The relationship between seismic activities and tidal periodicities could be important to understand some characteristics of the analyzed seismic zones. In addition, the statistical coefficient  $p$  could have a potential capacity to identify the existence of transient features around strong seismic events (Bernard, 2001). Thus, the new concept and methodology of the statistical tidal tomography could reveal important features in the behavior of a seismic zone.

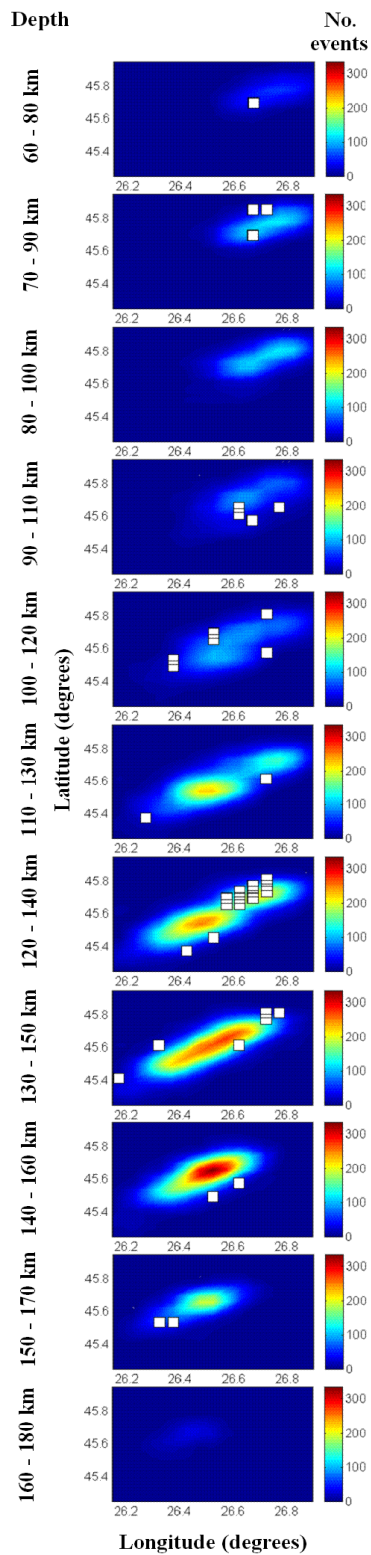


**Fig. 9.** Results of the statistical M2 tidal period tomography for the Vrancea seismic zone. Small white squares represent the positions of the elementary volumes with  $p < 5\%$  and colorbar gives the number of earthquakes for each small elementary volume at different levels.

**ACKNOWLEDGMENTS.** We thank Dr. Bernard Ducarme, Dr Pascal Bernard and Dr Dorel Zugravescu for their very useful comments and observations. We are very grateful to Dr. Mircea Radulian and Dr. Mihaela Popa, the National Institute for Earth Physics for providing the ROMPLUS catalogue.

## REFERENCES

- Bernard, P., 2001. From the search of ‘precursors’ to the research on ‘crustal transients’. *Tectonophysics* **338**, 225–232.
- Cadicheanu, N., van Ruymbeke, M., Zhu, P., 2007. Tidal triggering evidence of intermediate depth earthquakes in the Vrancea zone (Romania), *Nat. Hazards Earth Syst. Sci.* **7**, 733-740.
- Cadicheanu, N., Zhu, P., van Ruymbeke, M., 2008. Spatial and temporal variations of the correlation coefficient between M2 and S2 earth tides components and earthquake occurrence for the intermediate-depth seismic activity zones. *Acta Geod. Geoph. Hung.* **43**(2–3), 131–144.
- Cadicheanu, N., 2008. Etude des influences gravimétriques induites par les marées terrestres sur l’activité sismique intermédiaire dans la zone de Vrancea. Doctoral Thesis. Université catholique de Louvain.
- Cochran, E.S., Vidale, J.E., Tanaka, S., 2004. Earth tides can trigger shallow thrust fault earthquakes. *Science* **306**, 1164–1166.
- Emter, D., 1997. Tidal triggering of earthquakes and volcanic events. *Lecture Notes in Earth, Sciences* **66**, 293-309
- Enescu, D., Enescu, D.B., 1999. Possible cause – effect relationships between Vrancea (Romania) earthquakes and some global geophysical phenomena. *Natural Hazards, Kluwer Academic Publishers* **19**, 233–245.
- Heaton, T. H., 1975. Tidal triggering of earthquakes. *Geophys. J. R. Astron. Soc.* **43**, 307–326.
- Ismail-Zadeh, A., Müller, B., Wenzel, F., 2005. Modelling of Descending Slab Evolution Beneath the SE-Carpathians: Implications for Seismicity. *Perspectives in Modern Seismology Lecture Notes in Earth Sciences* **105**, 203-223
- Kasahara, J., 2002. Tides, earthquakes and volcanoes. *Science* **297**, 348–349.
- Melchior, P., 1978. *The Tides of the Planet Earth*. Pergamon Press, New York.
- Pegler, G., Das, S., 1998. An enhanced image of the Pamir-Hindu Kush seismic zone from relocated earthquake hypocentres, *Geophysical Journal International* **134** (2), 573–595.
- Ping Zhu, Michel van Ruymbeke, Nicoleta Cadicheanu, 2009. A stacking method and its applications to Lanzarote tide gauge records. *Journal of Geodynamics* **48**, 138–143
- Ping Zhu, 2010. Analysis of very weak signals in seismic, climatic and tidal observations. Doctoral Thesis. Université catholique de Louvain.
- Pitman, E.J.G., 1938. Significance tests which may be applied to samples from any population, Part III: The analysis of variance test. *Biometrika* **29**, 322–335.
- Pulido, N., 2003. Seismotectonics of the northern Andes (Colombia) and the development of seismic networks. *Bulletin of the International Institute of Seismology and Earthquake Engineering, Special Edition*, 69-76.

- Radulian M., Popa M., Cărbunar O., Rogozea M., 2008. Seismicity patterns in Vrancea and predictive features. *Acta Geod. Geoph. Hung.* 43(2–3), 163–173.
- Replumaz, A., Guillot, S., Villaseñor, A, Negredo, A.M., 2013. Amount of Asian lithospheric mantle subducted during the India/Asia collision. *Gondwana Research* 24, 936–945.
- Schuster, A., 1897. On lunar and solar periodicities of earthquakes, *Proc. R. Soc. Lond.* 61, 455–465.
- Souriau, M., Souriau, A., Gagnepain, J., 1982. Modeling and detecting interactions between Earth tides and earthquakes with application to an aftershock sequence in the Pyrenees. *Bull. Seismol. Soc. Am.* 72, 165–180.
- Stanica, D., Stanica, M., Piccardi, L., Tondi, E., Cello, G., 2004. Evidence of geodynamic torsion in the Vrancea zone (eastern carpathians). *Rev. roum. GÉOPHYSIQUE*, 48, 15–19.
- Stavinschi, M. and Souchay, J., 2003. Some correlations between earthquakes and Earth tides, *Acta Geod. Geoph. Hung.* 38, 77-92.
- Sturges, H. A., 1926. The choice of a class interval. *Journal of the American Statistical Association* 21, 65–66.
- Tanaka S., Sato, H., Matsumura, S., Ohtake, M., 2006. Tidal triggering of earthquakes in the subducting Philippine Sea plate beneath the locked zone of the plate interface in the Tokai region, Japan. *Tectonophysics* 417, 69–80.
- Tanaka, S., Ohtake, M., Sato, H., 2002. Evidence for tidal triggering of earthquakes as revealed from statistical analysis of global data. *J. Geophys. Res.* 107 (B10), 2211. doi:10.1029/2001JB001577.
- Tolstoy, M., Vernon, F.L., Orcutt, J.A., Wyatt, F.K., 2002. Breathing of the seafloor: tidal correlations of seismicity at Axial volcano. *Geology* 30, 503–506.
- Tsuruoka, H., Ohtake, M., Sato, H., 1995. Statistical test of the tidal triggering of earthquakes: contribution of the ocean tide loading effect. *Geophys. J. Int.* 122, 183–194.
- van Ruymbeke, M., Ducarme, B., De Becker, M., 1981. Parameterization of the tidal triggering of earthquakes. *B.I.M.* 86, 5521-5544.
- van Ruymbeke, M., Howard, R., Putz, P., Beauducel, F., Somerhausen, A., Barriot, J-P., 2003. An Introduction to the use of HICUM for signal analysis. *BIM* 138, 10955–10966.
- Wilcock, W.S., 2001. Tidal triggering of microearthquakes on the Juan de Fuca Ridge. *Geophys. Res. Lett.* 28, 3999–4002.
- Zarifi, Z., Havskov, J., 2003. Characteristics of dense nests of deep and intermediate depth seismicity. *Advances in Geophysics* 46, 237-278.
- Zugravescu, D., Fatulescu, I., Enescu, D., Danchiv, D., Haradja, O., 1989, Peculiarities of the correlation between gravity tides and earthquakes. *Revue Roumaine de Geologie, Geophysique et Geographie, Serie de Géophysique* 33, 3-11.

# Hydrological and tectonic strain forces measured in a karstic cave using extensometers

Ping ZHU\*<sup>1</sup>, Michel van Ruymbeke<sup>†1</sup>, Yves Quinif<sup>2</sup>, Thierry Camelbeeck<sup>1</sup> and Philippe Meus<sup>3</sup>

<sup>1</sup>Royal Observatory of Belgium, ORB-AVENUE CIRCULAIRE 3, 1180, Bruxelles, Belgium.

<sup>2</sup>Institut Jules Cornet (Géologie), Faculté Polytechnique de Mons, Rue de Houdain 9, 7000 Mons, Belgium

<sup>3</sup>Service Public de Wallonie Direction générale opérationnelle Agriculture, Ressources naturelles et Environnement Département de l'Environnement et de l'Eau Direction des Eaux souterraines 15 Avenue Prince de Liege, B-5100 Jambes, Belgium

---

\*ping.zhu@observatoire.be

†labvrui@oma.be

In order to monitor the hydrological strain forces of the karst micro fissure networks and local fault activities, six capacitive extensometers were installed inside a karstic cave near the midi-fault in Belgium. From 2004 to 2008, the nearby Lomme River experienced several heavy rains, leading to flooding inside the Rochefort cave. The highest water level rose more than thirteen meters, the karstic fissure networks were filled with water, which altered the pore pressure of the cave. The strain response to the hydrological induced pore pressure changes are separately deduced from fifteen events when the water level exceeded six meters. The strain measured from the extensometer show a linear contraction during the water recharge and a nonlinear exponential extension releasing during the water discharge. The sensitivity and stability of the sensor are constrained by comparing continuously observed tidal strain waves with a theoretical model. Finally, a local fault deformation rate around  $0.03 \pm 0.002\text{mm/yr}$  is estimated from more than four years' records.

**Keywords: Hydrologic, Tectonic, Tides, Strain, Deformation**

## 1 INTRODUCTION

The Rochefort karstic cave is located at a relatively stable continental region where the seismicity and the risk of seismic hazard are low. Palaeoseismology studies indicate that a maximum 0.3mm/yr deformation rate could account for coseismic effects from three large earthquakes during the Pleistocene and Holocene (Camelbeeck and Meghraoui, 1998). However, the recently growing stalagmite and falling rocks inside the cave, strongly evidence that the identified faults are active and expanding in the NW-SE direction, driven by the regional tectonic force (Vandycke and Quinif, 2001). But the continuous GPS measurements show motions less than 1mm/yr which is still inside the error bar. Hence, to constrain the results provided by the geological investigations, an in-situ strain measurement experiment was conducted since 1999.

Beyond its interest about the local faults activities, the experiment is also focusing on providing information about the hydrological impact on the formations process of micro fissure networks and karstification. There are two kinds of water flux which contribute to the process, the slow seepage and fast flow drainage. To monitor the strain inside a cave can help improving the understanding of the karst structure, especially it's porosity and fissure networks (Genty and Deflandre, 1998).

Six extensometers were set up near two identified faults inside the Rochefort cave, two aluminum extensometers No.1 (E1) and No.2 (E2) in 1997 and four Pyrex aluminum extensometers No.3 (E3), No.4 (E4), No.5 (E5), and No.6 (E6) in 2000. The hydrological strain forces, local faults activity, and the secular earth strain were detected from the recording of the extensometers.

## 2 EXPERIMENT SITE

The Rochefort karstic caves are located 20km away from the midi-fault, along which an Ms4.6 earthquake occurred on Aug. 08, 1988. At the far north-east direction, this area is a relatively active zone: all of the 'Roer Valley' graben is bounded by two normal faults, the Peel Fault (PF) and the Feldbiss Fault (FF). An Ms 5.3 earthquake occurred on Apr. 13, 1992 along the PF (Camelbeeck and Meghraoui, 1996). In this region, the majority of earthquakes were located at both sides of the midi-fault according to the Earthquake Catalog of Royal Observatory of Belgium (ROB) since 1910 (Fig.1). The Rochefort cave is buried 50 meters underground and constituted by two galleries: large one along the stratigraphic direction (N070E) named 'Fontaine Bagdad' and smaller one in the dip direction 'Val d'Enfer'. Inside the cave, two types of faults are recognized (Fig.1). The first type of fault is contemporaneous of the Variscan folding, characterized by reverse motion along the bedding planes. The second type is the present active faults. The recent faults are related with present-day tectonic activity which is evidenced by seismicity of the neighbor area. The stereographic projection of recent faults affecting Rochefort karstic network shows a principal NW-SE extension, nearly perpendicular to the present regional stress as illustrated by the analysis of the last strong regional earthquake (Vandycke and

Quinif, 2001).

Three water table probes have been successively installed inside the Rochefort karstic caves since 2005 (Fig.1). The first one (WI) was set up under the 'Val d'Enfer' room on March 2005. The site was at the bottom of an irregular shaft, about 77 meters deep and a few meters in section. The second one (WII) was installed at the 'Rivière des Touristes' in 2006. The 'Rivière des Touristes' is at one of the deepest points inside the cave. It is behaving as a river; the water comes from a sump and then flow out into another sump. During the flood period, the nearby conduits were filled and then the river becomes a lake. The third one (WIII) was placed at the 'Petit Noir' on 2007, located at a large funnel shape hall which is the ultimate point of the cave.

### 3 EXTENSOMETER

The Pyrex aluminum capacitive extensometers were designed and developed in 1999 at the Royal Observatory of Belgium in Brussels. The gauge is consisted of two round aluminum plates with 40mm diameter and it is fixed in the rock by two Pyrex rods. The extensometers were installed in two steps: first, two fiducial points are drilled 6cm into the limestone at two sides of a fault then the Pyrex rods are bonded to the hole by a chemical anchor capsules (Upat-UKA3); Second, about one month later, when the piers are adequately bounded with the rocks, we mount the extensometers with a 1300°C flame. The dielectricity of the capacitance is directly counted by an electric oscillator chip. EDAS data logger was used as acquisition systems (Van Ruymbeke et al., 2001; Sondag et al., 2003). The initial sampling interval is one minute. The laboratory calibration experiments show that the counting frequency is linearly proportional to the displacement when the relative displacement is less than 100 $\mu$ m. The stability and sensitivity of the gauges are influenced by the humidity, pressure, and temperature since the sensors are completely exposed to the environment. Fortunately, the meteorological conditions are very stable inside the cave. The continuous rock temperature monitoring near E4 gave an annual temperature variations of about 0.06°C, and the maximum daily changes were less than 0.02°C. The thermal expansion coefficient is  $22.3 \times 10^{-6}$  for aluminum and  $3.25 \times 10^{-6}$  for Pyrex glass. Thus, taking into account the laboratory tests, the expected strain resolution should be better than 0.1ppm. The original data were decimated into hour sampling rate (Fig.2). We selected the most homogeneous records of E4 (length 81mm, azimuth 84°), E5 (length 92mm, azimuth 136°) and E6 (length 75mm, azimuth 58°) since 2003, three years after the installation. Therefore we can believe that the extensometers are adequately coupled with the host rocks.

## 4 RESULTS

### 4.1 TIDAL STRAIN

The most difficult problem for such experiment is the calibration and evaluation of the stability of the sensors. The solid Earth Tides, continuously registered on the E4, E5 and E6, provide us a stable reference. The tidal strain measurement began from 1951 when Sassa, Ozawa and Yoshikawa published the first results obtained with a superinvar wire extensometer (Melchior, 1983). After that, a great effort have been paid to design high accuracy strainmeters by different groups, among them the most reliable gauges should be the Laser strain meter (Berger and Lovberg, 1970; King and Bilham, 1973; Berger and Wyatt, 1973; Sydenham, 1974; Beavan and Goult, 1977). With the new technology, the secular earth strain tides can be easily observed in different places. Thus, the interests of strain observations have been moved from the earth tide to seismic toroidal modes, tectonic activities, hydrological effects and transient pre-, co-, or post- seismic signals (Zadro and Braitenberg, 1999).

Due to the high accuracy of the tidal model, the tides are valuable input signals for the instruments. It can be applied to calibrate and check the sensitivity of any arbitrary records in situ such as the borehole strain measurements (Westerhaus and Zürn, 2001). The diurnal and semi-diurnal components have been found in the in situ relative seismic velocity variation records in Japan (Yamamura et al., 2003). It allows to measure directly the relation of relative seismic velocity variation with strain. The minimum resolution of our capacitive extensometer can reach  $10^{-7}$ . The synthetic volumetric earth strain tides computed with HW95 tidal potential (Wenzel, 1996) gave the amplitudes are between  $10^{-8}$  and  $10^{-9}$  at the surface of Rochefort karstic caves. Thus the gauges can hardly record the tidal strain by principle. But it is undoubtedly registered at the extensometer 4 and 5. To check the tidal frequency band signals, the data were band pass filtered between 0.6 cycles per day and 8 cycles per day. Two month's results between April, 1st and May 31st in 2005 were plotted (Fig.3 upper). The Amplitude Fourier Spectrum shows the diurnal and semidiurnal solar principal waves and its harmonic components until the fourth (Fig.3 lower). On the E4 these signals are dominated by a stronger one, probably due to the thermal elastic deformation. Similar phenomenon has been reported from a long base line laser strain meter measurements (Berger and Wyatt, 1973). The principal lunar diurnal wave O1 and semidiurnal wave M2 are permanently registered in the gauges E5 with unexpected high signal-to-noise ratio. The theoretical values of the volumetric strain in the azimuth of E5 are computed using Eterna3.3 (Wenzel, 1996) from Apr.01, 2005 to Sep.30, 2005. We compared the phases of O1, M2 and S2 with the records of E5 (Fig.4). The observed phases (O1, M2 and S2) were close to the values of the hydrostatic tidal strain (Table 1). It evidences that the sensors are recording the hydrostatic strains induced by pore pressure changes but the amplitudes were two orders larger than the synthetic values.

## 4.2 HYDROLOGICAL EFFECTS

The experiment site suffered a relatively dry season from the Feb, 2005 to the beginning of 2006, and then the precipitations were increased. It becomes a rainy season from the mid of 2007 to the end of 2008 (Fig.5 left). When the Lomme River was flooded, the water level rose and fell simultaneously at WI, WII and WIII. Due to the different capacities of three aquifers, they are discharging water with slightly different speeds (Fig.5 right). The WI water level gauge is the nearest probe to the extensometers so that the hydrological induced strain was directly measured on E5 and E6 from WI. To measure the strain changes from the extensometers, a hydrological event is defined when the water level becomes higher than 6 meters. We choice such a definition because the hydrological strain forces signal was superposed on a long term slip trends of fault motion. Sixteen events were located from the records of the water probe since 2005 until 2008. Due to the failure of the power supply, the E5 and E6 have missed one event. The E5 and E6 are well correlated with the processing of water charging and discharging at WI site (Fig.6). Obviously, the response of the extensometers to the charging and discharging procedure were different. The pore pressure was increased when the water level rose and decreased with water discharge.

The fifteen isolated hydrological events were divided into three categories according to the duration of the highest water level. In type one, the process of water charging and discharging is shorter than forty hours. The second type is longer than forty hours, and in the third type, the height of water table is exceeding 6 meters several times in a 150 hours window (Table 2). The highest water level was set as the boundary point between the water charging and discharging. We separately measured the strain changes as a function of water level. Six events were fall into the first category, seven events belong to the second category and two to the last category. During the water charging, the strain rate was linearly proportional to the water level and flux.

At the stage of the water discharge, the strain rate express an exponential recovery to the water level (Fig.7a). It evidently follows this pattern for all events of the second type (Fig.7b). The eighth and fifteenth events belong to the third type, the karst fissure networks were charging and discharging more than one times in a 150 hours window. Both extensometers were instantaneously responding to about one meter water level rising and falling (Fig.7c).

The extensometers simultaneously react to the pore pressure changes which suggest that the pore pressure was altered mainly due to the karst fissure networks were rapidly filling and run-off during the rainy season. In the regional scale, it shows that the complete karstic caves work as an elasticity and homogeneous media in a short term.

## 4.3 THE FAULT ACTIVITIES INSIDE THE KARSTIC CAVE

From the beginning of 2005 to the February of 2006, it was a relatively dry season. The water content was decreased inside the cave which altered hydrostatic strain inside the cave. The abnormal contraction appearing on the E6 can be explained by such effects (Fig.2). In 2006, the E5 and E6 were interrupted by a failure of the power supply. The E6

restarted to work after the power supply was repaired. The records of E4, E5, and E6 are decimated into daily sampling rate and low pass filtered to only keep the long term trends with frequency lower than one cycle per month (Fig.8). The annual rock temperature change is 0.06 near the E4. The annual thermal induced elastic deformation deduced from the E4 reaches an amplitude of  $7.3 \pm 1.9\mu\text{m}$ . The thermal effect is obviously weaker at the site of extensometer 5 and 6 where the water are penetrating through the karstic fissure networks and some new stalactites are growing nearby. Each of these three long term trenches was separately fitted by a linear function with 95% confidential boundary. The E4 shows a deformation rate of 0.028mm/yr and 0.026mm/yr for E6. The E6 is bonding across the fault 1 and E4 is to the fault2. It is reasonable to find that the E5 shows a slower expanding rate 0.010mm/yr than the E4 and E6 because the E5 is not directly attached to the identified active faults. The extension direction of the fissure where E5 installed, are nearly perpendicular to the fault 1 and 2.

## 5 DISCUSSION AND CONCLUSIONS

Diurnal and semidiurnal tidal constituents are continuously recorded by the E5. However, the amplitudes are much greater than the synthetic earth strain tides. But the observed tendency of O1 amplitudes distribution agree well with theoretical value which provides valuable constrains about the stability of the gauge. The solar principal wave S2 and its harmonic components are permanently recorded by the E4 and sometimes the E6. The semidiurnal S2 wave induced by thermal-elastic oscillation with amplitude around  $2.4 \times 10^{-7}$  is clearly observable on the E4. By inter comparing the S2 waves among three sensors, the S2 amplitudes differences were less than  $10^{-7}$ , which confirmed the sensor's stability can reach 0.1ppm (Fig. 4). The amplitudes of observed tidal strain waves are much greater than the theoretical value. It could be attributed to the cavity effects, but due to the chaos of the fractal cavities, it is difficult to model such effects.

Rock deformations induced by hydrological agents were observed from the E5 and E6. The water conductivity and porosity altered the pore pressure inside the cave. These hydrological induced deformations have been found in other geodetic observations. Several solutions are proposed to correct it from the geodetic observations, among them the mostly used methods are the rain function (Langbein et al., 1990) and the predictive filtering methods (Braitenberg, 1999). The E5 and E6 have different maximum strain response to water level. But the rate of strain accumulation and release accompanied by the processing of water charging and discharging, gave coherent results by both gauges for all fifteen events. During the water charging, it shows a linear contraction at E5 and E6 induced by the buoyancy force, at the period of the water discharge. The strain is recovering with an exponential trend due to the pore pressure alternation by the conductivity and porosity of the media during the flood periods. The contraction rate induced by the water level rising is slightly faster for E5 than than E6. After the water release, E5 and E6 share a similar extension rate.

The absolute gravity measurement at the site, shows gravity value increases  $90\text{nm/s}^2$

when the water level rose more than 10 meters (Van Camp et al., 2006). The gravity changes calculated from a 10 meters thick cylinder model in 60 meters depth and with 5% porosity, is  $250\text{nm/s}^2$  Dr. M. Van Camp (pers. comm.). The observed gravity changes are about 1/3 of the modeled value. Since the strain were linearly reacting to water charging, it suggested that both the strain and gravity changes, can be attributed to the buoyancy force during the water filling the karst fissure networks.

The E6 showed a 0.026mm/yr displacement of fault 1 and E4 gave a 0.028mm/yr displacement of fault2 which was superposed with a  $7.3 \pm 1.9\mu\text{m}$  annual oscillation term. A perpendicular fissure to the fault 1 measured by the E5, gave a 0.010mm/yr rate. The fissure is 20cm in width so that the formation of this fissure is about 20,000 years if we suppose that the activity of the region is relative stable since it. The expending rate deduced from the E4 and E6, agreed with the results obtained by stereographic projection (Vandycke and Quinif, 2001). It suggests that a local background driving displacement rate is about  $0.03 \pm 0.002\text{mm/yr}$ . A discussion and a tectonic interpretation of these observations can be found in (Camelbeeck et al., 2012).

A factual karstic cave is normally thought as an unfavorable site for the instrumental observations due to its complex geometry with strong heterogeneity and high humidity rates. But water drips monitoring under the stalactites, raised broad interest for the karstification process and palaeoclimatology study (Genty, 2008). The preliminary results of our strain measurement shed new light on the geophysical experiments. The result suggest that, if the sensor is properly installed, maximum following the characteristics of the nature, the ability of detecting very weak signals like the hydrology, local fault activities and secular earth strain can be achieved.

## ACKNOWLEDGMENTS

We are very grateful to the support of Dr. Ronald Van der Linden, director general of Royal Observatory of Belgium. We benefit a lot from the discussions with Dr. Michel Van Camp. We used the ROB earthquake catalog. The first author is financially supported by the Action 2 contract from the Belgian Ministry of Scientific Politics. The experiments in Rochefort were supported by the Ministry of the Walloon Region(Belgium).

## REFERENCES

- Beavan, R., Goult, N., 1977. Earth-strain observations made with the Cambridge laser strainmeter. *Geophys.J.R.Astr.Soc.* 48, 293–305.
- Berger, J., Lovberg, R., 1970. Earth strain measurements with a laser interferometer. *Science* 170, 296–303.
- Berger, J., Wyatt, F., 1973. Some observations of Earth strain tides in California. *Phil.Trans.R.Soc.Lond.A.* 274, 267–277.

- Braitenberg, C., 1999. Estimating the hydrologic induced signal in geodetic measurements with predictive filtering methods. *Geophys.Res.Lett.* 26, 775–778.
- Camelbeeck, T., Meghraoui, M., 1996. Large earthquakes in northern Europe more likely than once thought. *EOS Trans., Am. Geophys. Union* 77, 405–409.
- Camelbeeck, T., Meghraoui, M., 1998. Geological and geophysical evidence for large palaeoearthquakes with surface faulting in the Roger Graben (Northwestern Europe). *Geophys.J.Int.* 132, 347–362.
- Genty, D., 2008. Palaeoclimate research in Villars Cave (Dordogne, SW-France). *International Journal of Speleology* 37(3), 171–191.
- Genty, D., Deflandre, G., 1998. Drip flow variations under a stalactite of the Père Noël cave (Belgium). Evidence of seasonal variations and air pressure constraints. *Journal of Hydrology* 211, 208–232.
- King, G., Bilham, R., 1973. Tidal tilt measurements in Europe. *Nature* 243, 74–75.
- Langbein, J., Burford, R., Slater, L., 1990. Variations in fault slip and strain accumulation at Parkfield, California: initial results using two color geodimeter measurements. *J.Geophys.Res.* 95, 2533–2552.
- Melchior, P., 1983. *The Tides of the Planet Earth*, Pergamon Press. New York.
- Sondag, F., van Ruymbeke, M., Soubiés, F., Santos, R., Somerhausen, A., Seidel, A., Boggiani, P., 2003. Monitoring present day climatic conditions in tropical caves using an environmental data acquisition system (EDAS). *Journal of Hydrology* 273, 103–118.
- Sydenham, P., 1974. Where is experimental research on earth strain? *Nature* 252, 278–280.
- Van Camp, M., Meus, P., Quinif, Y., Kaufmann, O., van Ruymbeke, M., Vandiepenbeeck, M., Camelbeeck, T., 2006. Karst aquifer investigation using absolute gravity. *EOS Trans., Am. Geophys. Union* 87, 298–299.
- Van Ruymbeke, M., Beauducel, F., Somerhausen, A., 2001. The environmental data acquisition system (EDAS) developed at the Royal Observatory of Belgium. *Journal of the Geodetic Society of Japan* 47, 40–46.
- Vandycke, S., Quinif, Y., 2001. Recent active faults in Belgian Ardenne revealed in Rochefort Karstic network (Namur province, Belgium). *Netherlands Journal of Geosciences* 80, 297–304.
- Wenzel, H.-G., 1996. The nanogal software: Earth tide data processing package eterna 3.3. *Bulletin d'Informations Marées Terrestres* 124, 9425–9439.

- Westerhaus, M., Zürn, W., 2001. On the use of earth tides in geodynamic research. *Journal of the Geodetic Society of Japan* 47 No.1, 1–9.
- Yamamura, K., Sano, O., Utada, H., Takei, Y., Nakao, S., 2003. Long-term observation of in situ seismic velocity and attenuation. *J.Geophys.Res.* 108, doi:10.1029/2002JB002005.
- Zadro, M., Braitenberg, C., 1999. Measurements and interpretations of tilt-strain gauges in seismically active areas. *Earth-Science Reviews* 47, 151–187.
- Camelbeeck Th., van Ruymbeke M., Quinif Y., Vandycke S., de Kerkhove E., Zhu P., 2012. Observation and interpretation of fault activity in the Rochefort cave(Belgium). *Tectonophysics*, 581, 48-61.

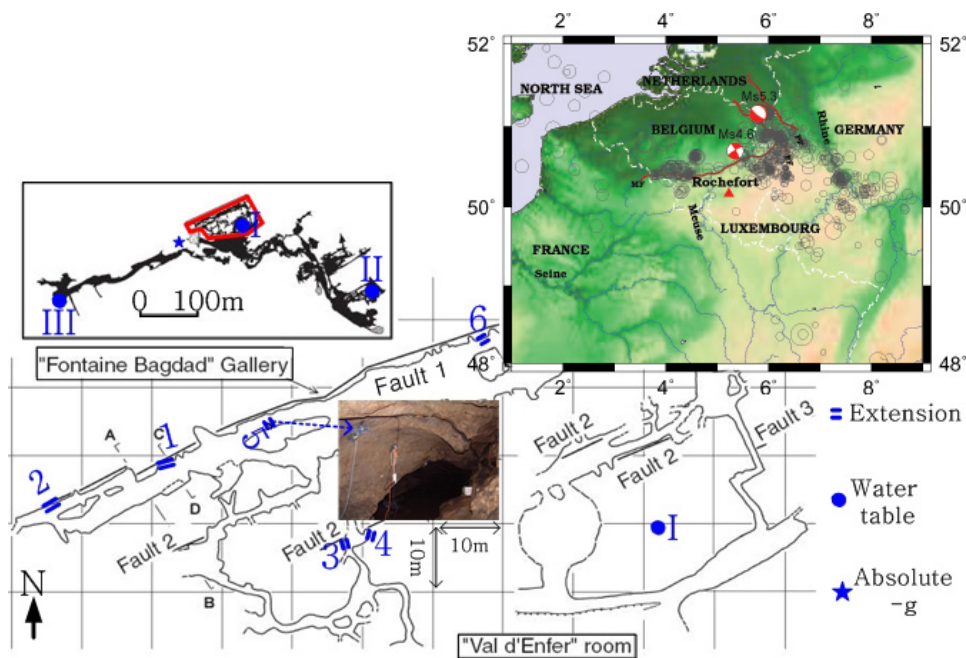


**Figure 1. The sketch plot of Rochefort karstic caves, the red box marks the area at which the extensometers were installed. Three type's measurements have been conducted: extension, water table and absolute gravity. The maps on the upper right show the geological background of the site. The small photo at the center is the place where E5 was installed.**

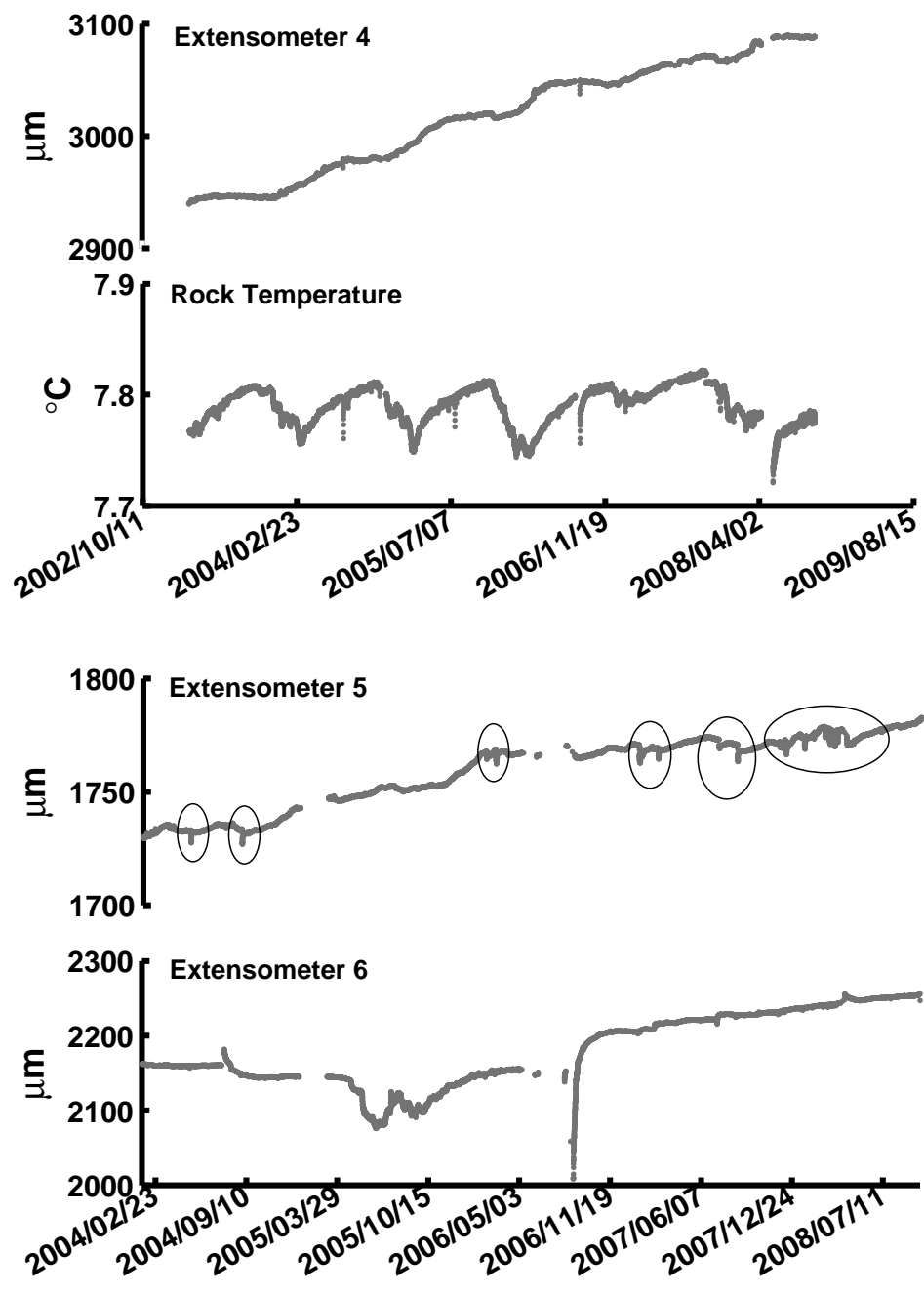


Figure 2. The original data were decimated into hour sampling rate. The annual periodical oscillations are observable from the E4 and Rock temperature. Six ellipsoidal circles mark the hydraulically induced deformation on E5. The pore pressure change during the dry season induced big gaps on E6.

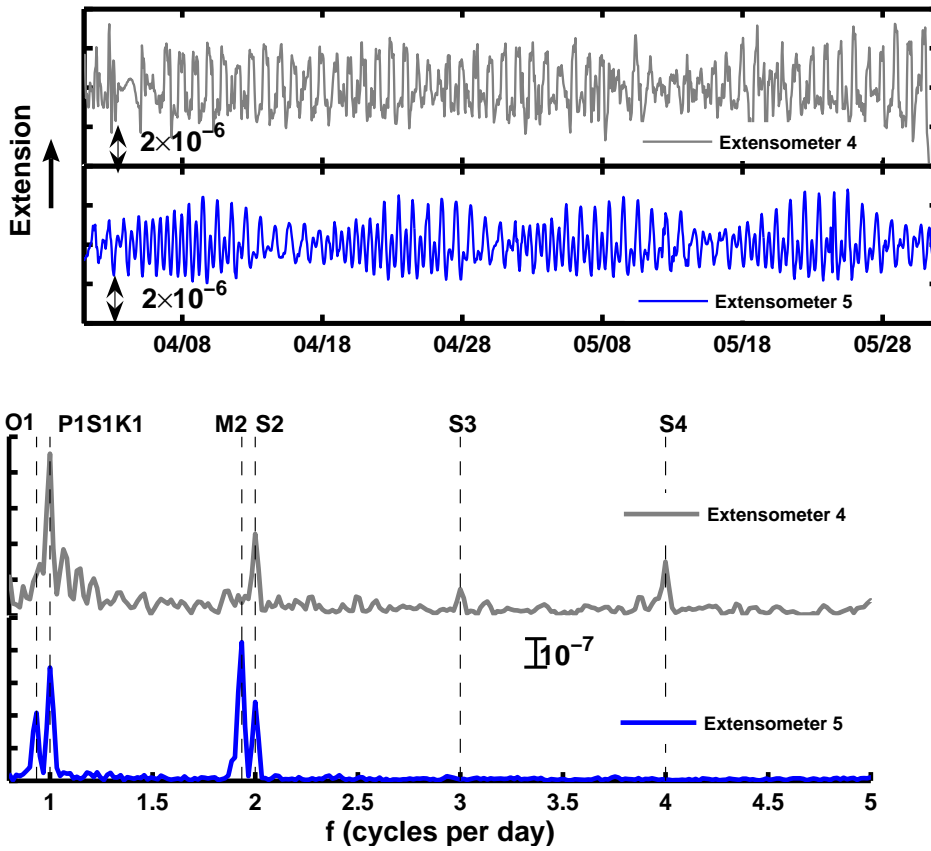


Figure 3. (Upper), The original data have been band pass filtered between 0.6 cpd and 8 cpd, the earth tides are obviously recorded by two gauges, (Lower), Amplitudes Fourier Spectrum of extensometer No. 4 and No.5.

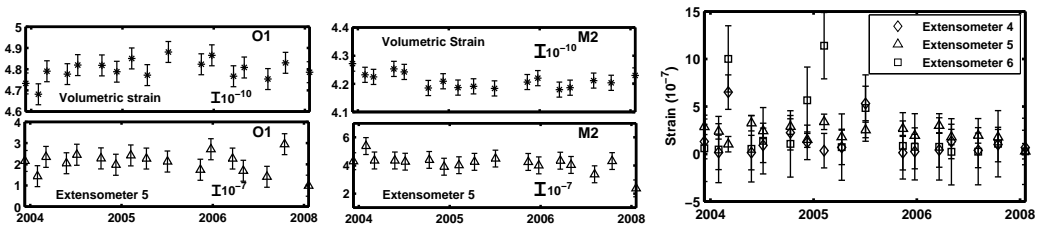


Figure 4. (a) O1 amplitudes distribution upper channel synthetic volumetric tidal strain, lower channel observed O1 tides from E5. (b) M2 amplitudes distribution upper channel synthetic volumetric tidal strain, lower channel observed M2 tides from E5. (c) S2 components separated from three sensors E4, E5 and E6.

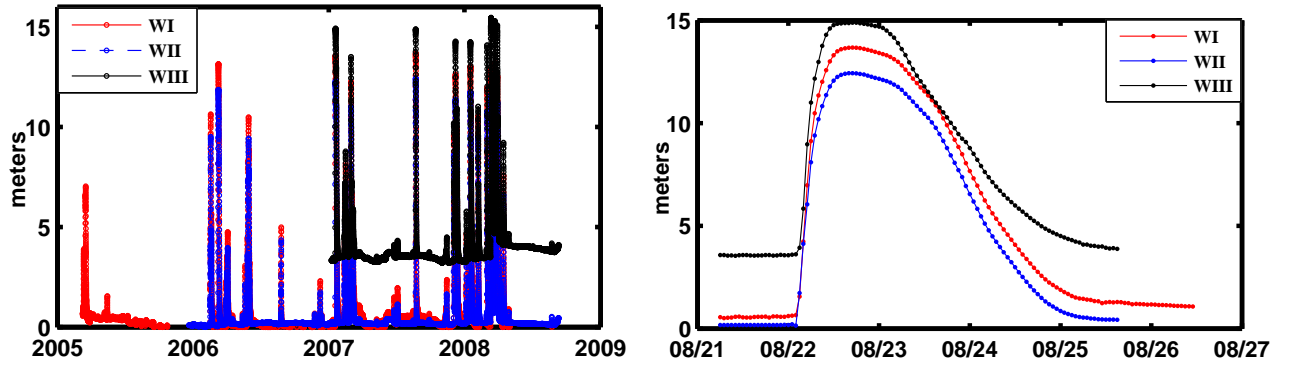


Figure 5. (Left), water table records at three locations in the karstic caves. The water level exceeded 6 meters at 16 occasions. (Right), a typical flood event recorded by three water tables.

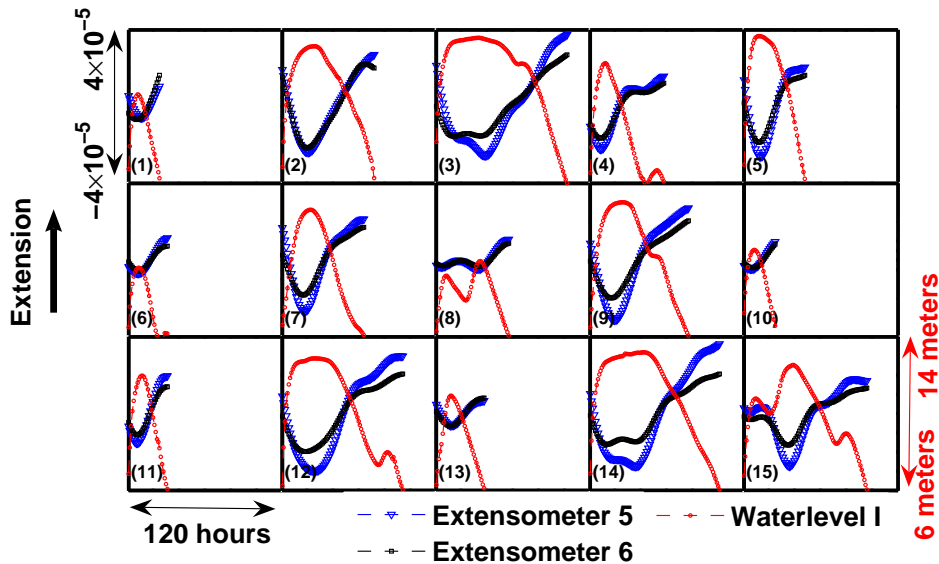


Figure 6. The water table WI, Extensometer 5, and 6 are plotted together when the water level is higher than 6 meters. The number of each box corresponds to the hydrological event listed in Table 2.

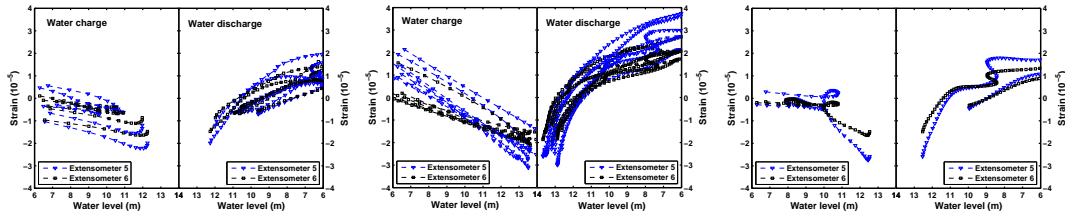


Figure 7. The strain versus water level. (a) The first type, the duration of water level higher than 6 meters is shorter than 10 hours. (b) The second type, the duration of water level higher than 6 meters is longer than 10 hours. (c) The third type, more than one times the water level rose higher than 6 meters.

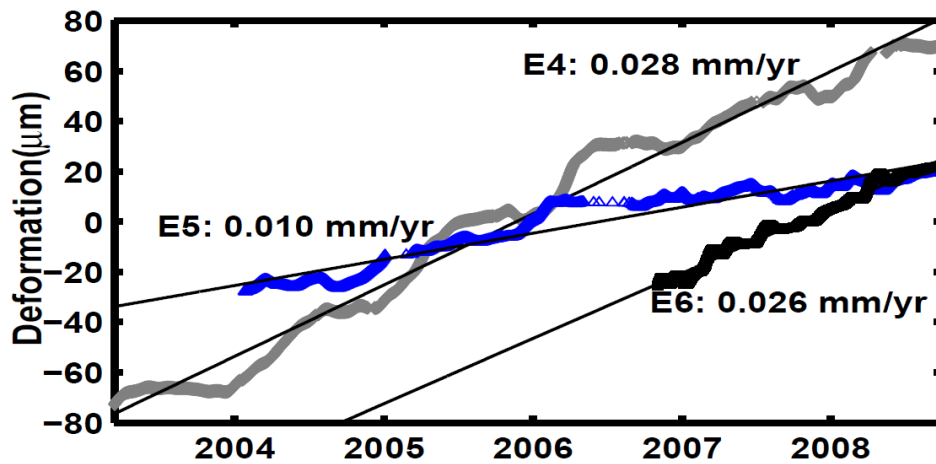


Figure 8. The long term trend of E4, E5 and E6 is fitted by a linear function with 95% confidential level.

**Table 1. Tidal analysis result of E5 records between Apr.01 and Sept.30 2005. Synthetic volumetric strain is compared with the observations.**

Wave	E5( $10^{-7}$ )	Syn( $10^{-9}$ )	Ratio	E5( $\phi$ )	Syn( $\phi$ )	Diff.
O1	2.219	5.006	44.3	138.311	125.186	13.125
M2	3.798	4.593	82.7	134.988	138.229	-3.241
S2	1.859	1.623	114.5	12.112	8.122	3.990

**Table 2. Hydrological events were separated into three groups, the maximum strain changes corresponding to the highest water is measured from each event.**

NO.	Date	Dur(hrs)	WI(m)	E5( $10^{-5}$ )	E6( $10^{-5}$ )
1	2006/02/17 00:00	25	10.6	-1.18	-0.33
4	2007/03/01 11:00	5	12.3	-1.20	-0.68
6	2007/12/03 03:00	31	9.6	-0.09	-0.13
10	2008/02/06 09:00	25	10.5	-0.04	-0.09
11	2008/03/01 09:00	9	11.9	-0.90	-0.65
13	2008/03/16 20:00	38	10.9	-1.11	-0.76
2	2006/03/09 06:00	72	13.1	-4.35	-3.69
3	2007/01/18 06:00	102	13.6	-4.75	-1.56
5	2007/08/22 05:00	48	13.7	-4.05	-2.05
7	2007/12/06 23:00	64	12.6	-4.42	-2.09
9	2008/01/16 02:00	77	13.0	-4.04	-1.92
12	2008/03/11 08:00	94	12.9	-3.93	-1.84
14	2008/03/21 06:00	101	13.2	-3.84	-1.49
8	2007/12/10 05:00	57	9.9	-0.19	-0.13
15	2008/03/31 22:00	96	12.5	-3.07	-1.49

# Calibration of pendulum by sinusoidal torque induced with the needles of a watch turning in the gravity field of the Earth

M. van Ruymbeke<sup>a,\*</sup>, F. Wielant<sup>b</sup>, J.-P. Noël<sup>a</sup>, Ph. Dumont

<sup>a</sup>Royal Observatory of Belgium, Avenue Circulaire 3, 1180, Brussels, Belgium  
Tel: +32 2 3730286, Fax: +32 2 3739822

<sup>b</sup>ICTEAM - INMA, Université Catholique de Louvain

---

## Abstract

An astatized symmetrical vertical pendulum is monitoring torque  $\Gamma_M$  resulting of gravitational attractions exerted by two external masses  $M$  moving up and down. Local gravity field  $\vec{g}$  produces the main pendulum restoring torque combined with a variable torque  $\Gamma_m$  of similar intensity induced by the rotation of the needles of a watch which is embedded on the pendulum. Transfer of fundamental units to calibrate the  $\Gamma_m$  torques is obtained by a reference torque  $\Gamma_\mu$  resulting of precise displacements of a well known mass  $\mu$ . We permanently monitored ratio between the gravitational effect  $\Gamma_M$  and calibrated  $\Gamma_m$  to determine  $G$ . The position of the pendulum is measured with a capacitive bridge. Bias voltages sent to two electrodes set-up at the bottom of the pendulum allows to feedback pendulum with a controlled electrostatic torque. We discuss potential interest of our prototype to design a multi pendulum system to check systematic effects for different geometries and various kinds of materials.

*Keywords:* tidal instrumentation, gravity,  $G$  gravitational constant, micro force, pendulum, calibration

---

## 1. Introduction

Newtons constant of gravitation  $G$ , is a fundamental constant of nature that determines the gravitational force between two massive bodies. The value of  $G$  varies by over 400 parts per million, 20 times greater than the uncertainty on any kind of measurement. So the precise value of  $G$  remains an open question for the physicists. To better understand this variation, we prepare a series of experiments designed with the expertise gained at the Royal Observatory of Belgium in the tidal instrumentation. Indeed very large dynamics are necessary in this domain with instrumental long term stability and stable sensitivity. Surface laboratory measurements are affected by various effects induced by thermal stress, infrasonic waves, atmospheric pressure waves, human activities effects, etc. For example, tiltmeter recording in a surface laboratory could not detect the tides. In an underground laboratory at a depth of fifty meter, we have access to a more than sixty dB on the same signal.

Analysing the patterns of various tidal instrumentation, we select a vertical pendulum approach with the local gravity field like restoring force. Capacitive transducer positioning sensor which reach sufficiently the precision needed. We induce electrostatic feedback similar to system applied in the tidal gravimeters. Calibration process is based on stacking filtering developed in the tidal waves detection within long series of registration and on inertial calibration developed by a vertical motion platform. Our new experiment allows  $G$  to be measured in two independent ways which are from angular deflection and from the electrostatic feedback force needed to compensate effect of gravitational induction. The operating mode consist in recording simultaneously the gravitational induction and a well known calibrated torque. We meter the ratio between the two effects which are modulated with different periodicities allowing separation by stacking. So we could ignore the sensitivity of the pendulum itself. This paper introduces the

---

\*Corresponding author

Email address: labvruiy@oma.be (M. van Ruymbeke)

different element of our research. Our  $G$  value obtained has less than one percent of discrepancy with CODATA value which could be attributed in the limitation of accuracy in the geometry and mass values determination. However the dynamics observed experimentally confirm potentiality of our method.

## 2. State of art

Physics of the gravitational forces continues to be mysterious. Since Galileo, this force become better and better described by theoretical models. But their origins stay an open question. Geophysicists in charge of determination of the Earth gravity field announce a very coherent pattern in relation with metrological standard units. Tidalists demodulate tidal signals induced by the permanent motions of Moon and Sun in the local coordinates. They reach dynamics better than  $10^{10}$ . This reality continue to be based on the Newton principle of gravitation expressed by the short formula:

$$F = G \frac{M_1 M_2}{r^2} \quad N \quad (1)$$

This simple representation of the gravitational interactions describes the astronomical observations and organises space navigation with enough accuracy.

Inversely the fixation of  $G$  value remains at the limit of instruments with systematic errors limiting the accuracy to 1/10000.

At the present time, the CODATA (Committee on Data for Science and Technology) recommended value of the Newton's constant,  $G$ , is announced with a relative uncertainty of  $1.2 \times 10^{-4}$  [Peter J. Mohr (2012)].

$$G = 6,67384(80)10^{-11} \quad m^3 kg^{-1} s^{-2} \quad \epsilon_r = 120 ppm \quad (2)$$

Noting that, on the one hand, the successively recommended values of  $G$ , and on the other hand the current measurement have no obvious overlap, the CODATA committee asked the scientific community to continue the experiments with various instruments and methods, to compare the systematic effects of each ones.

The main problem in  $G$  determination is that the system to measured is influenced by multiple various effects. The value of certain ones are several orders of size greater. Remembering that the gravitational force of the Earth is the main one, we have also to take into account forces induced by electrostatic and magnetic processes. In addition, the geometry is influenced by temperature gradients, and we have also to consider mechanical effects of displacements due to micro seismic events, industrial noises or airflows, thermal drift and so on. Those forces can totally overwhelm the force to measure, or combine with it in a non-linear fashion, preventing its evaluation.

In general, the experimental devices try to eliminate the Earth gravitation, and correct all other perturbations separately, e.g. by working in the vacuum.

Cavendish tried to get rid of the Earth gravitation by using a torsion balance whose movements are orthogonal to the Earth force. In fact, the Earth gravitation was present anyway through the weight of the balance applied to the rod that affects its torsional force. This effect occurs at the molecular level, along the complete rod.

Despite those difficulties, the resulting error obtained in 1798 was less that 1%, which is really outstanding.

In 2010, measurement techniques improved this result up to 4 significant digits. The internal coherency of the values issued from the CODATA referenced experiments, shows smaller value than the dispersion of the absolute values of the  $G$  constant. So, it seems that results are influenced systematically by undetermined parameters. Problems could be induced on the instrumentation or on gravity interaction into processes. Our goal will experience following earth tides instrumentation expertise : the simplest as possible techniques with a maximum of control for each kind of physical interactions. First assessment is that we could compare the modulated gravity action obtained by moving mass with the gravity action of the mass of the Earth.

Absolute gravimeters gives the  $g$  value with 0.01 ppm of accuracy by direct reference to the standard units. Objective of our method consists to use the pendulum principle to measure  $G$  referring to  $g$  with gravitational modulation function of mass expressed in *kilogram*, geometry and displacements in *meter*.

Let us recall that  $g$  is equal to  $G$  multiplied by the mass of the Earth divided by the square Earth mean radius. Our system based on the ratio between two actions becomes unable to detect a change of  $G$ .

### 3. Functional analysis of the G balance

In this context, we propose to exploit the earth local gravity field value  $g$ , to rely a gravitational force between two masses to the fundamental references.

From our expertise gained with experiences with tidal instrumentation, a list of specifications has been established for the design of an experimental device able to measure Newtons constant.

1. Our system uses a pendulum approach [Naslin (2009)] (see Fig. 1) referred to  $g$  with actions expressed in term of torques induced by various effects. The sum  $\sum \Gamma_i = 0$  corresponds to the equilibrium point.
2. Astaticization obtained with an horizontal axis of rotation just over centre of mass of pendulum allowing comparing very weak horizontal forces with larger vertical ones. Central positioning rejects largely translation mode of the micro seismic noise acting on the support.
3. Geometry defining the gravitational torque for different positions of the moving parallelepiped masses. Design decreases the effect of lateral discrepancy by larger attractive masses than the pendulum ones.
4. Axis of rotation experimental selection of cutter knives with their edges set perpendicular on a drill rig cylinders (see Fig. 3 and 4). This point determines the instrumentation approach because the position of the center of rotation directly involves the period and thus the sensitivity of the instrument.
5. Minimisation of thermal, acoustic and magnetic influences induced by the motion of the twin attractive masses. A constant loading effect on the ground rejecting risk of pendulum tilt.
6. Use of electronics based on symmetric phase detector connected to capacitive transducer [van Ruymbeke (1980)] with a limited gap between plates large enough for pendulum operating quite at critical damping just by air friction. It allows very high precision in the positioning without hysteresis.
7. Application of bias signal using the bottom capacitance plate to induce electrostatic torques for determination of step response or to apply electrostatic feedback to keep constant the position of the pendulum mass allowing neglecting the inelasticity of the suspension. Pulse Width Modulated (PWM) signals on both sides decrease non linear coupling between electrostatic induction and instantaneous position of the mass vibrating under environmental influences.
8. Filtering of random noise by stacking approach allows separating different signals just by linear averaging.

For this case of functional analysis, our approach is similar to a method of fundamental physics, where the simplification of our instruments is necessary to observe nature (and avoid to mask any phenomenon).

Therefore, the issues discussed above lead us to develop flexible simple instruments (with interchangeable pieces), ergonomic (for facilitated setting).

### 4. G Symmetrical Vertical Pendulum

A pendulum can be displaced from its rest position by an horizontal force that is significantly lower than the weight of the pendulum (remind that the torques  $\Gamma_i$  are the orthogonal projections of the forces  $F_i$  on the axis of rotation of the pendulum instrument). The ratio is equal to be displacement divided by the length of the pendulum. In such conditions, it is quite possible to measure horizontal force that is  $10^{-8}$  times smaller than the weight of the pendulum. Since in our case, the gravitational forces  $F_M$  are quiet orthogonal to  $\vec{g}$ , we have to take in account for the torque determination its orthogonal component if the pendulum is vertical.

The weakness of the gravitational attraction obliges to use an astatic pendulum which could have restoring force divided by more than 1000 compared to vertical pendulum.

The natural period of an astatic pendulum (between 15 and 20 seconds) minimizes external perturbations. A classical pendulum would need a length of more than 50 m to reach same sensitivity (see right side of Fig. 1).

For a simple pendulum, the restoring force is  $-mg\sin(\theta)$ . For the center of mass at a distance  $L$  of the axis of rotation, the restoring torque is  $\Gamma = -mgL\sin(\theta)$ . For a Symmetrical Vertical Pendulum (SVP) (see Fig.1, left), the restoring force depends of  $\theta$  proportionally to the addition of the lower torque  $\Gamma_l = -mg(L + \Delta L)\sin(\theta)$  and the upper torque  $\Gamma_u = -m(-g)(L - \Delta L)\sin(\theta)$ . If  $\frac{\Delta L}{L}$  decreases, sensitivity to external force increases until to reach an infinite value at the neutral equilibrium for  $\Delta L = 0$ .

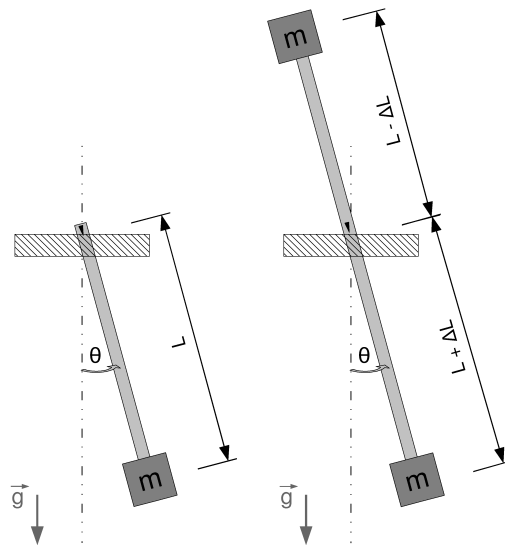


Figure 1: Principle of the simple pendulum (left) and of the astatized SVP pendulum (right).

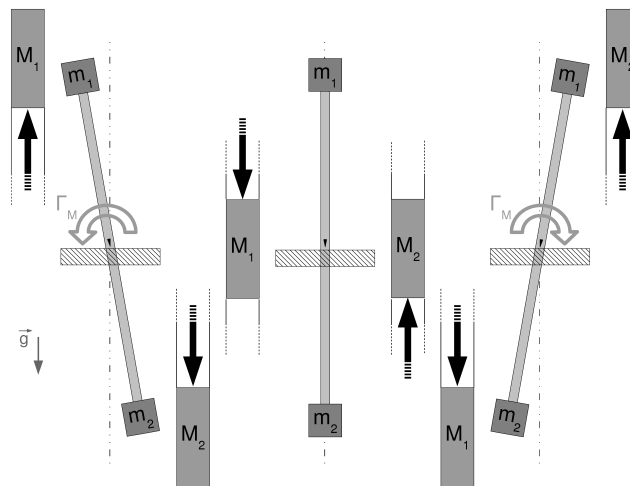


Figure 2: Principle for G measurement.

A belt rolling on a cylinder with horizontal axis of rotation supports two attractive masses which have inverse vertical motion. We control the mass displacement with a stepper motor and a gearbox driving the rotation of this cylinder. The loading of that system on the ground supporting the pendulums become constant (see Fig.2). The equilibrium position of the angular position  $\theta$  of the pendulum figures that the combination of all the torques, equals 0. An additional modulated electrostatic feedback loop could be adjusted to keep  $\theta$  constant.

Principle of SVP obliges to have a very high stability in the positioning of the axis of rotation. To select an appropriate system, a 10kg mass is fixed on a vertical beam supporting the axis of rotation prototype to evaluate (see Fig.3). An optical detector triggers a magnetic pulser keeping in oscillation the pendulum with a minimum of interaction. Periods are recorded by counting a quartz oscillator.

Series of tests confirms high quality of a support consisting in a Stanley<sup>TM</sup> cutter blade N° 1992 pushing perpendicularly on a 3mm in diameter drill rig cylinder used for PCB boring. The prototype pendulum oscillating on 1 second period with such heavy mass did not show abnormal features. The presented system referring to the randomness of

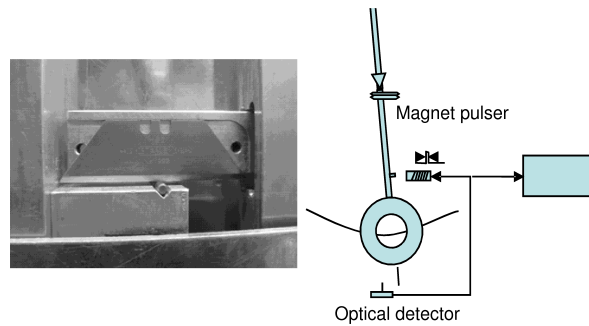


Figure 3: Detail of a blade swivel and the test pendulum principle.

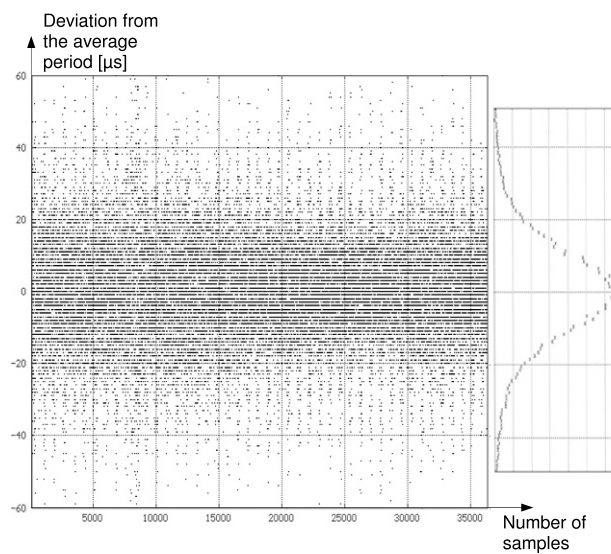


Figure 4: The figure shows an histogram of a series of 45000 periods measurements.

the histogram on 45000 periods (see Fig.4) is well adapted to the requirements of our heavy SVP device.

## 5. SVP scale factor determination

A calibration system is required to refer to the fundamental standards of mass and length with like a secondary standard the well known intensity of the local gravity field.

Figure 5 shows property of torque induction by mass motion. If we move for a pendulum of axis of rotation  $Y$ , a mass  $m$  from point  $P$  to  $P'$  in the earth gravity field parallel to  $Z$  axis, we only have to consider the motion  $x$  to  $x'$  which is the projection of  $P - P'$  on horizontal axis, perpendicular to the axis of rotation.

The low intensity of the measured gravitational forces compared to various random noise sources could reduce the signal / noise ratio. So, we choose filtering by averaging based on stacking method with well known frequencies and modulation on induced periodic phenomena. It improves dramatically the signal / noise ratio by effective rejection of all random noise [Zhu et al. (2009)] [Van Ruymbeke et al. (2003)]. To meet requirement of stacking, we place on the pendulum an analogue watch with tiny needles moved by Quartz mechanism (see Fig. 6). The rotation of two needles produce two periodic sine torque with periods of 1 minute and 1 hour and stable amplitude.

An analogue watch is a simple and suitable solution. Indeed, using current technologies, the electrical power supply and the long term stability of the movement are ensured. The sine torques generated by the rotation of the needles

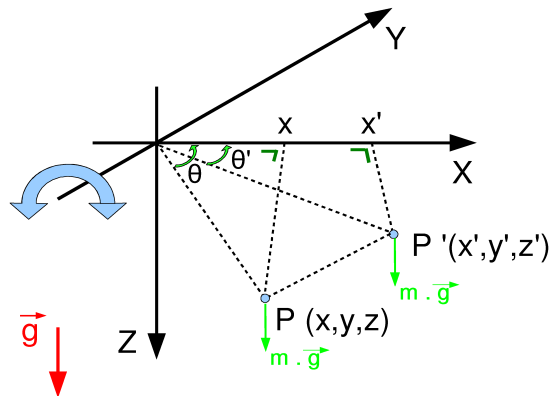


Figure 5: The torque produced by the motion of the mass  $m$  from  $P$  to  $P'$  is equal to  $d\Gamma = |mg(x - x')|$ .



Figure 6: Example of a solar watch mounted on a pendulum pivot for testing

are easy to model. Moreover, a waterproof watch allows to avoid the Archimedes effects due to the changes of atmospheric density. However, the watch manufacturer are unable to achieve needles systems with a repeatability needed for this metrological use. Moreover, the metallic needles are sensitive to thermal gradient (but can be modelled).

Before setting on a pendulum for the  $\Gamma_M \leftrightarrow \Gamma_m$  comparison, the watch has to be calibrated in absolute referring to the fundamental standards of *mass*, *length* and using the value of the Earth gravity field as a secondary standard (known with enough accuracy).

For this calibration of each watch, a specific lightweight optimized pendulum instrument (see Fig. 7) was designed. This instrument embeds the watch and an miniaturized electromechanical system in charge to produce a standard torque  $\Gamma_\mu$ .

Such a system is equipped with a micro brushless DC motor and an epicyclic reducer. The accuracy is limited by the errors of determination of the mass and the amplitude of displacement (see Fig. 8).

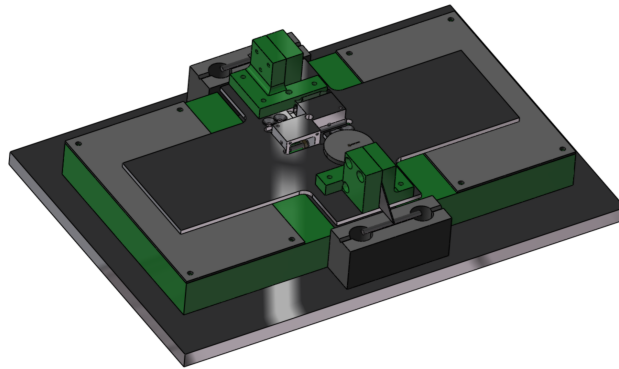


Figure 7: CAD view of the pendulum designed for watch calibration. The DC motor system is set up on the balance in parallel with the watch. The goal of this small lightweight pendulum becomes to conduct the calibration of the watches by direct comparison with two torques related to fundamental units.



Figure 8: Example of a micro motor used for calibration

Given its use of standard, this system has been designed to be embedded on a lightweight pendulum and to enable a relative uncertainty on the torque less than  $100ppm$ . For this specific problem, it is easy to separate the sine wave induced to the watch torque and to the slope generated by the linear motion of the small weight at very slow and constant speed (see Fig. 9).

The advantage of this calibration method is that each watch is individually calibrated. This allows the followings properties:

- As mentioned above, the position of the watch is not critical because, only the projection on the  $X$  axis is inducing a periodic torque (see Fig. 5).
- The individual calibration of each watch enables to mount a series of pendulum instruments, reacting to the movement of a couple of attractive masses. By extension, this allows gravitational optics experiments.
- We can validate the quality of our SVP instrument by monitoring the ratio between the amplitudes of the torques introduced by the rotation of the two needles which must be ideally constant.

The angular deviation of our pendulum instruments are measured through capacitive sensors. They are ideally suited for measuring displacements of such magnitudes. They also allow exerting reaction forces, to fully compensate the displacements. This allows controlling potential causes of errors:

- The mechanical properties of the pivots could induce perturbations like hysteresis.
- The gravitation forces are, of course, a non-linear function of the displacement; this aspect is made more complex due to the calibration features causing additional displacements.

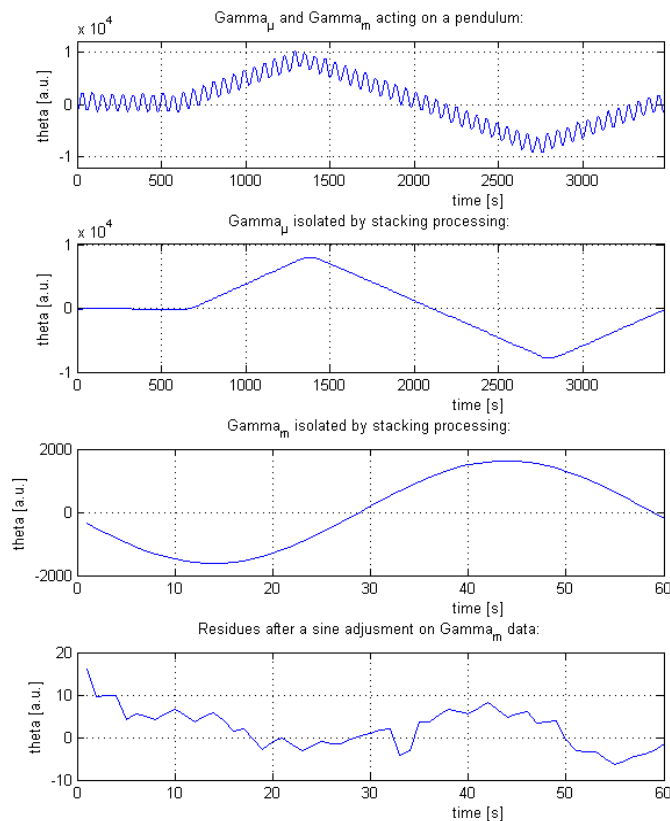


Figure 9: Exeprimental data obtained with a prototype pendulum in 2011 at ROB. The scale factor between the  $\Gamma_{\mu}$  torque (second graph from the top) and the  $\Gamma_{m}$  torque induced by the seconds needle of a watch (third graph from the top) can easily be compared after stacking processing. The amplitude of the residues proves the reality of the technique.

Mastery of these techniques of design, calibration and measurement enables to set up a system composed by three independent SVP, to conduct a new campaign of multi-dimensional gravitational interaction experiments (see Fig. 10). We can fix accurately the relative sensitivity between the three pendulums by the use of three calibrated watches.

The value of  $G$  is evaluated by comparing the measurement of the attractive forces on the 3 pendulum, with their theoretical value obtained by computation. This computation needs an integration by finite elements. We selected the parallelepiped for all elements influencing the result, that is in fact, all moving parts (including translating and rotating ones). Manufacturing parallelepipeds is obviously much easier than spheres

Let us remark that the distance between an attracting and an attracted object is conditioned by the protection features avoiding the pendulum being influenced by drafts, gradients of temperatures, and so on. This results in a minimal distance of 2 or 3 cm.

## 6. Conclusion

This paper describes how to generate calibrated torque on gravitational balance. Calibration of this torque is referenced to a known mass and a fixed motion with its speed expressed in meter and second. The well determined Earth gravity field  $g$  which is proportional to the product  $G \times M$  with  $M$  the Earth mass, induces the modulation of forces which produces the torque acting in the pendulum. So the procedure of calibration only consists in comparison of parameters with same physical dimensions.

Our prototype simply made with aluminium has promising characteristics. It operates without vacuum and shows a high rejection of ground vibration. A large enough support with metal strips fixing axis of rotation could work for



Figure 10: Picture of the set of 3 pendulums (each equipped with a calibrated watch), with a couple of attractive masses, moving vertically up and down. The gravitational torque on each pendulum is directly measured by comparison with two torques of the watches needles.

heavy masses without inelastic problem. The pendulum is calibrated by a fully independent action carried out simultaneously with gravitational measurements. Geometrical discrepancies are well rejected by a symmetrical approach. Improving our methods by a more careful setting of our balance could be justified.

Installing the pendulum in an underground laboratory at constant temperature and pressure could potentially increase the significance of results. We evaluate for the  $G$  SVP balance that the signal-to-noise ratio of 10000 is accessible. A new set of 3 SVP meters the attraction of the two attractive masses moving between them. So we have 3 signatures which allows to trace origin of systematic effects. By comparison of individual output signals it could be possible to detect eventualities of various kinds of effects susceptible to influence  $G$  constant value. By the simplicity of our prototype, this could be a good experimental system to study gravitational physics.

## 7. Acknowledgements

The authors are appreciative to the Royal Observatory of Belgium who provided the necessary support. Francis Renders has built the mechanical parts of SVP. We tank especially Anne-Marie Guillaume and Geneviève Tuts who participate to the development of this project. Funding by Eng. G.Berthault was determinant in the achievement of this research.

## 8. Bibliography

### References

- Naslin, S., 2009. Etude et réalisation d'un procédé expérimental novateur dédié à la mesure de la constante universelle de gravitation  $G$ . Ph.D. thesis. UCL.
- Parks, H.V., Faller, J.E., 2010. Simple pendulum determination of the gravitational constant. *Phys. Rev. Lett.* 105, 110801. URL: <http://link.aps.org/doi/10.1103/PhysRevLett.105.110801>, doi:10.1103/PhysRevLett.105.110801.
- Peter J. Mohr, Barry N. Taylor, D.B.N., 2012. CODATA recommended values of the fundamental physical constants: 2010. *Journal of Physical and Chemical Reference Data* 41.
- van Ruymbeke, M., 1979. Un pendule horizontal à méthode de zéro permet de mesurer la constante de la gravitation universelle  $G$ . Thèse annexe. UCL.
- van Ruymbeke, M., 1980. Description des principales étapes de la mise au point de capteurs capacitifs adaptés aux pendules horizontaux verbaandert-melchior. *B.I.M.*, 5323–5349.
- van Ruymbeke, M., Beauducel, F., Somerhausen, A., 1997. The environmental data acquisition system (edas) developed at the royal observatory of belgium. Short thermal and hydrological signatures related to tectonic activity, *Cahier du Centre Européen de Géodynamique et de Sismologie* 14, 163–174.
- van Ruymbeke, M., Naslin, S., Zhu, P., Renders, F., J-P, N., 2010. Royal observatory of belgium gravitational balance, in: Academia of the RAS, V.G.P. (Ed.), *IAG Symposium on Terrestrial Gravimetry : Static and Mobile Measurements Proceedings, IAG*. pp. 204–207.
- Tu, L.C., Li, Q., Wang, Q.L., Shao, C.G., Yang, S.Q., Liu, L.X., Liu, Q., Luo, J., 2010. New determination of the gravitational constant  $g$  with time-of-swing method. *Phys. Rev. D* 82, 022001. URL: <http://link.aps.org/doi/10.1103/PhysRevD.82.022001>, doi:10.1103/PhysRevD.82.022001.
- Van Ruymbeke, M., Howard, R., Pütz, P., Beauducel, F., Somerhausen, A., Barriot, J., 2003. An introduction to the use of hicup for signal analysis. *BIM* 138, 955–10.
- Wielant, F., van Ruymbeke, M., Naslin, S., Guillaume, A.M., Zhu, P., Tuts, G., J-P, N., 2012. Production d'un couple étalon adapté à une balance gravitationnelle réalisée à l'observatoire royal de belgique. *Revue scientifique des ISILF*, 41.
- Zhu, P., van Ruymbeke, M., Cadicheanu, N., 2009. A stacking method and its applications to lanzarote tide gauge records. *Journal of Geodynamics* 48, 138 – 143. URL: <http://www.sciencedirect.com/science/article/pii/S0264370709001057>, doi:<http://dx.doi.org/10.1016/j.jog.2009.09.038>. new Challenges in Earth's Dynamics - Proceedings of the 16th International Symposium on Earth Tides.

# Geodynamical observations using spatially distributed gravimeters, tiltmeters, and laser strainmeters

V. A. Volkov<sup>a</sup>, M. N. Dubrov<sup>b,\*</sup>

<sup>a</sup> *Shmidt Institute of Physics of the Earth, Russian Academy of Sciences, Bol'shaya Gruzinskaya, 10, Moscow, 123995, Russia*

<sup>b</sup> *Kotel'nikov Institute of Radioengineering and Electronics, Russian Academy of Sciences, Vvedensky sq. 1, Fryazino, Moscow Region, 141190, Russia*

## Abstract

The advanced methodology of geodynamical observations, which is based on accounting of all possible components of elastic body movements, is being developed. This approach means the allowance for simultaneous measuring the Earth surface spatial displacements, tilts (inclinations), and strains (deformations). For experimental workout of this methodology we use the spatially distributed system of pendulum (spring) gravimeters, inclinometers (tiltmeters), and laser deformometers (strainmeters) including equal-arm and unequal-arm configurations. The distance between separate instruments varies from a few hundred meters within local site installations, and up to hundreds kilometers for a different remote sites and observatories, which have been placed within the Moscow region. The experience of the developed method application is discussed and some observational results such as effects of powerful atmosphere and global ionosphere disturbances are presented.

Keywords: Gravimeter, Tiltmeter, Laser strainmeter, Earth oscillations, Earthquake precursors, Hurricane

## 1. Introduction

Investigators when studying geophysical processes have to concern with a wide variety of natural and artificial phenomena and occurrences. Nevertheless, all processes in the Earth can be divided in two basic categories:

- (i) The processes occurring in the Earth continuously and being excited by the external forces: the tidal deformations of the whole Earth due to tidal gravity forces of the Moon and the Sun, microseismic oscillations spreading along the Earth crust under influence of permanent dynamical processes in atmosphere and oceans.
- (ii) The processes that occur after any events: earthquakes, volcanic eruptions, typhoons (hurricanes), etc. They are the seismic waves, the free oscillations of the Earth, the fault creeps, and slow earthquakes, tectonic shifts and other spontaneous occurrences in the solid Earth body. These processes are so-called the event-processes.

For an instrumental recording of tidal processes the extended class of devices with high sensitivity, stability, and wide dynamic range has been developed: tidal gravimeters (seismo-gravimeters), tiltmeters (seismo-tiltmeters), and extensometers (strain-seismometers). These instruments being good for measurements the diurnal (semidiurnal) and seasonal tidal deformations of the Earth with the high accuracy also can be used to record the ultra-small ground oscillations (i) occurring in a wide frequency range permanently, as well as to detect non-periodic event processes (ii) in the Earth crust. Comprehensive investigations of all these phenomena are important for understanding both origins of natural disasters (earthquakes, hurricanes), and mechanisms of coupling the processes observed at the solid Earth and in the adjacent geospheres.

---

\* Corresponding author. Tel.: +7 496 56 52440

E-mail address: mnd139@ire216.msk.su (M.N. Dubrov)

Selected experimental results, which were obtained during past decades, are presented and discussed in this paper. The results show a measure ability of the developed instrumental techniques and demonstrate their application for research of poorly studied phenomena.

## **2. Methodology and Instrumentations**

Gravimeters especially super-conducting (cryogenic) gravimeters are the most precise devices for the tidal processes investigation now. But the gravity tides that are measured by these instruments contain only the vertical component of the tidal force. If we want to study completely Earth crust deformations, it is necessary to measure also the horizontal components. The contribution of the elastic deformation of the Earth to the direct gravimetric signal is close to 25% or 15% if we consider the atmospheric pressure or tidal force variations respectively, while it reaches 30% for tidal tilts (Melchior, 1983). Strainmeters, especially laser strainmeters are the only ground based instruments measuring directly the Earth deformation with accuracy  $10^{-10}$  and better (Takemoto et al., 2006; Kravtsov et al., 2011) that can be compared with the accuracy of the modern gravimeters. At last, the full representation of the Earth surface motions requires simultaneous observations with gravimeters, clinometers and strainmeters.

From the other hand the necessity of horizontal deformation measurements is caused by the constitution of upper layers of the solid Earth which are fragmented and consist of a number of geo-blocks. The vertical dimensions of the lithosphere strata are less than 1% of the globe radius. The rest of the Earth body includes the solid or liquid strata: asthenosphere, mantle, and core where transversal tensions are small. Therefore the effective scale estimations of horizontal inhomogeneities of the observed deformations of the Earth are very important, and they could be determined as a result of our measurements. These estimations may elucidate the nature and origins both the continuous (i) and event (ii) processes mentioned above owing to the characteristics of their spatial distribution. These features can be specified in every observed phenomenon just by spatially distributed instruments, which are fit to measure both the vertical deformation (through variations of gravity) and horizontal tilts and strains of the Earth surface. With application of such techniques the distinctions between local and global processes and similarly between endogenous and exogenous phenomena in the Earth will be available.

Three different kinds of precise geophysical instruments have been applied to deformation measurements of the Earth surface. Two of them use the inertial and gravitational properties of mass of the accurate pendulum: gravimeter (seismo-gravimeter) and tiltmeter (seismo-tiltmeter). The third one: precise laser interferometric strainmeter measures relative displacements of two points at the Earth surface to which the interferometer is anchored.

The improved and modernized ASCANIA gravimeter GS-11 and portable tiltmeter station have been used in presented experiments. The objective in improvement of pendulum registration systems was to extend the characteristics of instruments: sensitivity, stability, dynamical and frequency ranges. Research and developments have been fulfilled in the Institute of Physics of the Earth. The design of a capacitive displacement transducer of pendulum in an electric field (Volkov et al., 1985) allowed the next instrument characteristics to be obtained: pendulum displacement resolution of 10 nm, tidal gravimeter resolution of 0.2  $\mu\text{Gal}$ , vertical accelerometer resolution of 20 nGal with a bandwidth from 200 s to 5000 s. Additionally two long-period seismic channel with bandwidths 10-100 s and 10-1000 s have been realized. Selective results of processes (i) and (ii) registration by seismo-gravimeter are shown in Fig.1 (a, b) and Fig.4 (c).

### *2.1. Two-components tiltmeter NP-IM*

The composition of tiltmetric station includes: sensor, control electronics, and recording equipment. Sensor operation is based on the principle of vertical pendulum. Sensor consists of 100 mm vertical pendulum which is mounted on the base with three adjustable screws. The main components are mounted

in the case which is protected by the sealed cap. The control unit can be connected to the sensor by signal cable with lengths up to 1 km.

Tiltmetric station is designed for the measurement of the relative slopes of the Earth surface in two mutually perpendicular directions. The aims: studying the tidal deformation; studying the modern movements of the Earth crust; finding earthquake precursors in the form of abnormal tilts and strains; tests of bases and parts of large engineering structures. Tiltmeter resolution is estimated as 1 milliarcsecond (mas) of in tidal channel and 0.1 mas in seismic-accelerometer channel. Tiltmeter with horizontal pendulum installation has been also used in our observations (Kalinina et al., 2004). The highest resolution of this instrument is estimated as 0.1 mas in tidal channel and 0.01 mas in seismic-accelerometer channel. Selective results of registration of processes (i) and (ii) are shown in Fig.2 (a, b).

## 2.2. Laser interferometers, extensometers, and strain-seismometers

Investigations and developments of laser interferometers for geophysical measurements are being carried out in the Institute of Radio-engineering and Electronics (IRE RAS) in cooperation with the Institute of Physics of the Earth (IPE RAS) since 1970th (Dubrov et al., 1989). The number of new prototypes of laser interferometers, deformometers, and strain-seismometers have been developed and tested during last decades. Laser deformometers (strainmeters) with horizontal and vertical arm orientations both equal-arm and unequal-arm configurations have been investigated. The original optical schemes of laser instruments provided with special procedures of recording and signal selection were used and the field observation experience was accumulated.

Two versions of laser strainmeters for geophysical and seismological application have been developed. They include jam-proof laser feedback interferometer prototypes (path length varies from 10 m up to 850 m), and unequal-arm Michelson interferometers with length of 1-10 m. The first one has resolution of 1 nm on the basis up to 300 m. The resolution of Michelson interferometer recorder is about 1 pm under 180-190 dB dynamic ranges in 1 Hz frequency band. The top relative strain resolution is  $dL/L = 10^{-11} - 10^{-12}$ , frequency range  $10^{-6} - 10^2$  Hz. The digital PC data acquisition systems extend the recording and analyzing range up to 0.1-1 kHz. The instruments allow the wide variety of the Earth surface displacements and strains to be measured with high accuracy without vacuum or evacuated facility. The number of spatial distributed laser instruments were installed and tested both in non-seismic area (Moscow Region) and in active seismic (Pamir and Tien Shan) regions. Selective results of registration of processes (i) and (ii) by different laser strainmeters are shown in Fig.3 (a, b) and Fig.4 (a, b).

The example of records of microseismic storms 4-6 s (0.17-0.25 Hz) presented in Fig. 4(a) has been made by simultaneously operated and spatially distributed laser strainmeters. The first of them (IRE RAS testing site, Fryazino) has measuring arms about 500 m, and the length of the second strainmeter (Observatory Protvino) is 16 m, distance between these instruments is 135 km (Dubrov et al., 1989). Both strainmeters have recorded the clear pulsing waves with the relative amplitudes  $dL/L \sim 10^{-10}$  and about of 1 minute retardation; instrumental resolution is the order of  $10^{-11}$  relative units.

High frequency microseisms or “micro-tremors” (1-100 Hz) have artificial origin on the whole. They are generated by human activity and sometimes occur as a result of sharp weather changes. These microseisms contain both surface and body waves which lay the information not only about of industrial machine operations but also on the Earth interior especially on upper layers of the solid Earth, where the earthquake precursors may develop (Dubrov et al., 1987). Fig. 4(b) shows the results of time-frequency analysis of microseism recordings made by two laser strainmeters: (1) within 2-3 m underground at IRE RAS testing site (Fryazino), and (2) about 30 m in depth (Obninsk Observatory) being 140 km apart. Two instruments near of the same lengths (100 m and 90 m respectively) record quite different tremors in 0.5-3.5 Hz frequency band (Kravtsov et al., 2011). The weak spectral components with amplitudes up to  $dL/L \sim 10^{-12}$  can be resolved.

### 2.3. Records with gravimeters

The example of data processing in ultra-low frequency band is shown in Fig. 4(c). Free oscillations of the Earth, being excited after powerful Sumatra M=9.1 earthquake and recorded by seismo-gravimeter in Obninsk (Fig. 1 a, b) have been filtrated in frequency band of the fundamental mode  ${}_0S_2$ . The rotational overtones of the main mode  ${}_0S_2$  (53.94 minutes) produced the pulsing signal of 27 days duration (Fig. 4 c). In result of spectral splitting four overtones: 52.33 minutes, 53.11 minutes, 54.79 minutes, and 55.48 minutes have been revealed. The regular discrepancy of the order of 0.3% - 0.7% with Bullen's model have been found. It demonstrates that improved and modernized vertical pendulum gravimeter with accurate recording system is available for high precision measurements when combining with sensitive tiltmeters and laser strainmeters. The suggested methodology and instrumentations, which are based on the multicomponent and spatially distributed measurements of the Earth motions, are the new approach to geophysical observations.

### 3. Results and Discussion

During long-term observations many authors detected the Earth background free oscillations excited on seismically quiet days, see e.g. review in (Petrova, 2000). The oscillations have a time-dependent intensity and intensity increases have been observed before strong earthquakes (Petrova and Volkov, 1996; Volkov et al., 1999).

There are two types of background signals in frequency band 0.05-0.5 mHz: (1) the oscillations existing in frequencies known as modes of free Earth oscillations after earthquakes, and (2) the oscillations which are not identified with those modes. The nature of these continuously excited background signals is under debate now. The amplitudes of free oscillation modes (1) are too high to be attributed to weak earthquakes and their origin has been related to atmospheric disturbances (Kobayashi and Nishida, 1998). The oscillations of type (2) may be connected with such powerful processes in the World Ocean as tropical cyclones: typhoons and hurricanes (Golovachev et al., 2011). Therefore the disturbances in atmosphere and hydrosphere of the Earth are much probable sources of continuous processes as well as event processes that force the Earth crust (Klügel and Wziontek, 2009).

The multiform interactions of lithosphere and atmosphere disturbances have been first investigated and analyzed in detail by the synchronous operating and spatial distributed seismo-gravimeter, tiltmeter, and laser strainmeter (Dubrov et al., 2000). The joint data analysis from sites being apart at 140 km one from another has been carried out. The dynamic disturbances in the atmosphere were found to have the wave microstructure and to be accompanied by complicated Earth surface strains, tilts, and gravity variations. These interactive "waves" propagate along the atmosphere-ground boundary with the velocities of 30 - 50 km/h. Owing to partial coherency they would hamper the precise geophysical data acquisition. However the correct knowledge of those ground motion mechanisms would provide new technique for the Earth material testing (Volkov et al., 1999).

The ultra-long period (3 minutes...6 hours) oscillations of the Earth together with the atmospheric pressure micro-variations in the same period range were investigated during last decades (Petrova and Volkov, 1996). This type of disturbances were for the first time identified in the result of data analysis of observations made by seismo-gravimeters of different design in 1987 (St. Petersburg and Obninsk) and 1992 (St. Petersburg, and Borovoe, Kazakhstan). The similar signal was found when analyzing synchronous observations made with a seismo-gravimeter installed in St. Petersburg and a quartz strainmeter in Apatity during May 3-10, 1993. The essential growth of 4-5 hour period disturbances during 2 days before the earthquake March 25, 1998,  $M_p,s=7.0-7.9$  have been observed by a laser strainmeter and seismo-gravimeter in Moscow region (Volkov et al., 1999).

The growths of oscillation intensities discovered before the earthquakes in April 29, 1987 (Iran), December 12, 1992 (Indonesia), and May 11, 1993 (Philippines), were identified as traveling disturbances lasting 85 – 120 h and having slight excess about the mean amplitude, common spectral components, and stable shapes of the envelope along the propagation path. It is important that these observations were conducted during the periods of low seismic activity, and the disturbances were observed before strong earthquakes.

### *3.1. Co-seismic processes preceding the Sumatra M=9.1 earthquake*

The analysis of the “bursts” of periodic oscillations and their synchronization before strong earthquakes have been recently reported (Sobolev, 2011). Three earthquakes with magnitudes  $M = 7.8 - 9.1$  were considered: Kronotskoe earthquake (December 5, 1997), the Hokkaido earthquake (September 25, 2003), and the Sumatra earthquake (December 26, 2004). It is important that “bursts” before two of these earthquakes could be attributed to powerful atmospheric excitations in result of strong tropical cyclones in the North-West Pacific Ocean. They are: typhoon PAKA, November 27 - December 21, 1997 (Sobolev, 2011) and super-typhoon MAEMI, September 09-13, 2003, which was followed by two less intensive tropical cyclones in NW Pacific (Golovachev et al., 2011). The both powerful cyclones PAKA and MAEMI had the highest Category 5 SSHS with maximum wind velocities of 260 km/h and 280 km/h respectively. The third event of the “burst” oscillations before the strongest Sumatra  $M=9.1$  earthquake on December 26, 2004 was assumed (Sobolev, 2011) to be attributed to another remote earthquake which occurred 3 days earlier (Macquarie earthquake, December 23, 2004,  $M = 8$ , 49.31 S–143.91 E, see Fig.1a) and any typhoons had not been taken into account. It was the cause what made this kind of earthquake precursors ambiguous (Sobolev, 2011).

Let us consider co-seismic processes preceding the Sumatra  $M=9.1$  earthquake (Fig.1 a, b, Fig.2 b, and Fig.4 c) in more detail. Data from tiltmeters and strainmeters, which measure horizontal components of deformation, seem to be more appropriate for this goal than gravimeters, which measure vertical motions of the Earth surface (Section 2). Results of tilt measurements from Observatory Jezeri (Czech) obtained in November-December 2004 were taken for analysis. Two months of 10-minutes sampling data have been divided in two fragments of 30 days durations which are presented in Fig.5 (a, b). Peak-to-peak amplitudes of the semidiurnal tidal waves vary in the range of 0.2–0.4 msec and slightly irregular drifts of 0.1–0.2 msec per day are observed.

These fragments, each containing 4320 samples have been developed by computer spectral-temporal subroutine with 25% analyzed window. The results of Time-Frequency analysis of these data fragments are presented in Fig.5 (c, d). Diurnal and semidiurnal tidal waves are marked on both diagrams as two contrast horizontal bands at frequencies near 0.012 mHz and 0.022 mHz. Their maximum amplitudes vary between 0.03-0.04 relative units (see column to the right of each diagram). The November time-frequency diagram contains additionally the intense disturbance of spectral components at ultra-low frequencies beyond 0.003 mHz with amplitudes up to 0.1 relative units. This disturbance has probable strain-baric origin and may be related to occurrence of Intense Tropical Cyclone BENTO Category 5 (SSHS) in South-West Indian Ocean during November 19 – December 4, 2004. The peculiarity of December diagram consists in a especial sort of disturbances with increasing frequencies from 0.002 mHz to 0.006 mHz during December 14-21, 2004. The amplitudes of spectral components have the order of tidal wave amplitude and they have appeared a few days just before the powerful earthquake into consideration. No more tropical cyclones with Category  $> 1$  (SSHS) were observed in Pacific, Atlantic or Indian Ocean in the second half of December, 2004 while extra-tropical cyclonic activity was recorded by observatories in Europe and Asia in this period (<http://www.eas.slu.edu/GGP/sumatra2004/>). The spectral and temporal features of the considered eventual perturbations are similar to the other events of oscillation “bursts” mentioned in (Sobolev, 2011). Therefore, in the all three occurrences of powerful earthquakes (December 5, 1997; September 25, 2003; December 26, 2004) the hurricanes or typhoons

were followed by the arising of the Earth oscillations. This result makes such kind of short-term earthquake precursor to be more attractive and sufficiently probable.

### 3.2. Global geophysical disturbances on March 15, 2013

The geophysical event-processes (ii) may have their origin in the Earth interior (earthquakes, volcanoes), in atmosphere and ocean (typhoons, hurricanes), as well as in ionosphere (geomagnetic storms, auroras), and in the space (sun flare and ejections, flight of comets or meteorites). All of them eventually may have sufficiently high power and bring considerable victims and destructions.

Let us consider the recent example of geophysical disturbances of extra-terrestrial origin, which have been recorded by spatially distributed instruments on March 15, 2013. Data from three measuring sites in the East Europe are presented: Geophysical Observatory Jezeri (Czech), IRE RAS Testing Site (Fryazino) and IZMIRAN Space Weather Prediction Center (Troizk, Moscow Region).

After the Last Quarter Moon on March 4, 2013 the Observatory Jezeri NS tiltmeter has recorded near a smooth sinusoidal semi-diurnal tidal wave with rising amplitude from 2 msec to 8 msec till the New Moon on March 11. The oscillating disturbances with 1-2 h periods appeared at smooth recording traces on March 14-15 (see Fig.6 a). The maximum 1-2 msec amplitude of these oscillations was observed between 12-14 h on March 15. The synchronous atmospheric pressure variations with opposite sign are clearly seen at the atmospheric pressure trace (Fig. 6 b) in Jezeri. Much more contrast irregular waves of atmospheric pressure with amplitudes up to 0.7-0.8 hPa were recorded in Troizk (<http://forecast.izmiran.ru/>) about two hours later and Fryazino about three hours later (between 14-16 h, Fig. 6 c, d).

Atmospheric conditions in two close sites Troizk and Fryazino were strongly correlated owing to powerful snowfall in Moscow region on March 15, 2013. The correlation of geophysical processes recorded at the remote sites (Czech - Moscow region) is indirectly confirmed by the comparison of geomagnetic data from Troizk (Fig. 7 a) and tiltmeter data in Jezeri (Fig. 7 b). The mentioned above low period disturbances on tiltmeter track being started at ~5h30m in Jezeri coincides with the beginning of magnetic field variations in Troizk (they are indicated by arrows in Fig. 7 a, b). Distance between these sites is near 1600 km; therefore geophysical processes in consideration may not to be attributed to any local phenomena. Similarly the spreading of irregular tilt-baric waves from Czech to Moscow region cannot be related to atmosphere motion: the value of signal retardation is too small to substantiate this way of its propagation. Existence of magnetospheric disturbances in the observed processes means that ionospheric layers have to be also involved (Dubrov and Smirnov, 2013) and extra-terrestrial phenomena origin would be quite probable. Indeed, it is the comet C/2011 L4 (PanSTARRS) transited between the Earth and the Sun on March 2013 that may ground the occurred situation. Comet PanSTARRS was closest to the Earth on March 5, 2013 (approach about  $1.6 \cdot 10^8$  km) and it was closest to the Sun on March 10; since then it has been receding from the Sun and Earth, heading back to the outer solar system. During its transit in March 10-18, 2013 the geostationary satellite GOES15 of Space Weather Prediction Center (NOAA, USA, <http://www.swpc.noaa.gov/index.html>) recorded every day events of an arising X-ray flux. The maximum of those events occurred on March 15 and had outstanding intensity above  $1 \cdot 10^{-5}$   $W \cdot m^{-2}$  this day (see Fig.7 c). The beginning of this X-ray event was happened in ~5h30m on March 15 and coincided with the start of geomagnetic variations and low-period disturbances in tiltmeter data (see arrows in Fig.7 a, b, c). Satellite GOES13 being  $14^\circ$  to the East on the geostationary orbit began to record the essential growth of proton flux after 19 h this day (see Fig.7 d). The synchronization of X-ray (c) variations detected at high space orbit together with ground-based magnetometer (a) and tiltmeter (b) is observed with small retardation, which is used to be a few orders greater for common solar occurrences. This moment has been critical for Troizk instruments - pressure and geomagnetic recordings were stopped this time (Fig.6c and Fig.7a) for 2 days. The growth of proton flux was being continued for 2 days, reaching above two order of magnitude with maximum level over  $10$  particles $\cdot$ cm $^{-2}$  $\cdot$ s $^{-1}$  $\cdot$ sr $^{-1}$  and was

finished by strong geomagnetic storm with  $K_p=6$  on March 17. Furthermore, Friday March 15, 2013 was an unusual day also due to other events: besides the Troizk instrument irregularities, the operations of laser strainmeter (Fryazino), tiltmeter (Pribram, Czech), and X-ray receiver at GOES15 were partially broken too; heavy snow precipitations provoked many destructions and edifice fractures in Moscow Region this day.

#### **4. Conclusion**

The extended abilities of the wide-band tidal recording instruments for non-traditional geodynamic observations have been shown. Two specific examples of global high power processes in atmosphere and space are presented and their probable influence upon the Earth surface deformations has been manifested. The results have been obtained by using the system of simultaneously operating and spatially distributed wide-band tidal recording instruments: pendulum gravimeters, tiltmeters, and laser strainmeters. Such complementary information seems to be very important when poorly studied phenomena are investigated. The main feature of our approach is the simultaneous application of various spatial components of earth ground motion (vertical displacements, horizontal strains and tilts.)

Two types of background signals have been observed in ultra-low frequency band 0.002-0.5 mHz: (1) frequency modes of free Earth oscillations, and (2) the oscillations which are not identified with those modes. These signals being partial coherent could hamper the precise geophysical data acquisition. However the correct knowledge of those ground motions would bring the new technique for the Earth material testing. There is an opportunity to use atmospheric variations as sounding signal to study the elastic properties of the crust.

Comparison of spatially distributed ground-based data with accompanying processes in atmosphere, ocean and ionosphere seems to be presented at first time. We suppose that deployment of the detailed mechanism of the atmosphere and adjacent geospheres connections with processes in the solid crust would give a chance to understand the physical mechanisms of interaction of powerful processes at the Earth and in the Solar system, as well as to find the regularity and origins of such natural disasters as earthquakes and hurricanes.

#### **Acknowledgements**

Tiltmeter data sets from Geophysical Observatory Jezeri are kindly provided by Institute of Geophysics, Czech Academy of Sciences. We thank Dr. Jan Mrlina, as well as the engineers Peter Skalsky and Vaclav Polak for supplying data sets and their assistance in the recording data interpretation. We express our gratitude to Prof. B. Ducarme for the valuable comments and kind assistance in gravity tides estimating, which have made this publication to be possible.

#### **References**

- Boyarsky E.A., Vasil'ev I.M., Suvorova I.I. 2001. The Study of Tilts and Strains at the Protvino Geophysical Station, *Izvestiya, Physics of Solid Earth*. 37, 764-770.
- Dubrov, M.N., Karmaleeva, R.M., 1976. Analysis of operation of equal-arm laser extensometer and its comparison with bar extensometer, *Izv. Akad. Nauk SSSR Fiz. Zemli*, N7, pp. 81-89 (in Russian).
- Dubrov M.N., Yakovlev A.P., Alyoshin V.A., 1987. On a link of high frequency microseismic deformations with a stress condition of lithosphere. *Dokl. Akad. Nauk SSSR*. 293, 1085-1089.
- Dubrov M. N., Alyoshin V.A., Yakovlev A.P., 1989. Wideband laser strainmeters as a new instrument for geophysical research, *Gerlands Beitr. Geophysik*. 98, 292-300.

- Dubrov M.N., Matveev R.F., Volkov V.A., Latynina L.A., Ponomarev A.V., 2000. Strain, tilt, and gravity monitoring of long period and seismogravity oscillations. Proceeding of the Ninth International Symposium on Recent Crustal Movements CRCM'98, November 14-19, 1998, Cairo, Egypt, NRIAG, 2000, vol. 1, pp.167-178.
- Dubrov, M.N., 2010. Earthquake precursors: stratification and detection by laser strainmeter system, Proceeding of 5th International conference "Sun-Earth links and physics of earthquake precursors", Paratunka, August 2-7, 2010, Petropavlovsk-Kamchatskiy, IKIR DVO RAN, 2010, pp.368-371. (ISBN 978-5-7442-1498-2, in Russian)
- Dubrov, M.N., Smirnov V.M., 2013. Interdependent Perturbations of the Earth's Surface, Atmosphere, and Ionosphere, Geomagnetism and Aeronomy, vol. 53, No. 1, pp. 49–59. © Pleiades Publishing, Ltd., 2013.
- Golovachev S.P., Dubrov M.N., Volkov V.A., 2011. The Interaction between the Tropical Cyclogenesis and Seismic Activity as Derived from Spacecraft and Ground-Based Measuring Systems, "The Modern Problems of Remote Sensing the Earth from the Space", vol. 8, N1, pp.232-238 (in Russian).
- Klügel, T., Wziontek, H., 2009. Correcting gravimeters and tiltmeters for atmospheric mass attraction using operational weather models. *J. Geodyn.* 48, 204-210.
- Kalinina A.V., Volkov V.A., Gorbatikov A.V., Arnosó J., Vieira R., Benavent M., 2004. Tilt observations in the normal mode frequency band at Geodynamic Observatory Cueva de los Verdes, Lanzarote. *Pure and Applied Geophysics. Special issue "Geodetic and geophysical effects associated to seismic and volcanic hazards"*, N161, pp. 1597-1611
- Kobayashi, N., Nishida, K., 1998. Continuous excitation of planetary free oscillations by atmospheric disturbances. *Nature.* 395, 357-360.
- Kravtsov V.V., Dubrov M.N., Remontov M.S., 2011. Detection of solid Earth excitations by laser seismo-acoustic antenna array. Proceeding of the VIII International Conference on Antenna Theory and Techniques, September 20-23, 2011, Kyiv, Ukraine, pp.117-119.
- Melchior P., 1983. *The tides of the Planet Earth*, Pergamon Press, 2nd edition, 641 pp.
- Petrova, L., Volkov, V., 1996. Dynamic features of seismo-gravitational oscillations of the Earth. *Report Acad. Sci.* 41, 683-686.
- Petrova, L., 2000. The seismic process in the frequency range 0.05-0.5 mHz: patterns and peculiarities, *Volc. Seis.*, 21, 573-585.
- Sobolev G.A., 2011. Seismicity dynamics and earthquake predictability. *Nat. Hazards Earth Syst. Sci.* 11, 445–458.
- Takemoto, S., H. Momose, A. Araya, W. Morii, J. Akamatsu, M. Ohashi, A. Takamori, S. Miyoki, T. Uchiyama, D. Tatsumi, T. Higashi, S. Telada and Y. Fukuda: A 100 m laser strainmeter system in the Kamioka Mine, Japan, for precise observations of tidal strains, *J. Geodyn.*, 41, 23-29, 2006.
- Volkov V.A., Iordanov I.D., Rogatnev I.I., 1985. Preliminary results of observations by means of capacitive seismogravimeter. Collected articles "Slow deformations of the Earth and its rotation", *Acad. Sci. USSR, Soviet Geophys. Comm.*, Moscow, 1985 (in Russian).

Volkov V.A., Dubrov M.N., Matveev R.F., 1999. The lithosphere and atmosphere interaction activity and its possible connection with coseismic process. IUGG'99 (XXII General Assembly of the International Union of Geodesy and Geophysics, Birmingham, 18-30 July, 1999), Abstracts (week A and B), p.171  
<http://www.iugg.org/assemblies/1999birmingham/1999abstracts.pdf> (accessed Sep. 2013)

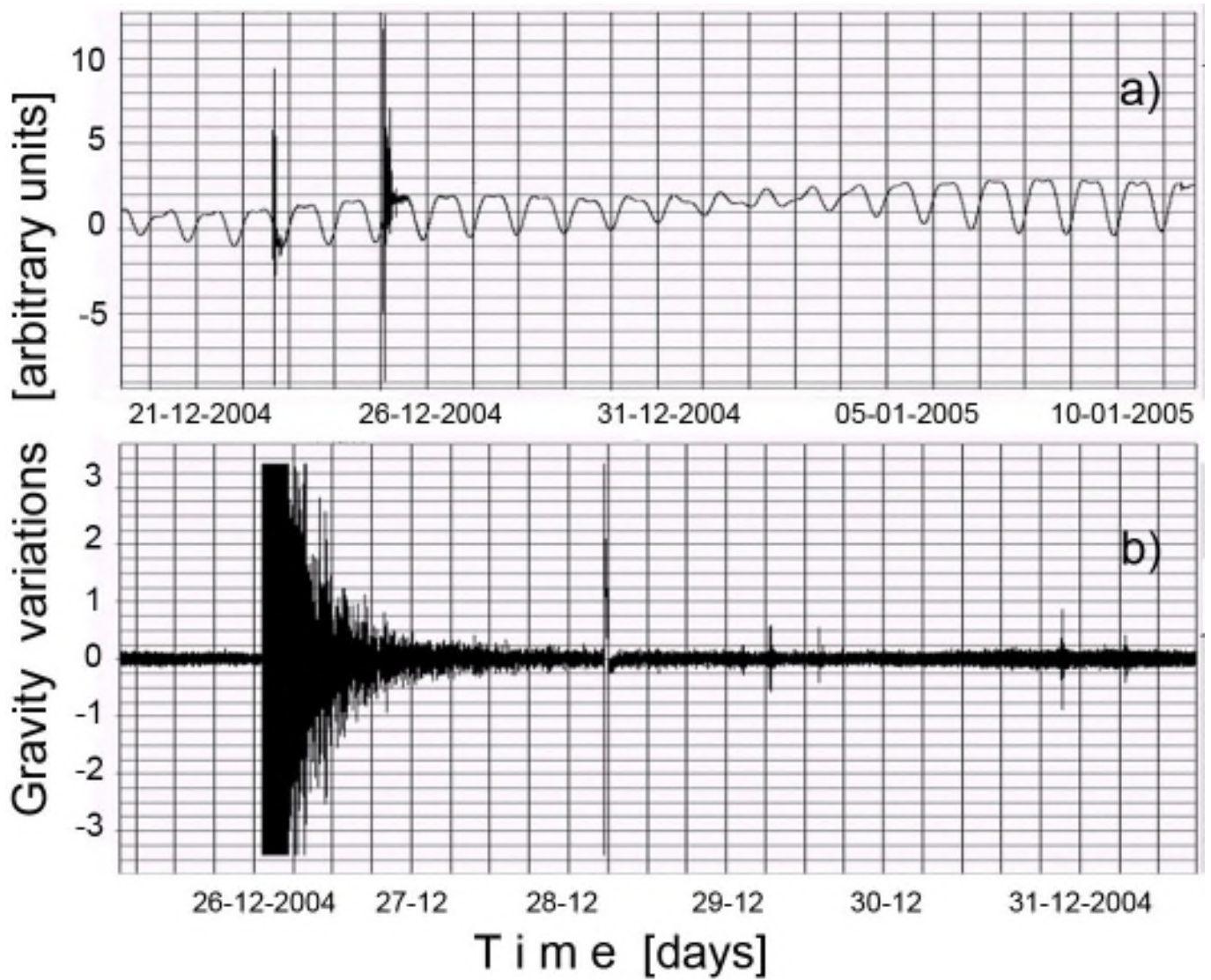


**Fig. 1.** Seismo-gravimeter records from Obninsk Geophysical Observatory: a) unfiltered tides together with Macquarie (December 23, 2004,  $M = 8$ ) and Sumatra (December 26, 2004,  $M=9.1$ ) earthquakes; b) acceleration channel, Sumatra, December 26, 2004,  $M=9.1$  earthquake.

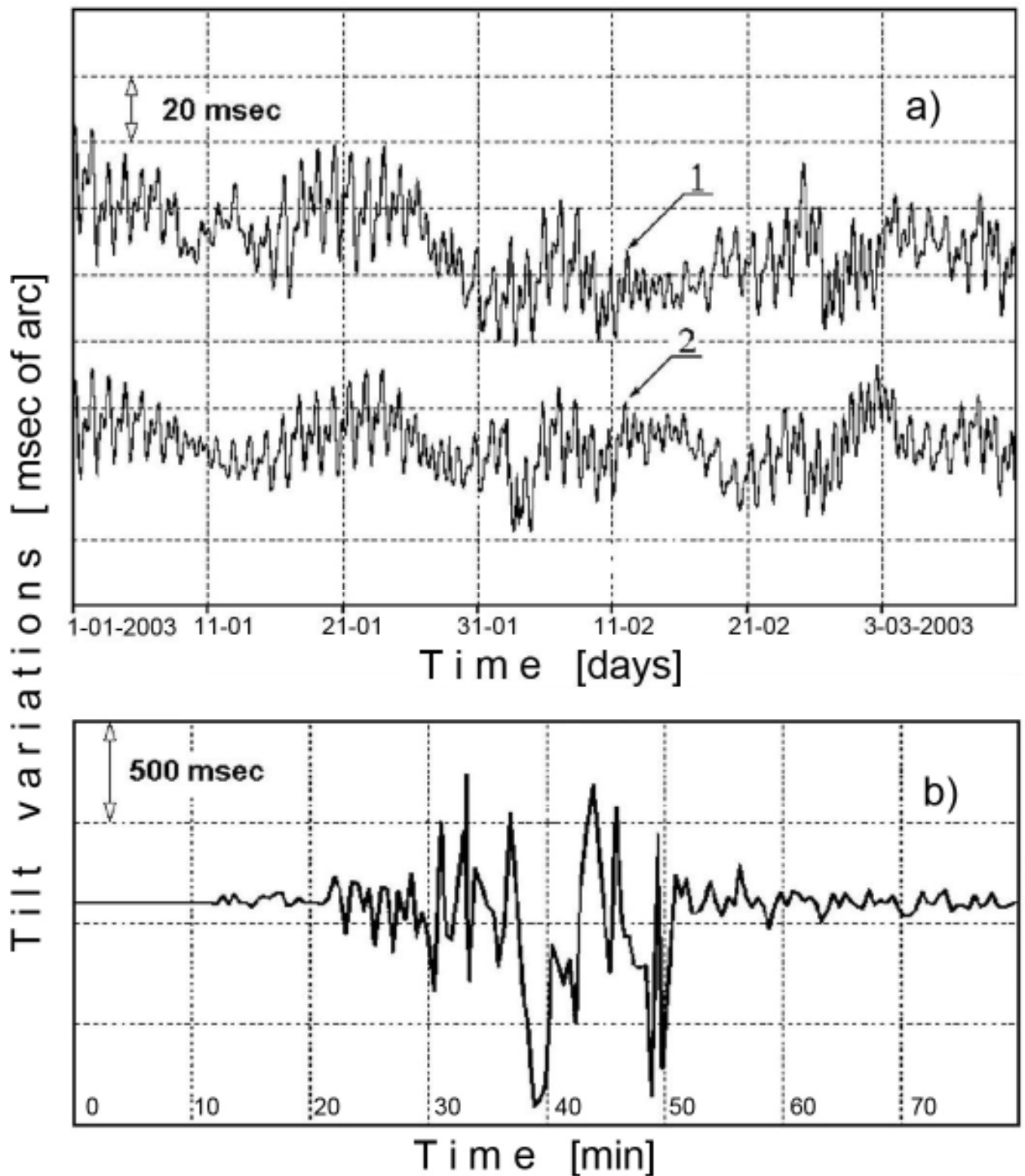


**Fig. 2.** Samples of tiltmeter records from Protvino Geophysical Observatory in Moscow region – installation on the massive concrete bases 15 m underground (Boyarsky et al., 2001): a) two-month unfiltered signal in tidal band (sensors 1 and 2 are located about of  $D=15$  m apart); b) seismic channel, Sumatra, December 26, 2004,  $M=9.1$  earthquake.

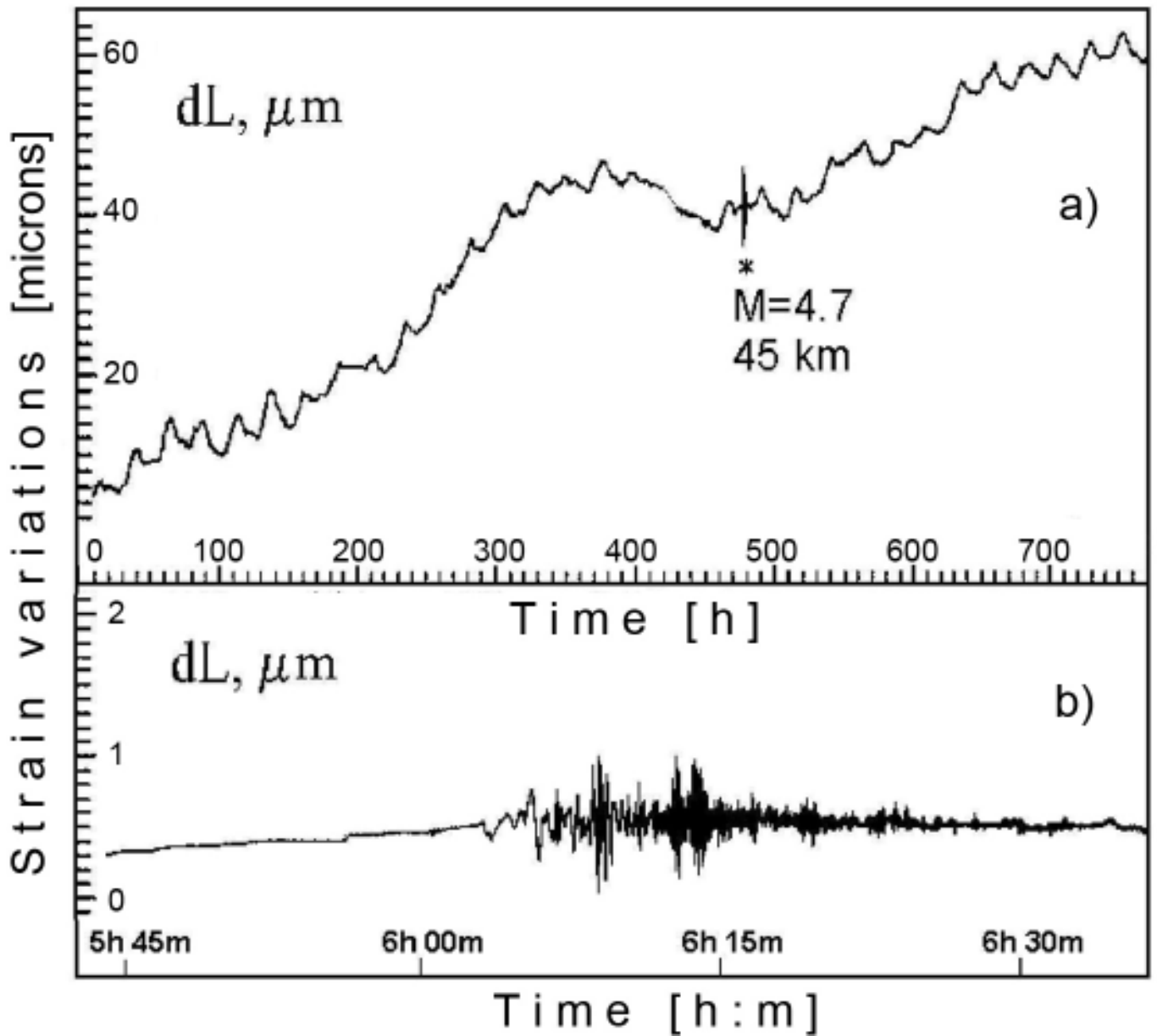


**Fig. 3.** Recordings made by two different laser strainmeters with 100 m measuring arms: a) tidal-band deformations of the Earth surface (anomalous variation of a mean diurnal velocity of rock tension) before regional earthquake  $M=4.7$  in Pamir (Dubrov, 2010); b) Laser extensometer (equal-arm interferometer at IRE RAS underground beam wave-guide, Moscow region) records the earthquake in Atlantics (Dubrov and Karmaleeva, 1976).

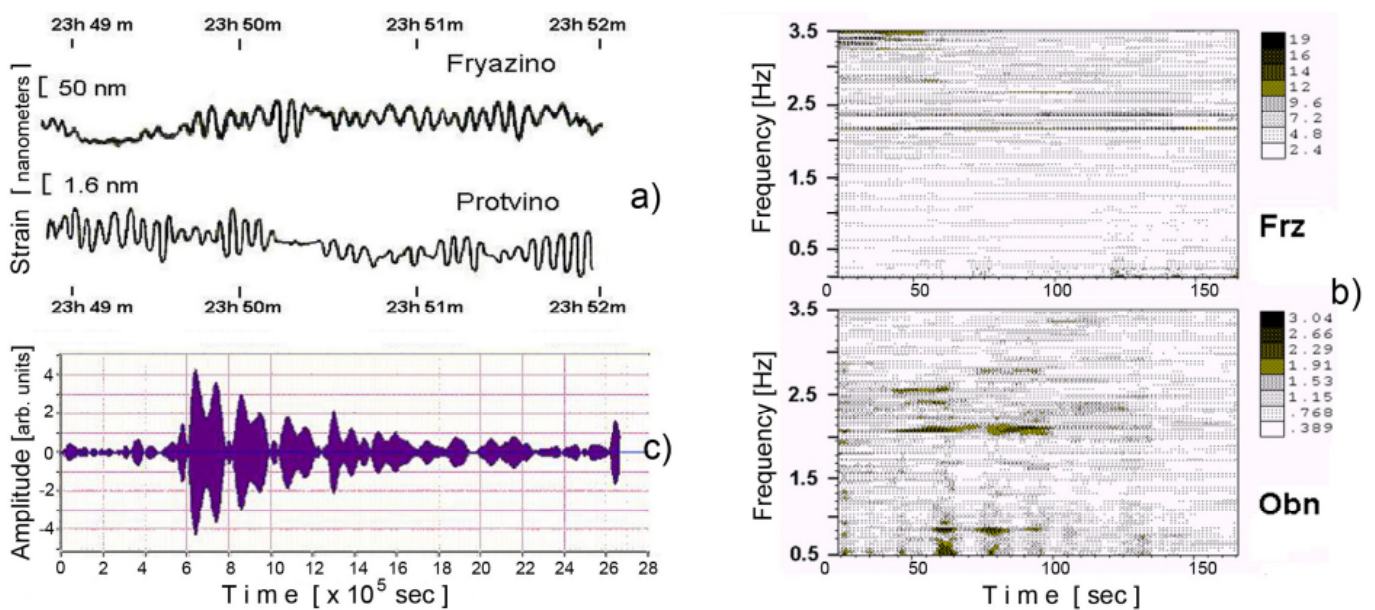


**Fig. 4.** Results of continuous (i) and event (ii) processes registration: a) long-path laser strainmeter in Fryazino (500 m) and Protvino (16 m) synchronous records of storm microseisms from Atlantic; b) time-frequency diagrams of high frequency microseisms detected by laser strainmeters in Fryazino (Frz) and Obninsk (Obn); c) free oscillations of the Earth in frequency band of the fundamental mode  ${}_0S_2$  recorded by seismo-gravimeter in Obninsk during December 20, 2004 – January 22, 2005.

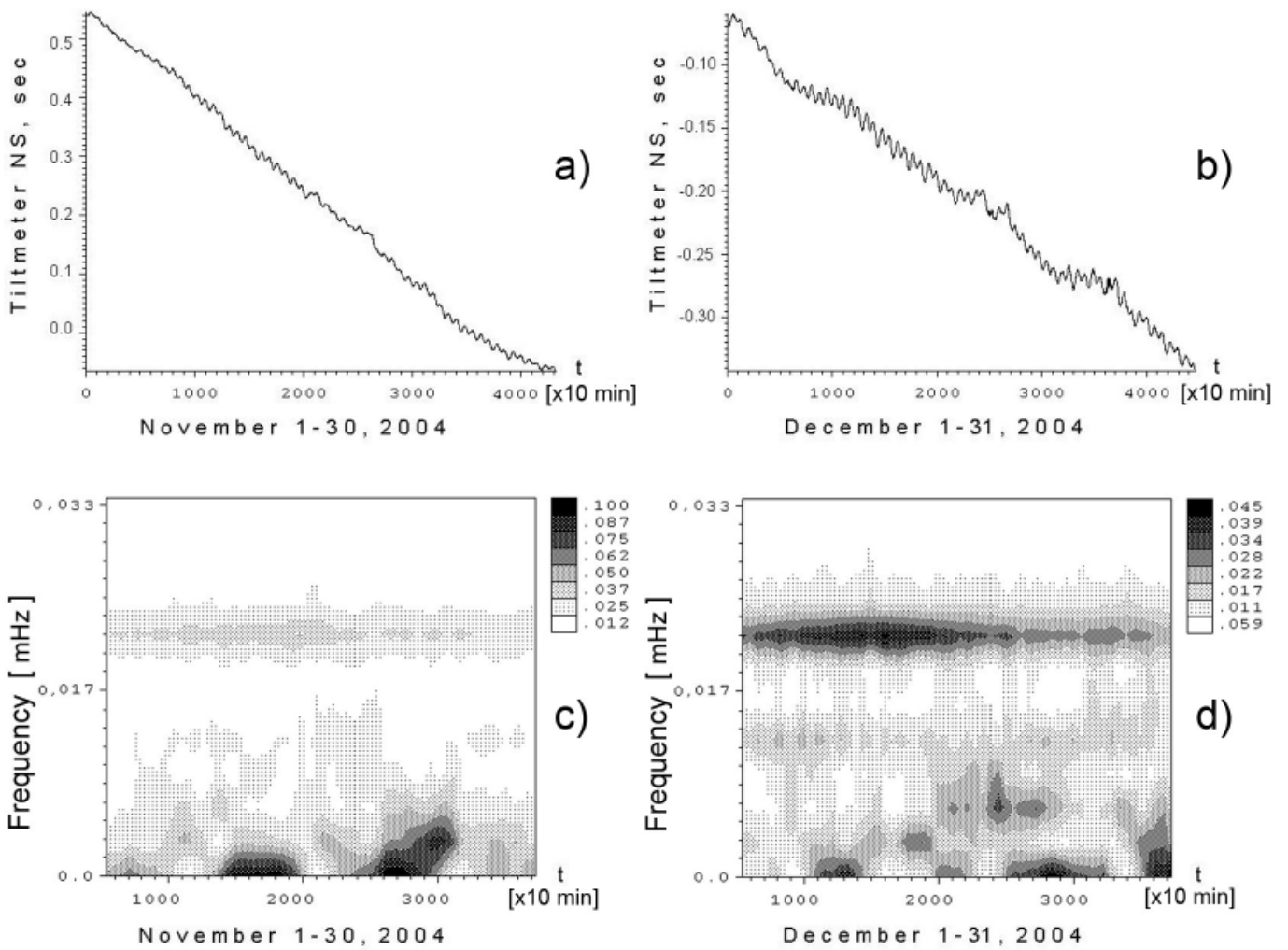


**Fig. 5.** Tiltmeter records from Observatory Jezeri-2 (NS component) during November 01 – December 31, 2004 (a, b) and time-frequency diagrams for corresponding periods (c, d); growth of spectral component intensities near 0.002-0.006 Hz in the second half of December is clearly seen.

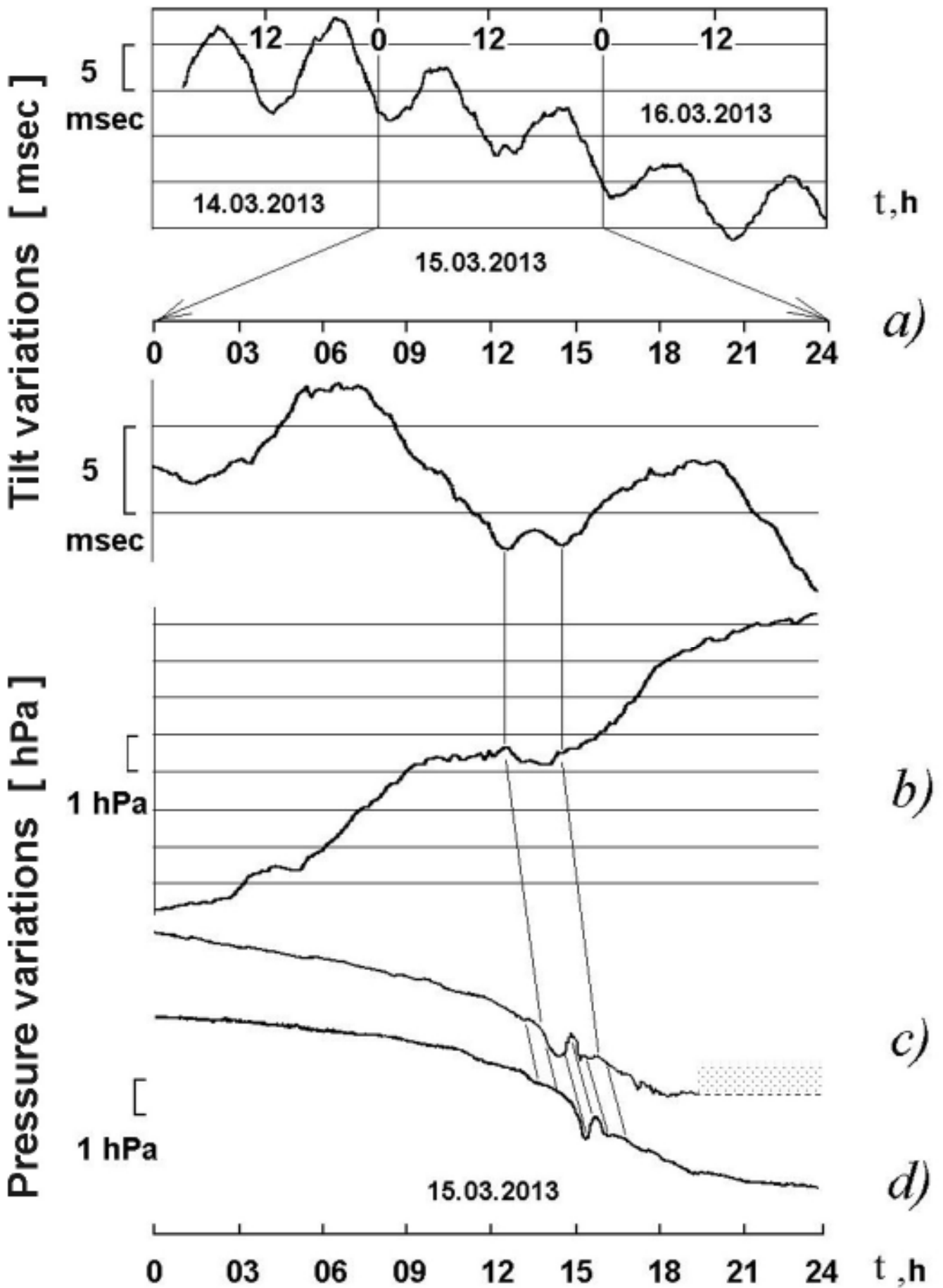


**Fig. 6.** Global disturbances recorded on March 14-16, 2013: tiltmeter (a) and atmospheric pressure (b) in Observatory Jezeri; atmospheric pressure in Troizk (c) and Fryazino (d).

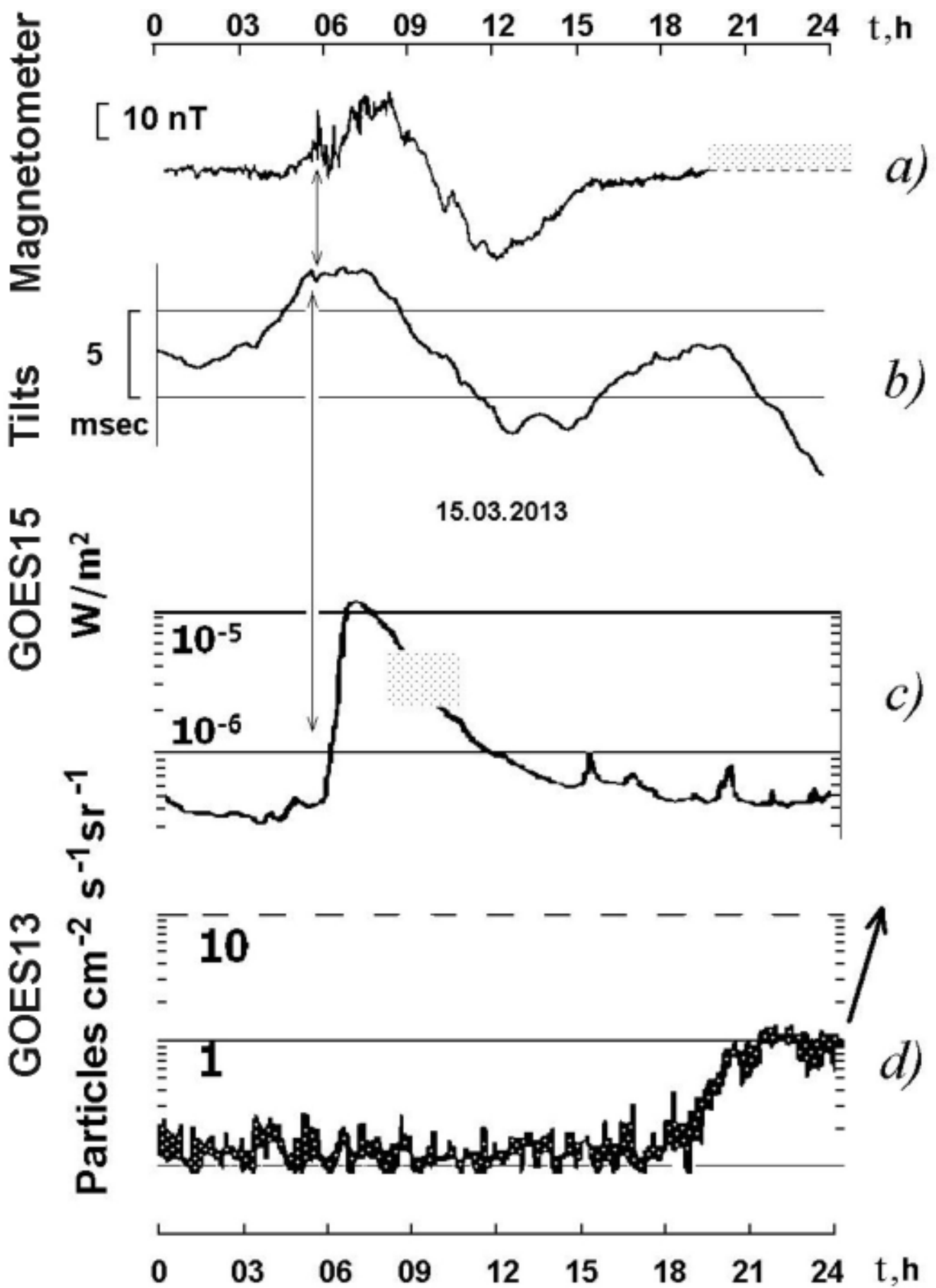


**Fig. 7.** Geomagnetic and ionosphere disturbances recorded on March 15, 2013: a) magnetometer in Troizk; b) tiltmeter in Observatory Jezeri; c) X-ray flux, satellite GOES15; d) proton flux, satellite GOES13.

---

## Comparison of noise levels of the new *iGrav-007* superconducting gravimeter and the SG-065 superconducting gravimeter in Wuhan (China)

Zhang Miaomiao<sup>1,\*</sup>, Xu Jianqiao<sup>1</sup>, Sun Heping<sup>1</sup>, Shen Wenbin<sup>2</sup>, Chen Xiaodong<sup>1</sup>

<sup>1</sup>State Key Laboratory of Geodesy and Earth's Dynamics, Institute of Geodesy and Geophysics, Chinese Academy of Sciences, Wuhan, 430077, China

<sup>2</sup> Department of Geophysics, School of Geodesy and Geomatics, Key Laboratory of Geospace Environment and Geodesy of the Ministry of Education, Wuhan University, Wuhan 430079, China

\*Corresponding author. E-mail: zhangmm@whigg.ac.cn

### Abstract

The new GWR *iGrav*<sup>®</sup> superconducting gravity meter is designed with the characteristics of an ultra-low drift, a virtually constant scale factor, and being less expensive, more portable and simpler to use than the traditional Observatory Superconducting Gravimeter. This paper aims to test the performance of the new *iGrav-007* in Wuhan in terms of noise levels in the seismic band (2 min – 1 h), sub-seismic band (1 h to 6 h) and tidal band (above 6 h) with respect to the collocated SG-065 superconducting gravimeter. In the seismic band, based on the Seismic Noise Magnitude (SNM), 0.97 and 0.37 respectively, we see that the *iGrav-007* is noisier than the SG-065; what's more, the Power Spectral Densities (PSD) curve of the *iGrav-007* is slightly higher than that of the SG-065, with the maximum difference of 10 dB. Similar to the comparison in the seismic band, the *iGrav-007* is also noisier than the SG-065 in the sub-seismic band in terms of the Sub-Seismic Noise Magnitude (SSNM), 1.96 and 1.86 respectively, and the slightly higher PSD curve of the *iGrav-007*, with the maximum difference of no more than 10 dB. Nevertheless, because of the small SNMs (below 1.0) and SSNMs (below 2.0), we can infer that both instrument-site combinations in Wuhan have low noise and a good quality in the seismic and sub-seismic bands. Furthermore, the above results in the seismic and sub-seismic bands have been confirmed by the comparison of the amplitude spectra between 0.2 and 1.7 mHz obtained from the residuals of the *iGrav-007* and the SG-065 after the 2013/11/17 Mw=7.8 Scotia Sea earthquake and the background free oscillations of the Earth observed in both SGs records. In the tidal band, however, by using the ETERNA 3.4 Earth Tide Analysis program we find that the *iGrav-007* performs slightly better due to the lower average noise amplitudes, especially in the 1 circle/day frequency band where the *iGrav-007* is 3 times quieter than the SG-065. Nonetheless, the tidal parameters obtained from the two SGs are almost same, with the maximum discrepancies of 0.4‰ for amplitude factors and -0.03° for phase lags respectively, and match well with those given in the theoretical models; besides, the unfiltered residuals of both SGs are highly correlated. Given the above discussion in the tidal band, we imply that both SGs perform well and similar in this band, even though the noise levels are different. Additionally, the mechanical instability of the SG-065 revealed by the signal difference has been improved recently. Compared with the noise levels of the old C032, the two new SGs perform much better in all the above bands and even Wuhan can be regarded as one of the quietest sites in the GGP network for seismic and sub-seismic study at present. Knowledge of the noise levels of the new *iGrav-007* and the SG-065 in Wuhan in the different frequency bands provides us with a necessary precondition and reference to make full use of these two SGs for the global and regional research.

**Keywords:** *iGrav-007* superconducting gravimeter; SG-065 superconducting gravimeter; noise levels; Wuhan tidal station

---

## 1. Introduction

With an extremely high sensitivity, an extremely long-term stability, an extremely wide dynamic linearity measuring range and an extremely low noise level (Heping Sun et al., 1999; H. P. Sun et al., 2001), superconducting gravimeters (SGs) have been known to be the most precise and stable relative gravity meter in existence (Goodkind, 1991) and regarded as an important tool in the research fields of geophysics, geodynamics and geodesy. As one of the earliest SG stations in the world and the sole international tidal gravity fundamental station in China (Hsu & Sun, 1998), Wuhan SG station has accumulated a great many of tidal gravity observations since 1985. It is playing a very important role in both global and regional research projects, such as the Global Geodynamics Project (GGP), the Asia-Pacific Space Geodynamics Project (APSG) and the Crustal Movement Observation Network of China (CMONOC), which can contribute to the study of Earth tides, the nearly diurnal-free wobble and modes of the Earth's core, Earth's rotation and polar motion, interaction of the Earth with atmosphere and oceans, gravity changes due to tectonic motions, regional seasonal effect and seismic effect, seismic modes, and so on (Courtier et al., 2000; Crossley et al., 1999; Heping Sun & Xu, 1997). Until now a series of research successes have been achieved at Wuhan SG station, including the accurate determination of the Earth tidal parameters, the establishment of international tidal gravity references, the construction of synthetic tidal gravity signals, the retrieval of atmospheric and oceanic gravity signals and the determination of free core nutation parameters and so on (Heping Sun et al., 2002).

On 5 March 2013, the new GWR *iGrav*-007 superconducting gravity meter and the SG-065 superconducting gravimeter were installed at Wuhan SG station by Wuhan University and the Institute of Geodesy and Geophysics, Chinese Academy of Sciences, to replace the GWR C032 superconducting gravimeter (stopped on 29 July 2012). Both SGs operate under almost the same environmental conditions and the same processing procedure, about 20 m apart from each other. Designed to replace mechanical spring-type gravity meters with SGs for geophysical applications that require much higher stability and precision, the new GWR *iGrav*<sup>®</sup> superconducting gravity meter not only maintains the same operating features as the traditional Observatory Superconducting Gravimeter, but also has such superiorities as an ultra-low drift of less than 0.5 microgal / month and a virtually constant scale factor; it is also much less expensive, portable and much simpler to use (Warburton et al., 2010) (cf. Fig. 1). Till now we have few studies of the performances of the new *iGrav* meters, and this paper aims to test the performance of the *iGrav*-007 in terms of noise levels in the seismic (2 min to 1 h), sub-seismic (1 h to 6 h) and tidal bands compared with the SG-065, by using one-minute and one-hour decimated data spanning from 30 March 2013 till 31 December 2013.

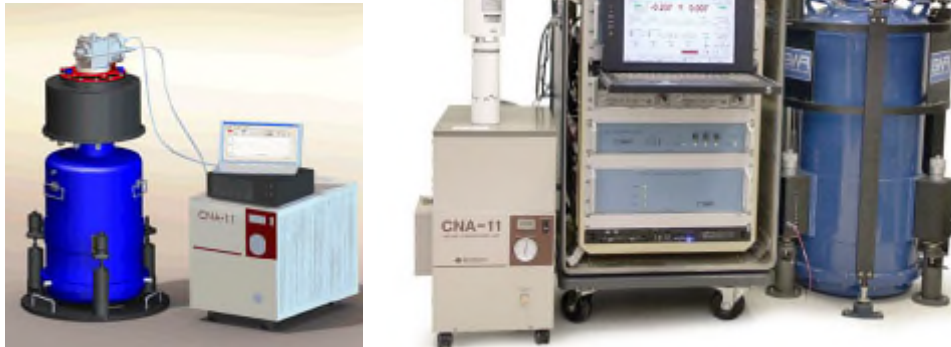


Figure 1. Comparison between *iGrav*<sup>®</sup> and OSG. *iGrav*<sup>®</sup> system is much less complex than the Observatory SG shown on the right side. (Warburton et al., 2010)

## 2. Noise levels in the seismic (2 min to 1 h) and sub-seismic (1 h to 6 h) bands

Here we first compare the noise levels of the *iGrav*-007 and the SG-065 in the seismic band with the processing procedure proposed by Banka and Crossley (Banka, 1997; Banka & Crossley, 1999) and recommended by GGP (<http://www.eas.slu.edu/GGP/ggphome.html>). The concept of Seismic Noise Magnitude (SNM) similar to earthquake magnitude is introduced in this procedure to quantify and quickly compare the noise levels at seismic frequencies. Then, following almost the same procedure, the noise levels of both SGs in the sub-seismic band are also compared with respect to the term Sub-Seismic Noise Magnitude (SSNM) (Rosat & Hinderer, 2011; Rosat et al., 2004; Rosat et al., 2003) generalized from SNM. Based on this method, Rosat *et al* (Rosat et al., 2004; Rosat et al., 2003) have enabled the quantitative comparison of noise levels of GGP stations in these two bands. Knowledge of the noise levels at each station in the seismic and sub-seismic bands is significant for site selection, instrumental modifications, evaluation of the recent potential of SGs to contribute to seismic normal mode studies and the search for the Slichter mode, and combination of the SGs to determine global Earth parameters (Banka, 1997; Rosat et al., 2004; Rosat et al., 2003). We describe briefly the processing procedure for studying the noise levels in the seismic band as follows.

The one-minute interval raw gravity and pressure daily files of the *iGrav*-007 and the SG-065, spanning from 30 March 2013 till 31 December 2013, are assembled and calibrated in amplitude from volts to microgal and to mbar respectively. The pressure files should be fixed for spikes, gaps, and offsets to avoid transferring problems in the pressure into the gravity data. A synthetic elastic tide, based on a modern tidal potential (Tamura, 1987; Xi, 1989) or later with recent values for the elastic tidal Love numbers, is subtracted and the influence of the air pressure is reduced with an admittance factor of  $-3 \text{ nm/s}^2 \text{ hPa}^{-1}$ . In order to eliminate the instrument drift and any residual tidal signal, a best-fitting 9th degree polynomial is subtracted. Then we compute the RMS of the reduced gravity data for each of the days, and select the 5 quietest days with the lowest RMS. We take a FFT for the data in each of the 5 quietest days through windowing with the Hann window and padding the data with zeros to the (next+1) power of 2, and then compute the average of the 5

unnormalized amplitude spectra. According to the average FFT spectrum, we can plot the Power Spectral Densities (PSD) and compute the mean PSD in the period range 200-600 sec to acquire the SNM through the relation(Banka, 1997):

$$\text{SNM} = \log_{10} (\text{mean PSD} / (\text{nm/s}^2)^2 / \text{Hz}) + 0.5 \quad (1)$$

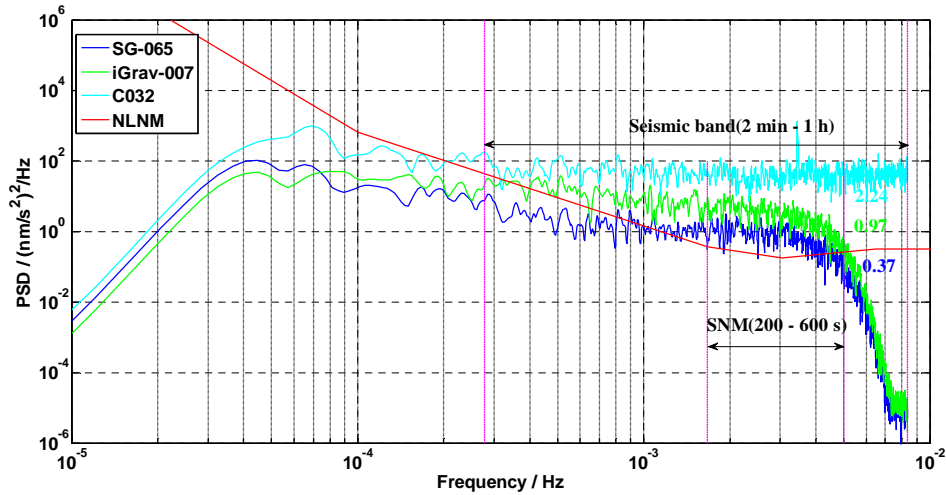


Figure 2. PSD noise levels in the seismic band for the *iGrav-007*, the SG-065 and the C032.

The SNMs for *iGrav-007* and SG-065 are 0.97 and 0.37 respectively. Additionally, the SNM for the old C032 computed based on the one-min interval data spanning from 30 March 2011 till 31 December 2011, equals to 2.24, which is far beyond those for the *iGrav-007* and the SG-065 indicating that these two new instrument-site combinations have much lower noise than the old one in the seismic band. The PSDs of them are shown in Figure 2, referring to the New Low Noise Model (NLNM) (Peterson, 1993) which is a reference noise model in seismology and represents the lower bound for the best seismometers. As a matter of fact, removing a 9<sup>th</sup> degree polynomial artificially decreases the PSDs at low frequencies, resulting in the lower PSD curve of the SG with respect to that of the seismometer; but in the period range 200-600 sec, the PSD curve of the SG is always higher than that of the seismometer. Based on the SNMs and Figure 2, we can conclude that *iGrav-007* is slightly noisier than SG-065 in the seismic band with the maximum PSD difference of 10 dB, corresponding to a factor of 10 in power and a factor of about 3 in amplitude. Nonetheless, the SNMs for *iGrav-007* and SG-065 are small (below 1.0) enough, indicating that both instrument-site combinations in Wuhan SG station have low noise and a good quality in the seismic band, and even now Wuhan is one of the quietest sites in the GGP network (cf. Fig. 3).

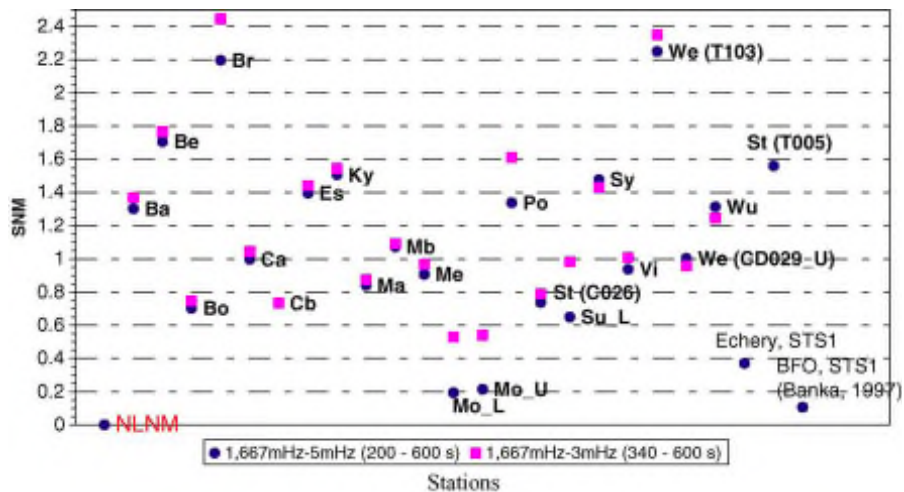


Figure 3. Seismic noise magnitudes in the frequency bands 200–600 s and 340–600 s for the 19 GGP stations. (Rosat et al., 2004).

Slightly different from the above mentioned processing procedure, we replace subtracting a 9<sup>th</sup> degree polynomial by high-pass filtering with a corner period of 8h; instead of computing the RMS for each day and selecting the 5 quietest days with the lowest RMS, we compute the RMS with a moving window of 15 days shifted by 1 day and then choose the quietest 15 continuous days with the lowest RMS (Rosat et al., 2004). In addition, the PSD is smoothed in the frequency domain with a 101-point Parzen window.

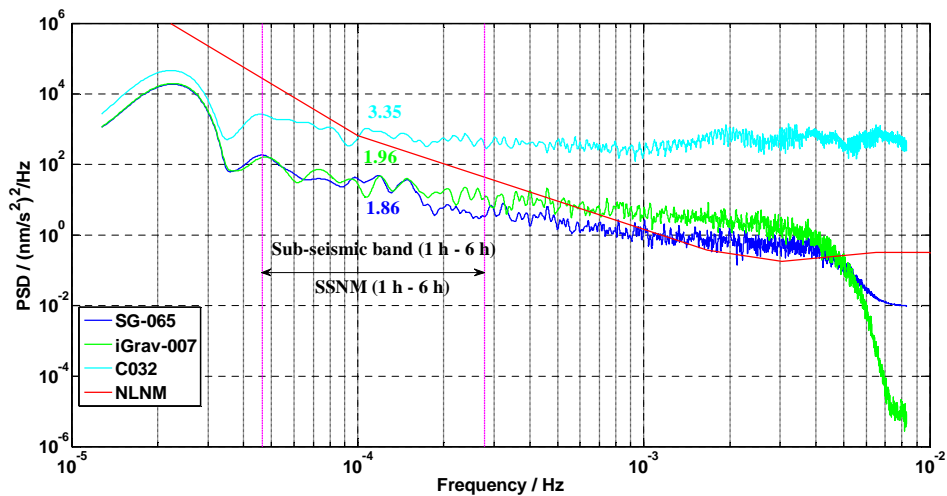


Figure 4. PSD noise levels in the sub-seismic band for the *iGrav-007*, the SG-065 and the C032.

The SSNMs for *iGrav-007* and SG-065 are 1.96 and 1.86 respectively. We also give the SSNM (3.35) for the old C032 by using the one-min interval data spanning from 30 March 2011 till 31 December 2011; with respect to it, we imply that the performances of these two new SGs have been quite improved in the sub-seismic band. From Figure 4, the maximum difference between the PSDs of the *iGrav-007* and the SG-065 in the sub-seismic band is no more than 10 dB, i.e., a factor of 10 in power and a factor of about 3 in amplitude. Similar to the comparison of noise levels of both SGs in the seismic band, the *iGrav-007* is slightly noisier than the SG-065 in the sub-seismic band while both instrument-site combinations are not noisy in terms of the small

SSNMs (below 2.0) and even now Wuhan is one of the quietest sites in the GGP network (cf. Fig. 5). In fact, the results in this study are consistent with the conclusion that there exists high linear correlation between the noise levels in the seismic and sub-seismic frequency bands, and thus estimating the noise level in only the seismic frequency band would be sufficient (Rosat & Hinderer, 2011; Rosat et al., 2004). However, no conclusions can be drawn for other *iGrav* superconducting gravimeters, considering the slightly lower noise level of *iGrav* 001 in the seismic band compared to the OSG 061 operating at GWR (Warburton et al., 2010). In addition, due to almost the same environmental conditions and the same processing procedure for the two SGs in Wuhan, there is the possibility that the slightly higher noise levels of the *iGrav*-007 in the seismic and sub-seismic bands are due to instrumental effects. After reviewing the dewar operating conditions, the higher noise levels of the *iGrav*-007 in the seismic and sub-seismic bands can be to a large extent attributed to the operating conditions with only a simple damper inserted in the neck and could probably be reduced by inserting a 2 inch spacer below the coldhead (Richard Warburton 2014, private communication).

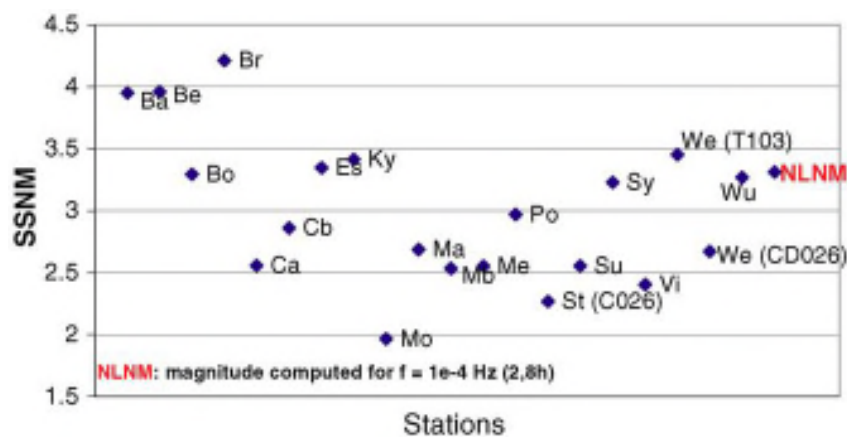


Figure 5. Sub-seismic noise magnitudes in the frequency band 1–6 h for the 19 GGP stations. (Rosat et al., 2004).

Furthermore, on the one hand, we have confirmed the above results by comparing the SNRs of the *iGrav*-007 and the SG-065 in the frequency band between 0.2 and 1.7 mHz (i.e. 83 and 10 min in period), where the ultra-low-frequency free modes of the Earth have their eigenfrequencies and are not excited to large amplitudes even by very large earthquakes (Freybourger et al., 1997; Richter et al., 1995). Figure 6 shows the amplitude spectra of the residuals (with the local tides and the barometric pressure effect subtracted by using tidal parameters and the barometric pressure admittance derived from tidal analysis) for time window from 5 to 85 h after the 2013/11/17 Mw=7.8 Scotia Sea earthquake. Obtained by parallel registration with AG measurements, the scale factors of the *iGrav*-007 and the SG-065 are  $-91.6402 \pm 0.0852 \mu\text{Gal/V}$  and  $-92.3533 \pm 0.0854 \mu\text{Gal/V}$ , equivalent to a precision of 0.093% and 0.092% respectively, which have been proved to be correct within the error bars considering the closeness of the analyzed tidal amplitudes of both SGs and the theoretical ones discussed in the section 3. Clearly, the SG-065 performs better in general and has slightly larger SNRs for most peaks ( ${}_0S_4$ ,  ${}_0S_5$ ,  ${}_3S_1$ ,  ${}_0S_6$ ,  ${}_1S_4$ ,  ${}_0S_7$ ,  ${}_2S_4$ ,  ${}_0S_8$ ,  ${}_1S_6$ ,  ${}_0S_9$ ,  ${}_1S_7$ ,  ${}_2S_6$ ) in this band. In addition, between 0.6 and 1.7 mHz, the strong similarities and the large SNRs of the two spectra imply that both SGs perform well and

similarly for the study of the modes of the Earth in the seismic and even sub-seismic bands.

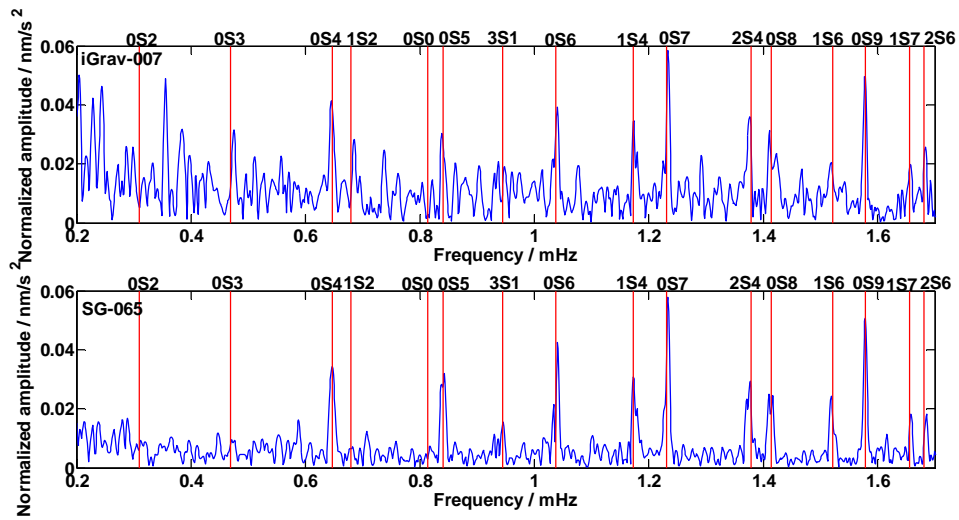


Figure 6. Amplitude spectra for time window from 5 to 85 h after the 2013/11/17 Mw=7.8 Scotia Sea earthquake obtained from the residuals of the *iGrav-007* and the *SG-065*. Vertical red lines indicate theoretical eigenfrequencies for some modes from Earth Model PREM (Dziewonski & Anderson, 1981).

On the other hand, the background free oscillations of the Earth, which are commonly called ‘hum’ and provide a good reference for the evaluation of the noise level in the milliHertz band (Nawa et al., 2000), are observed in both SGs records and thus indicate they have low noise in the seismic and even sub-seismic bands. Following the method recommended in Nawa et al. (2000), we removed the local synthetic tides and the pressure effect with an admittance of  $-3 \text{ nm/s}^2 \text{ hPa}^{-1}$  from the one-min interval data and computed power spectra for every seismically quiet period, which is defined as a 3-day-long interval not containing the day of or day immediately after any earthquakes with moment magnitude greater than 5.7 listed in the Harvard CMT catalogs; then, we stacked these power spectra to obtain the averaged power spectrum and smoothed it with an 11-point rolling average. Figure 7 shows the averaged power spectrum between 1 and 5 mHz for almost the same period in 2013 for the *iGrav-007*, the *SG-065*, for MO (Moxa, Germany) which is the quietest SG station in GGP and for ME (Metsähovi, Finland) where the background free oscillations were detected in 1995 (Nawa et al., 2000). We can see the spectral peaks of the background free oscillations for both the *iGrav-007* and the *SG-065* data especially at frequencies between 3 and 5 mHz, though these peaks are slightly less clear for the *iGrav-007*. In contrast, the peaks are clearly visible at MO while less clear at ME. In addition, our results are consistent with the critical noise level,  $10^{-17} \text{ m}^2 \text{ s}^{-3}$  or  $10 \text{ (nm/s}^2\text{)}^2 \text{ Hz}^{-1}$  (Nawa et al., 2000), below which the background free oscillations can be identified easily.

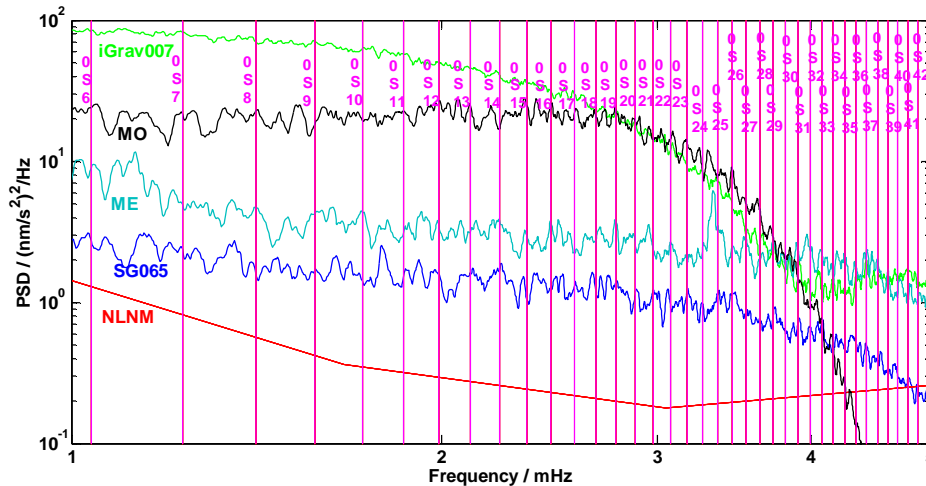


Figure 7. Averaged power spectra between 1 and 5 mHz (with logarithmic scale for both axes) for seismically quiet periods with a cutoff magnitude of 5.7 in 2013 for the *iGrav-007*, the SG-065, MO, and ME. Vertical magenta lines indicate theoretical eigenfrequencies for some modes from Earth Model PREM (Dziewonski & Anderson, 1981).

### 3. Noise levels in the tidal band (above 6 h)

In this part, the comparison of noise levels of the *iGrav-007* and the SG-065 in the tidal band is also carried out by using the ETERNA 3.4 Earth Tide Analysis program (Wenzel, 1996). After numerical filtering and decimation from 1 s to 1 min, the data are preprocessed for gaps, spikes, steps and other disturbances with the TSoft software (Van Camp & Vauterin, 2005), and then decimated to the hourly data spanning from 31 March 2013 till 31 December 2013. By applying high-pass filtering, the tidal potential development of Tamura (1987) and a linear regression with air pressure, ETERNA 3.4 performs the tidal analysis on the hourly data of both SGs. Here it is worth to note that there is a gap between 2013/05/25 09:00:00 and 2013/05/27 17:00:00 in the data of the *iGrav-007* and thus the whole data of the *iGrav-007* have been separated into two sets, spanning from 2013/03/31 00:00:00 till 2013/05/25 08:00:00 and from 2013/05/27 18:00:00 till 2013/12/31 23:00:00 respectively.

The noise levels estimated from the Fourier spectral analysis of the *iGrav-007* and the SG-065 residual records after tidal analysis with ETERNA are normalized by the number of samples and then listed in table 1. We can find that in all the tidal frequency bands the average noise amplitudes of the *iGrav-007* are always lower than those of the SG-065, especially in the 1 cycle/day frequency band where a factor of 3 is obtained. In addition, we also list the average noise amplitudes of the old C032 hourly data spanning from 31 March 2011 till 31 December 2011, which are always much higher than those of the *iGrav-007* and in general slightly higher than those of the SG-065 except for the 1 cycle/day frequency band. Table 2 shows the tidal parameters (amplitude factors  $\delta$  and phase lags  $\Delta\phi$ ) and their Root-Mean-Square (RMS) errors for the four main tidal waves ( $O_1$ ,  $K_1$ ,  $M_2$ ,  $S_2$ ). For these tidal waves, the RMS errors of the amplitude factors and phase lags for the *iGrav-007* are always smaller than those for the SG-065, with a ratio of nearly 3 for  $O_1$ , 4 for  $K_1$ , 1.5 for  $M_2$  and nearly 2 for  $S_2$ . To be exact, the internal precision of the tidal analysis results obtained by the *iGrav-007* is higher, at 0.12‰, 0.1‰, 0.04‰, 0.12‰ for

the  $O_1$ ,  $K_1$ ,  $M_2$  and  $S_2$  waves, respectively; the determined average internal precision of the phase lags is also superior with  $\pm 0.0051^\circ$ . In fact, the higher internal precision of the tidal parameters for the *iGrav-007* is a consequence of smaller residual noise levels in table 1 (Freybourger et al., 1997).

Table 1. Estimates of noise levels in different tidal frequency bands normalized by the number of samples

Frequency band (cycles/day)	Noise level of <i>iGrav-007</i> record ( $\text{nm s}^{-2}$ )	Noise level of SG-065 record ( $\text{nm s}^{-2}$ )	Noise level of C032 record ( $\text{nm s}^{-2}$ )
1	0.031945	0.095074	0.068411
2	0.025210	0.038842	0.063672
3	0.012210	0.025697	0.024384
4	0.007420	0.014807	0.018439

Table 2. Results obtained by tidal analysis of the *iGrav-007* hourly data and the SG-065 hourly data for main tidal waves

Wave group	<i>iGrav-007</i>		SG-065		Difference ( <i>iGrav- SG</i> )	
	$\delta$ & RMS error	$\Delta\varphi(^{\circ})$ & RMS error	$\delta$	$\Delta\varphi(^{\circ})$	$\Delta\delta(\times 1000)$	$\Delta\Delta\varphi(^{\circ})$
$O_1$	1.17436 $\pm 0.00012$	-0.5009 $\pm 0.0059$	1.17416 $\pm 0.00033$	-0.5016 $\pm 0.0162$	+0.20	+0.0007
$K_1$	1.14842 $\pm 0.00010$	-0.5626 $\pm 0.0052$	1.14802 $\pm 0.00040$	-0.5529 $\pm 0.0202$	+0.40	-0.0097
$M_2$	1.17094 $\pm 0.00004$	-0.4724 $\pm 0.0017$	1.17092 $\pm 0.00006$	-0.4456 $\pm 0.0027$	+0.02	-0.0268
$S_2$	1.16509 $\pm 0.00012$	-0.6857 $\pm 0.0077$	1.16487 $\pm 0.00020$	-0.6549 $\pm 0.0126$	+0.22	-0.0308

From the last two columns in table 2, we can conclude that the calibrations of both instruments agree within 0.4‰ in amplitude and  $0.03^\circ$  in phase. Meanwhile, the tidal parameters of the *iGrav-007* and the SG-065 match well with those given in the theoretical model  $\square$  (Dehant (1997) model (Dehant et al., 1997)+ TOPEX/POSEIDON satellite altimetry ocean data) and in the theoretical model  $\square$  (Dehant (1997) model (Dehant et al., 1997)+ Schwiderski global ocean data + local Chinese data) mentioned by Xu *et al* (Xu et al., 2000); the averaged discrepancies between observed tidal amplitude factors and those given in the theoretical models  $\square$  and  $\square$  are 3.8‰ and 3.0‰ (*iGrav-007*), 3.9‰ and 3.2‰ (SG-065) respectively; the mean differences between observed phase lags and those given in the theoretical models  $\square$  and  $\square$  are  $0.104^\circ$  and  $0.223^\circ$  (*iGrav-007*),  $0.093^\circ$  and  $0.207^\circ$  (SG-065) respectively.

Furthermore, a correlation analysis of the unfiltered residuals of both SGs is carried out for the two periods (2013/03/31 00:00:00 – 2013/05/25 08:00:00 and 2013/05/27 18:00:00 – 2013/12/31 23:00:00) respectively. The unfiltered residuals are obtained by subtracting synthetic tides, air

pressure effect (using adjusted tidal parameters and air pressure regression parameters derived from the above mentioned tidal analysis) and polar motion effect from the hourly data (Figure 8). It is worth to note that, in order to observe the correlation between the two data sets more easily, this figure is obtained by offsetting both records (so that they start close to zero and are close to overlapping-but not quite) and then expanding the scale. The correlation coefficients for the two periods are very high, with 0.9871 and 0.9106 respectively. It reflects the fact that there are still common signals such as an installation drift during the 100 first registration days, unmodelled gravity signals from the Earth (especially the long period wave *Mf*), atmosphere and hydrosphere in both SGs observations (Richter et al., 1995). Given to the small discrepancies for tidal parameters and the high correlation coefficients between both SGs residuals, we can infer that both SGs perform well and similar in the tidal band, even though the noise levels are different.

However, the individual residuals are not matching well at certain areas and many of the problems with SG-065 can be seen either on its residual or more easily on the signal difference between SG-065 and *iGrav-007* (cf. Figure 8 and 9). The signal difference shows that apart from the relative drift between these two SGs and concrete identified events in the auxiliary data, there are some other disturbances which appear mainly on SG-065, such as the offset marked by the red circle in Figure 9. Recently, further experiments and analysis conducted by the GWR team (including closing compressor, tilt desensitizing, purging coldhead, cleaning neck, interchanging the electronics between the X and Y axis, field servicing of X and Y axis thrusters, greasing all three post slides and so on) have revealed that we could associate many of these disturbances to the mechanical instability of Tilt X and Y thermal levelers of the SG-065 caused by small temperature changes. Meanwhile, the mechanical instability of SG-065 has been improved, which will be useful for lowering its noise level in the tidal band.

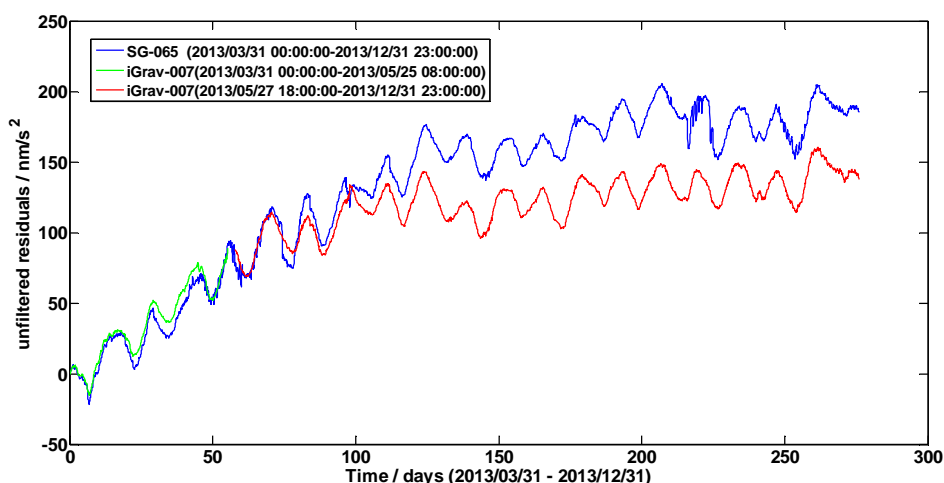


Figure 8. Residual curves of tidal records from the *iGrav-007* and the SG-065 with tides, air pressure effect and polar motion effect subtracted

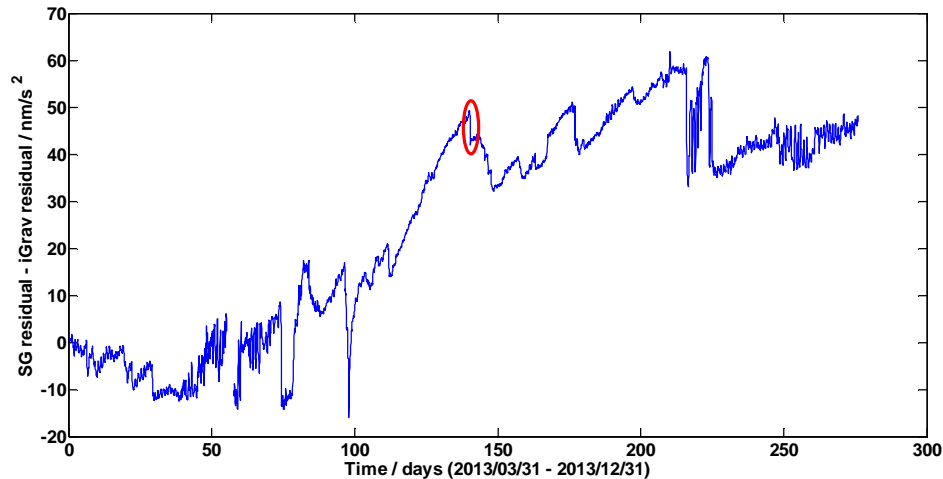


Figure 9. The difference between the SG-065 and the *iGrav-007* residuals (i.e. SG-065 residual – *iGrav-007* residual). An offset is marked by the red circle.

#### 4. Conclusions

We have investigated the performance of the new *iGrav-007* superconducting gravimeter in Wuhan in terms of noise levels in the seismic band (2 min – 1 h), sub-seismic band (1 h to 6 h) and tidal band (above 6 h) by comparing with the SG-065 superconducting gravimeter.

In the seismic and sub-seismic bands, the *iGrav-007* is noisier than the SG-065, with the maximum PSD difference of 10 dB, corresponding to a factor of 10 in power and a factor of 3 in amplitude. Given the small SNMs (0.966 and 0.366) and SSNMs (1.9604 and 1.8631), we can infer that both instrument-site combinations in Wuhan have low noise and a good quality in these two bands. Moreover, we confirm the conclusion in these two bands by comparing the amplitude spectra between 0.2 and 1.7 mHz obtained from the residuals of the *iGrav-007* and the SG-065 after the 2013/11/17 Mw=7.8 Scotia Sea earthquake, and by the background free oscillations of the Earth observed in both SGs records especially at frequencies above 3 mHz. Thus both SGs are suitable for the geophysical research such as seismic normal mode and Slichter mode. Additionally, the higher noise levels of the *iGrav-007* in the seismic and sub-seismic bands are to a large extent attributed to the operating conditions only with a damper inserted in the neck and are probably to be lowered by inserting a 2 inch spacer below the coldhead.

In the tidal band, the *iGrav-007* performs slightly better with respect to the lower average noise amplitudes, especially in the 1 circle/day frequency band where the *iGrav-007* is 3 times quieter than the SG-065, which contributes to the higher accuracy of the tidal parameters. However, the tidal parameters obtained by tidal analysis of the *iGrav-007* record are to a large extent in good agreement with those of the SG-065 record, and match well with those given in the theoretical models. In addition, the unfiltered residuals of both SGs are highly correlated, which reflects that there are still common signals such as unmodelled gravity signals from the Earth, atmosphere and hydrosphere in both SGs observations. As a result, we imply that both SGs perform well and similarly in the tidal band, and thus can collaborate with or refer to each other for the studies of

---

Earth tides, the validation of solid Earth and ocean tidal models (Baker & Bos, 2003; Boy et al., 2003) and so on. In addition, further investigation of the individual residuals and the signal difference revealed the mechanical instability of the SG-065 and hopefully the recent improvement of the operation of the SG-065 will contribute to lowering its noise level in the tidal band.

Here, it is worthy to note that, due to almost the same environmental conditions and the same processing procedure, the differences between the noise levels in each band for the two SGs should be of instrumental origin mainly.

In addition, compared with the noise levels of the old C032, we can conclude that the two new SGs in Wuhan perform much better in all the above bands; specially, in both the seismic and sub-seismic bands, Wuhan can be regarded as one of the quietest sites in the GGP network at present. Knowledge of the noise levels of the new *i*Grav-007 and the SG-065 in Wuhan in the different frequency bands provides us with a necessary precondition and reference to make full use of these two SGs for the global and regional research, such as the Global Geodynamics Project (GGP), the Asia-Pacific Space Geodynamics Project (APSG) and the Crustal Movement Observation Network of China (CMONOC).

### **Acknowledgments**

The authors are grateful to the GWR team (Mr Richard Warburton, Mr Richard Reineman and Mr Harish Pillai) for helping analyze some of data sets. This work was jointly supported by the National Basic Research Program of China (Grant No. 2014CB845902), and the National Natural Science Foundation of China (Grant Nos. 41274085, 41374084, 41321063).

### **References**

- Baker TF, Bos MS. (2003). Validating Earth and ocean tide models using tidal gravity measurements. *Geophysical Journal International*, 152, 468-485. doi: 10.1046/j.1365-246X.2003.01863.x.
- Banka D. (1997). Noise levels of superconducting gravimeters at seismic frequencies. GDMB - Information - gesellschaft mbH.
- Banka D, Crossley D. (1999). Noise levels of superconducting gravimeters at seismic frequencies. *Geophysical Journal International*, 139, 87-97. doi: 10.1046/j.1365-246X.1999.00913.x.
- Boy JP, Llubes M, Hinderer J, Florsch N. (2003). A comparison of tidal ocean loading models using superconducting gravimeter data. *Journal of Geophysical Research: Solid Earth*, 108, 2193. doi: 10.1029/2002JB002050.
- Courtier N, Ducarme B, Goodkind J, Hinderer J, Imanishi Y, Seama N, Sun H, Merriam J, Bengert B, Smylie DE. (2000). Global superconducting gravimeter observations and the search for the translational modes of the inner core. *Physics of the Earth and Planetary Interiors*, 117, 3-20. doi: [http://dx.doi.org/10.1016/S0031-9201\(99\)00083-7](http://dx.doi.org/10.1016/S0031-9201(99)00083-7).
- Crossley D, Hinderer J, Casula G, Frnacis O, Hsu HT, Imanishi Y, Jentzsch G, Kääriänen J, Merriam J, Meurers B, Neumeyer J, Richter B, Shibuya K, Sato T, van Dam T. (1999). Network of superconducting gravimeters benefits a number of disciplines. *Eos, Transactions American Geophysical Union*, 80, 121-126. doi: 10.1029/99EO00079.
- Dehant V, Defraigne P, Wahr JM. (1997). Tides for Earth in a non-hydrostatic equilibrium. In: *In Proc.*

- 
- 13th Int. Sympos. on Earth Tides (eds. Ducarme, B., Paquet, P.), Brussels: Royal Observatory of Belgium, pp. 261-263.
- Dziewonski AM, Anderson DL. (1981). Preliminary reference Earth model. *Physics of the Earth and Planetary Interiors*, 25, 297-356.
- Freybourger M, Hinderer J, Trampert J. (1997). Comparative study of superconducting gravimeters and broadband seismometers STS-1 / Z in seismic and subseismic frequency bands. *Physics of the Earth and Planetary Interiors*, 101, 203-217. doi: [http://dx.doi.org/10.1016/S0031-9201\(97\)00003-4](http://dx.doi.org/10.1016/S0031-9201(97)00003-4).
- Goodkind JM. (1991). The superconducting gravimeters principles of operation, current performance and future prospects. In: *Proceedings of the workshop on non-tidal gravity changes*, Luxembourg, pp. 81-90.
- Hsu HT, Sun H. (1998). Progress status of the experimental study on tidal gravity in China. *Advance in earth sciences*, 13, 415-421.
- Nawa K, Suda N, Fukao Y, Sato T, Tamura Y, Shibuya K, McQueen H, Virtanen H, Kääriäinen J. (2000). Incessant excitation of the Earth's free oscillations: global comparison of superconducting gravimeter records. *Physics of the Earth and Planetary Interiors*, 120, 289-297. doi: [http://dx.doi.org/10.1016/S0031-9201\(00\)00158-8](http://dx.doi.org/10.1016/S0031-9201(00)00158-8).
- Peterson J. (1993). Observations and modelling of background seismic noise. Open-file report 93-322. US Geological Survey, Albuquerque, New Mexico.
- Richter B, Wenzel HG, Zürn W, Klopping F. (1995). From Chandler wobble to free oscillations: comparison of cryogenic gravimeters and other instruments in a wide period range. *Physics of the Earth and Planetary Interiors*, 91, 131-148. doi: [http://dx.doi.org/10.1016/0031-9201\(95\)03041-T](http://dx.doi.org/10.1016/0031-9201(95)03041-T).
- Rosat S, Hinderer J. (2011). Noise Levels of Superconducting Gravimeters: Updated Comparison and Time Stability. *Bulletin of the Seismological Society of America*, 101, 1233-1241.
- Rosat S, Hinderer J, Crossley D, Boy JP. (2004). Performance of superconducting gravimeters from long-period seismology to tides. *Journal of Geodynamics*, 38, 461-476. doi: 10.1016/j.jog.2004.07.005.
- Rosat S, Hinderer J, Crossley D, Rivera L. (2003). The search for the Slichter mode: comparison of noise levels of superconducting gravimeters and investigation of a stacking method. *Physics of the Earth and Planetary Interiors*, 140, 183-202.
- Sun H, Xu H. (1997). Execution and prospect for the Global Geodynamics Project cooperation. *Advance in earth sciences*, 12, 152-157.
- Sun H, Xu H, Ducarme B. (1999). Comprehensive comparison and analysis of the tidal gravity observations obtained with superconducting gravimeters at stations in China, Belgium and France. *Chinese science bulletin*, 44, 750-755.
- Sun H, Xu J, Xu H. (2002). Progress in application study of gravity observations recorded with a GWR superconducting gravimeter in China. *Journal of Geodesy and Geodynamics*, 22, 106-111.
- Sun HP, Takemoto S, Hsu HT, Higashi T, Mukai A. (2001). Precise tidal gravity recorded with superconducting gravimeters at stations Wuhan (China) and Kyoto (Japan). *Journal of Geodesy*, 74, 720-729. doi: 10.1007/s001900000139.
- Tamura Y. (1987). A harmonic development of the tide-generating potential. *Bulletin d'Informations Marees Terrestres*, 99, 6813-6855.
- Van Camp M, Vauterin P. (2005). Tsoft: graphical and interactive software for the analysis of time series and Earth tides. *Computers & Geosciences*, 31, 631-640.
- Warburton RJ, Pillai H, Reineman RC. (2010). Initial Results with the New GWR iGrav™ Superconducting Gravity Meter. *Proc. IAG Symp. on Terrestrial Gravimetry: Static and Mobile*

---

Measurements (TG-SMM2010), 22 - 25 June 2010, Russia, Saint Petersburg, 138

Wenzel HG. (1996). The nanogal software: Earth tide data processing package ETERNA 3.30. Bull. Inf. Marées Terrestres, 124, 9425-9439.

Xi Q. (1989). A new complete development of the tide-generating potential for the epoch J2000.0. Bulletin d'Informations Marees Terrestres, 99, 6766-6812.

Xu H, Sun H, Xu J, Tao G. (2000). International tidal gravity reference values at Wuhan station. Science in China Series D: Earth Sciences, 43, 77-83. doi: 10.1007/BF02877832.

|

BLANK PAGE